EXPERIMENTAL AND NUMERICAL INVESTIGATION OF LAMINAR FLAME SPEEDS OF $H_2/CO/CO_2/N_2$ MIXTURES

A Dissertation

Presented to

The Academic Faculty

by

Jayaprakash Natarajan

In Partial Fulfillment

of the Requirements for the Degree

Doctor of Philosophy in the

School of Aerospace Engineering

Georgia Institute of Technology

May 2008

EXPERIMENTAL AND NUMERICAL INVESTIGATION OF LAMINAR FLAME SPEEDS OF $H_2/CO/CO_2/N_2$ MIXTURES

Approved by:

Dr. Jerry M. Seitzman, Advisor
School of Aerospace Engineering
Georgia Institute of Technology

Dr. Timothy C. Lieuwen
School of Aerospace Enginnering
Georgia Institute of Technology

Dr. Suresh Menon
School of Aerospace Engineering
Georgia Institute of Technology

Dr. Jechiel I. Jagoda
School of Aerospace Engineering
Georgia Institute of Technology

Dr. Scott Martin
Gas Turbine Combustion Technology
Siemens Power Generation

Date Approved: February 29th 2008

To my parents

ACKNOWLEDGEMENTS

It is pleasure to thank all the people who made this thesis possible. First and foremost I would like to express my deep sense of gratitude to my thesis advisor Dr. Jerry Seitzman, for his valuable guidance, continuous support and encouragement throughout the course of this work. I would also like to express my sincere thanks to Dr. Tim Lieuwen for his guidance and support.

I would like to acknowledge the helpful comments and guidance from the thesis reading committee, Dr. Scott Martin, Dr. Suresh Menon and Dr. Jechiel Jagoda. I greatly appreciate their time and efforts in helping me to improve this document.

I would like to thank all the graduate students at the Georgia Tech combustion lab for their help and encouragement, with special recognition to Nori, Yash, Qingguo, Murgi, Bobba, Preetham, Santosh, and Priya. Working with them was indeed a pleasurable experience that I shall cherish throughout my life.

I would also like to acknowledge the financial support from Siemens Power Generation and General Electric Global Research for the successful completion of this work.

Finally, I thank my parents and my brothers for their love and being a constant source of encouragement. Above all, I thank God for all the blessings showered during the days of this work.

TABLE OF CONTENTS

ACKNOWLEDGEMENTS ..... **iv**

LIST OF TABLES ..... **viii**

LIST OF FIGURES ..... **ix**

SUMMARY ..... **xvi**

CHAPTER 1: INTRODUCTION **1**

1.1 Motivation 1

1.2 Literature Review 3

1.3 Overview of Present Work 6

CHAPTER 2: BACKGROUND **8**

2.1 Laminar Flame Properties of H_2/CO Mixtures 8

2.1.1 Adiabatic flame temperature 8

2.1.2 Flame structure 10

2.1.3 Laminar flame speed 15

2.2 Flame Speed Measurement Approaches 24

2.2.1 Bunsen flame approach 25

2.2.2 Spherically expanding flame method 28

2.2.3 Stagnation flame approach 29

CHAPTER 3: MEASUREMENT AND MODELING APPROACHES **33**

3.1 Measurement Approaches 33

3.1.1 Bunsen flame approach 33

3.1.2 Stagnation flame approach 44

3.2 Modeling Approaches 51
3.3 Measurement Uncertainties 52
3.3.1 Bunsen flame approach 54
3.3.2 Stagnation flame approach 55
CHAPTER 4: INFLUENCE OF PREHEAT TEMPERATURE 65
4.1 Validation – Bunsen flame approach 65
4.1.1 Atmospheric pressure 66
4.1.2 Elevated pressure 68
4.2 Atmospheric pressure results 69
4.2.1 Medium H_2 content fuels 72
4.2.2 Low H_2 content fuels 76
4.2.3 High H_2 content fuels 78
4.3 Elevated pressure results 85
4.3.1 Elevated preheat temperature 88
4.3.2 Room temperature (no preheat) 89
4.4 Sensitivity analysis 92
4.4.1 Medium H_2 content fuels 92
4.4.2 High H_2 content fuels 97
CHAPTER 5: INFLUENCE OF DILUENTS 100
5.1 Effects of CO_2 dilution 100
5.1.1 Atmospheric pressure results 101
5.1.2 Elevated pressure results 111
5.2 Effects of N_2 dilution 113

5.2.1 Eleveated preheat temperature reactants 114

5.2.2 Room temperature reactants 120

CHAPTER 6: CONCLUSIONS AND FURTHER RECOMMENDATIONS 123

6.1 Summary and conclusions 123

6.2 Recommendations for further studies 128

REFERENCES 131

LIST OF TABLES

Table 3.1. List of fuel mixtures and test conditions considered for the flame speed measurements. 50

Table 5.1. Measured and OPPDIFF predicted unstrained flame speed by linearly extrapolating to zero strain and their comparison with Bunsen flame measurements and PREMIX predictions for 40:40:20 H_2:CO:CO_2 mixture at three different equivalence ratios. 105

Table 5.2. Variation of the measured and models predicted unburned strain sensitivities for mixtures of H_2 with N_2 diluted air (O_2:N_2 1:9) at 700 K preheat temperature. 119

LIST OF FIGURES

Figure 1.1. Illustration of all the syngas (H_2/CO) flame speed data available prior to this study and the region of interest (pressure, equivalence ratio and preheat temperature space) for modern gas turbines. 5

Figure 2.1. Adiabatic flame temperatures for CH_4, H_2, CO and typical syngas (35% H_2, 35% CO and 30% CO_2) fuels with air..... 9

Figure 2.2. Chemical structure of a lean (Φ=0.6) H_2/CO fuel mixture with 5% of H_2 at normal temperature and pressure conditions..... 11

Figure 2.3. Chemical structure of a lean (Φ=0.6) H_2/CO fuel mixture with 95% of H_2 at normal temperature and pressure conditions..... 13

Figure 2.4. Laminar flame speeds for a range of H_2/CO fuel mixtures at a fixed equivalence ratio of 0.6, p=1 atm and T_u=300 K. 16

Figure 2.5. Laminar flame speed and mass burning rate as a function of pressure for 50:50 H_2/CO fuel mixture at Φ=0.6 and 300 K. 18

Figure 2.6. Laminar flame speed and mass burning rate as a function of pressure for 50:50 H_2/CO fuel mixture at Φ=1.0 and 300 K. 19

Figure 2.7. Variation of reaction order with pressure for 50:50 H_2/CO fuel mixture at two equivalence ratios. Symbols: numerical predictions, and lines: logarithmic fits.. 21

Figure 2.8. Normalized flame speeds as a function of preheat temperature for 50:50 H_2/CO fuel mixtures at three fixed equivalence ratios and T_u=300 K..... 22

Figure 2.9. Bunsen flame with three standard optical accessible flame edges. 26

Figure 2.10. Definition of the unburned flame speed based on the half cone angle. 27

Figure 2.11. Schematic of freely expanding spherical flame. 28

Figure 2.12. Schematic of the stagnation flow field with flame. 30

Figure 3.1. Schematic of the Bunsen flame experimental setup used for flame speed measurement at atmospheric pressure (TC=thermocouple). Mixing is achieved through long flow lines. 36

Figure 3.2. Images of flame emission for various fuels and conditions: (a) H_2:CO=95:5, Φ=0.61 without knife edge, (b) same as (a) but with knife edge, (c) H_2:CO=95:5 and 20% CO_2, Φ=0.62 without knife edge, (d) same as (c) with knife edge. The color scale represents the intensity variation of the 12 bit flame images. 38

Figure 3.3. (a) Schematic high pressure Bunsen flame experimental setup (TC=thermocouple). Mixing is achieved through long flow lines. (b) Typical image of flame emission at 15 atm and 600 K preheat temperature (80:20 H_2/CO fuel mixture, 10:90 O_2:He oxidizer). 40

Figure 3.4. A sample flame images of 50:50 H_2/CO fuel mixture at Φ=0.6, p=10 atm, and T≅600 K with (a) standard air, and (b) 10:90 O_2/He mixture. 42

Figure 3.5. Schematic of the experimental setup (TC=thermocouple). 45

Figure 3.6. Schematic of the burner stabilized stagnation flame. 46

Figure 3.7. Typical measured axial velocity along the stagnation streamline. Figure insert shows layout of nozzle generated wall stagnation flame. 48

Figure 3.8. Variation of the measured flame speed with strain rate for H_2:CO:CO_2 40:40:20 fuel mixture at Φ=0.59, p=1atm and T≅300K. 49

Figure 3.9. Numerical simulation of counter flow flame (CFF) and wall stagnation flame (WSF) for H_2 with N_2 diluted air (O_2:N_2 1:9) at Φ=0.8 and 700 K preheat temperature. 57

Figure 3.10. Model predicted strained flame speeds for CFF and WSF with two different wall temperatures. The fuel mixture is H_2 with N_2 diluted air (O_2:N_2 1:9) at Φ=0.8 and 700 K preheat temperature. The vertical bars indicate 3% deviation from CFF. 59

Figure 3.11. Numerical simulation of stagnation flame with plug and potential flow boundary conditions for the same strain rates. The fuel mixture is H_2 with N_2 diluted air (O_2:N_2 1:9) at Φ=0.8 and 700 K preheat temperature. 61

Figure 3.12. Model predicted strained flame speeds with plug and potential flow boundary conditions. The vertical bars indicate 2% deviation. 62

Figure 3.13. Comparison between the extrapolated flame speed (OPPDIFF) and the true unstrained flame speed (PREMIX) for 50:50 H_2:CO fuel mixture at Φ=0.6, T≅700K, and p=1atm. Both simulations are performed with GRI Mech 3.0. 63

Figure 4.1. Measured laminar flame speeds in Bunsen flame for CH_4 flames at p=1atm and T_u≅300K, including previous counter-flow flame experiments [,]. 66

Figure 4.2. Measured laminar flame speeds in Bunsen flame for H_2:CO 50:50 and 5:95 compositions at p=1atm and T≅300K, including previous spherical flame experiments [11,14,15]. 67

Figure 4.3. Comparison of measured laminar flame speeds obtained with conical flame and spherical flame [15] approaches for a 50:50 H_2/CO fuel mixture (O_2:He 1:7 oxidizer) at p=10 atm and T_u=300K. 68

Figure 4.4. Measured and models predicted laminar flame speeds for three H_2:CO compositions at p=1atm and $T_u \cong 300K$; Bunsen flame measurements (symbols) and PREMIX predictions (lines). 70

Figure 4.5. Laminar flame speed for fuels with 50:50 H_2:CO composition for various preheat temperatures at p=1atm; Bunsen flame measurements (symbols) and PREMIX predictions (lines). 73

Figure 4.6. Strained laminar flame speeds for lean mixtures with 50:50 H_2:CO fuel composition at p=1atm and T=700K; stagnation flame measurements (symbols and linear fit) and OPPDIF predictions (lines) 74

Figure 4.7. Laminar flame speed for fuels with 5:95 H_2:CO composition for various preheat temperatures at p=1atm; Bunsen flame measurements (symbols) and PREMIX predictions (lines). 77

Figure 4.8. Laminar flame speed for fuels with 95:5 H_2:CO composition with 20% CO_2 dilution for various preheat temperatures at p=1atm; Bunsen flame measurements (symbols) and PREMIX predictions (lines). 79

Figure 4.9. Strained laminar flame speeds for mixture of H_2 with air at Φ=0.3 and 700 K preheat temperature; stagnation flame measurements (symbols and linear fit) and OPPDIF predictions (lines). 81

Figure 4.10. Strained laminar flame speeds for mixture of H_2 with air at Φ=0.5 and 700 K preheat temperature; stagnation flame measurements (symbols and linear fit) and OPPDIF predictions (lines). 82

Figure 4.11. Ratios of the models predicted (PREMIX) and measured unstrained laminar flame speeds for lean mixtures of H_2 with standard air at 300 K and 700 K preheat temperatures. 85

Figure 4.12. Laminar flame speed for fuels with 50:50 H_2:CO composition for various preheat temperatures at p=1 atm; Bunsen flame measurements (symbols) and PREMIX predictions (lines). 87

Figure 4.13. Laminar flame speeds for a range of H_2/CO fuel mixtures (O_2:He 1:9 oxidizer) at a fixed equivalence ratio of 0.6, p=15 atm and T_u=600 K; Bunsen flame measurements (symbols) and PREMIX predictions (lines). 88

Figure 4.14. Laminar flame speeds for a range of H_2/CO fuel mixtures (O_2:He 1:9 oxidizer) at a fixed equivalence ratio of 0.8, p=15 atm and T_u=300 K; Bunsen flame measurements (symbols) and PREMIX predictions (lines). 90

Figure 4.15. Normalized sensitivity coefficients of the laminar flame speed to the pre-exponential rate constants. The fuel mixture is 50:50 H_2/CO and the oxidizer is standard air. 93

Figure 4.16. Variation of the reaction rates for R3, R13 and R15 reactions in the H production and consumption layers for preheated and room temperature reactants. The fuel mixture is 50:50 H_2/CO and the oxidizer is standard air. 95

Figure 4.17. Normalized sensitivity coefficients of the laminar flame speed to the pre-exponential rate constants. The fuel H_2 and the oxidizer is standard air. 98

Figure 5.1. Laminar flame speeds for fuels with 50:50 H_2:CO composition, and 0 and 20% CO_2 dilution of the fuel at p=1atm and $T_u \cong 300$K; Bunsen flame measurements (symbols) and PREMIX predictions (lines). 102

Figure 5.2. Strained flame speeds for lean mixtures with 50:50 H_2:CO fuel with 20% CO_2 dilution (i.e., 40:40:20 H_2:CO:CO_2) at p=1atm and $T_u \cong 300K$; Stagnation flame measurements (symbols and linear fit) and OPPDIF predictions (lines). 104

Figure 5.3. Strained laminar flame speeds for lean mixtures of fuel with 50:50 H_2:CO and 40% CO_2 dilution at p=1atm and T_u=700K; stagnation flame measurements (symbols and linear fits) and OPPDIF predictions (lines). 106

Figure 5.4. Laminar flame speed for fuels with 95:5 H_2:CO composition, and 0 and 20% CO_2 dilution at p=1atm and $T_u \cong 300K$; Bunsen flame measurements (symbols) and PREMIX predictions (lines). 108

Figure 5.5. Laminar flame speed for fuels with 5:95 H_2:CO composition, and 0 and 10% CO_2 dilution at p=1atm and $T_u \cong 300K$; Bunsen flame measurements (symbols) and PREMIX predictions (lines). 110

Figure 5.6. Laminar flame speeds for a range of H_2/CO fuel mixtures (O_2:He 1:9 oxidizer) with 0% and 40% CO_2 dilution at a fixed equivalence ratios, p=15 atm and T_u=600 K; Bunsen flame measurements (symbols) and PREMIX predictions (lines). 112

Figure 5.7. Strained laminar flame speeds for mixture of H_2 with N_2 diluted air (O_2:N_2 1:9) at Φ=0.8 and 700 K preheat temperature; stagnation flame measurements (symbols and fits) and OPPDIF predictions (lines). 114

Figure 5.8. Variation of the heat release rates for R3, R13 and R15 reactions for pure H_2 with standard air and N_2 diluted air (O_2:N_2 1:9) at Φ=0.385 and Φ=0.8, respectively 116

Figure 5.9. Strained laminar flame speeds for stoichiometric and rich mixtures of H_2 with N_2 diluted air (O_2:N_2 1:9) at 700 K preheat temperature; stagnation flame measurements (symbols and fits) and OPPDIF predictions (lines)..... 118

Figure 5.10. Ratios of the models predicted (PREMIX) and measured unstrained laminar flame speeds for lean mixtures of H_2 with N_2 diluted air (O_2:N_2 1:9) at 300 K and 700 K preheat temperatures..... 121

SUMMARY

Coal derived synthetic gas (syngas) fuel is a promising solution for today's increasing demand for clean and reliable power. Syngas fuels are primarily mixtures of H_2 and CO, often with large amounts of diluents such as N_2, CO_2, and H_2O. The specific composition depends upon the fuel source and gasification technique. This requires gas turbine designers to develop fuel flexible combustors capable of operating with high conversion efficiency while maintaining low emissions for a wide range of syngas fuel mixtures. Design tools often used in combustor development require data on various fundamental gas combustion properties. For example, laminar flame speed is often an input as it has a significant impact upon the size and static stability of the combustor. Moreover it serves as a good validation parameter for leading kinetic models used for detailed combustion simulations.

Thus the primary objective of this thesis is measurement of laminar flame speeds of syngas fuel mixtures at conditions relevant to ground-power gas turbines. To accomplish this goal, two flame speed measurement approaches were developed: a Bunsen flame approach modified to use the reaction zone area in order to reduce the influence of flame curvature on the measured flame speed and a stagnation flame approach employing a rounded bluff body. The modified Bunsen flame approach was validated against stretch-corrected approaches over a range of fuels and test conditions; the agreement is very good (less than 10% difference). Using the two measurement approaches, extensive flame speed information were obtained for lean syngas mixtures at

a range of conditions: 1) 5 to 100% H_2 in the H_2/CO fuel mixture; 2) 300-700 K preheat temperature; 3) 1 to 15 atm pressure, and 4) 0-70% dilution with CO_2 or N_2.

The second objective of this thesis is to use the flame speed data to validate leading kinetic mechanisms for syngas combustion. Comparisons of the experimental flame speeds to those predicted using detailed numerical simulations of strained and unstrained laminar flames indicate that all the current kinetic mechanisms tend to over predict the increase in flame speed with preheat temperature for medium and high H_2 content fuel mixtures. A sensitivity analysis that includes reported uncertainties in rate constants reveals that the largest contribution to the uncertainty in the predicted flame speed is from the HO_2 destruction reaction ($HO_2+H \leftrightarrow OH+OH$). This reaction, in conjunction with the HO_2 formation reaction ($H+O_2+M \leftrightarrow HO_2+M$), is primarily responsible for the heat release in the very early part (the "low temperature" regime) of flames with significant H_2 fuel content. An increase in preheat temperature significantly alters the temperature range over which these reactions occur. Hence, error in the temperature dependence of the HO_2 destruction reaction seems to be the most likely cause for the observed higher preheat temperature dependence of the flame speeds. To enhance the accuracy of the current models, a more detailed sensitivity analysis based on temperature dependent reaction rate parameters should be considered as the problem seems to be in the intermediate temperature range (~800-1200 K).

CHAPTER 1

INTRODUCTION

1.1 Motivation

There is increasing interest in clean coal technologies for power generation applications as there is increasing risk associated with the supply and cost of petroleum and natural gas, and because conventional coal combustion systems are environmentally damaging. One promising approach towards clean coal burning is to gasify the coal, removing some of the pollutants, and subsequently burning the gas in fuel lean condition to achieve low pollution emissions with high conversion efficiency, e.g., integrated gasification combined cycle (IGCC) plants. These coal derived gasification products, called synthetic gas (syngas) fuels, are typically composed primarily of H_2 and CO, with various levels of diluents such as N_2, CO_2, and H_2O [1,2]. They can also contain small amounts of CH_4 and other higher order hydrocarbons. The specific composition depends upon the fuel source and processing technique. In a typical syngas, the H_2 content in the fuel mixture varies from 10 to 60% (by volume) and the amount of CO varies from 1 to 55%. Similarly syngas mixtures have varied amount of diluents (sum of N_2, CO_2, and H_2O) from as small as 5% to as high as 70%. This substantial variability in composition, and hence in heating value, provides one of the largest barriers towards their usage in power generation application. For example, a gas turbine combustor designed to produce low emissions with a particular syngas composition may not achieve the same emission goals on a different syngas composition. Moreover, the fuel composition is strongly

coupled with the static and dynamic stabilities of the combustor which raises unwanted operability issues such as flash back, blow-off and combustion induced instabilities [3,4].

Extensive research is ongoing to understand the impact of this variability on emission and stability characteristics of the combustor. Various combustor design tools/methodologies are in the development to aid the design of an efficient "fuel flexible" combustor operating with wide range of syngas fuel mixtures in lean premixed conditions. These design tools primarily requires an understanding of the fundamental combustion properties of these mixtures such as ignition characteristics, laminar flame speed, strain sensitivity and extinction strain rates. For example, understanding the ignition characteristics would help to optimize the mixing time in the pre-mixer for better emission characteristics and simultaneously avoid potential auto ignition which could be detrimental to the hardware. This is particularly important as the chemical/induction time could vary by an order of magnitude considering the variation in the amount of H_2 content in the syngas fuel mixtures.

Similarly, laminar flame speed is another important parameter as it contains fundamental information regarding reactivity, diffusivity, and exothermicity of the fuel mixture. Often many reduced order models to predict the static stability of the combustor heavily rely on laminar flame speed information as it has a significant impact upon the propensity of a flame to flashback and blowoff. Also it serves as a key scaling parameter for other important combustion characteristics, such as the turbulent flame structure, turbulent flame speed and flame's spatial distribution etc.

Moreover with the ever improving computational power and capability of combustion modeling, one needs a good kinetic model for the detailed simulation of these

flames in a real combustor operating at elevated pressure and preheat conditions. Since the current leading kinetic models for syngas combustion have not been tested/optimized at realistic engine operating conditions, the predictive capabilities of the models is questionable. Traditionally the laminar flame speed serves as a good validation parameter for these kinetic models. Hence laminar flame speed information is highly desirable for syngas fuel mixtures at realistic engine operating conditions. It is also important to understand the strain sensitivity, which is defined as sensitivity of flame speed to aerodynamic strain, of syngas fuel mixtures as it has rich information about non-equi-diffusive nature of fuel mixtures, which is essential for turbulent flame simulations. Hence the prime objective of this study is to characterize the laminar flame speed and strain sensitivity of practical syngas fuel mixtures at realistic engine condition.

1.2 Literature Review

Several prior studies have focused on measurements of flame speeds for syngas-type mixtures. Laminar burning velocities of syngas mixtures have been measured with conical flames stabilized with Mach Hebra nozzle burners [5] and with Bunsen burners [6]. Laminar flame speeds of CO/H_2 mixtures have also been measured with spherically expanding flames [7] and flat flames [8]. There are two shortcomings of these earlier flame speed studies. Firstly, all of these measurements neglected the effect of stretch on the measured flame speed. Since the CO/H_2 fuel mixtures are expected to be strongly stretch sensitive, there is substantial scatter in the reported data that can not be explained solely by measurement uncertainties [9]. Secondly, most of these flame speed measurements are for stoichiometric and fuel-rich mixtures, while many modern low

emissions combustion approaches, especially in gas-turbines, emphasize lean premixed combustion.

Recently stretch corrected measurements of laminar flame speed and strain sensitivity of H_2/CO fuel mixtures have been obtained in counter-flow flames [10] and spherically expanding flames [11-15], and they are in fair agreement with each other. Vagelopoulos *et al.* [10] measured the laminar flame speed and extinction strain rates of H_2/CO mixtures at atmospheric pressure and room temperature for near stoichiometic mixtures. Mclean *et al.* [11,12] reported laminar flame speeds for H_2/CO mixtures measured with spherically expanding flames for a range of H_2/CO ratio and equivalence ratios. All these stretch corrected measurements are mostly for atmospheric pressure; exceptions are the work of Hassen *et al.* [13] and Sun *et al.* [15].

Hassen *et al.* [13] measured the laminar flame speed and Markstein length with spherically expanding flames at 4 atm for H_2/CO fuel mixtures with only 5% H_2. They reported that the onset of severe instabilities restricts the flame speed measurements for high H_2 content mixtures even at a few atmospheres. More recently, Sun *et al.* [15] measured H_2/CO laminar flame speeds with an O_2/He oxidizer at up to 10 atm for fuels containing up to 50% H_2, and extended the measurements up to 40 atm for mixtures with only 5% H_2. While flame speed information is available up to 40 atm, it is limited to very low levels of H_2 in the fuel mixture and also to stochiometric and fuel rich conditions, especially for pressures above 10 atm. More importantly, all the available data (both at atmospheric and elevated pressure) for H_2/CO fuel mixtures are restricted to room temperature measurements. To illustrate more clearly, Figure 1.1 shows the disparity between the available and desirable flame speed information.

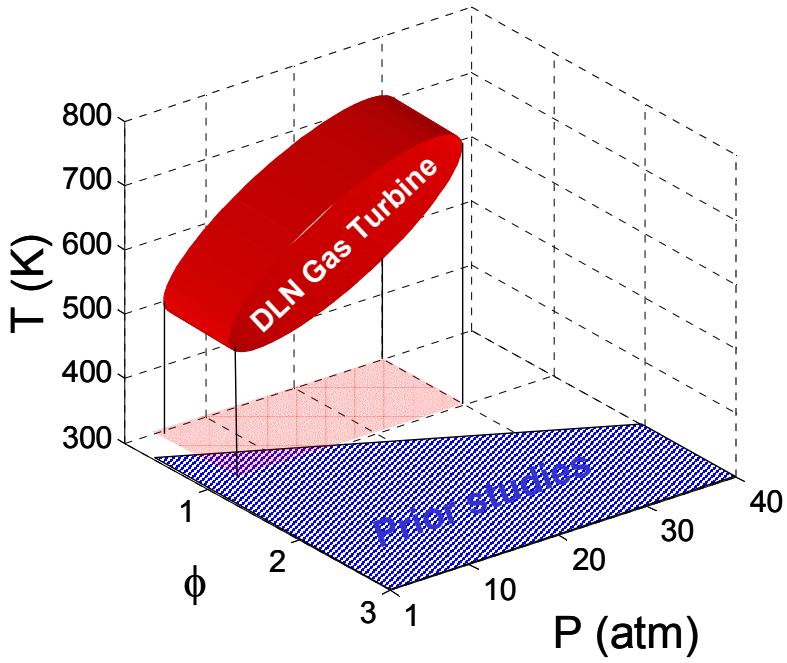

Figure 1.1. Illustration of all the syngas (H_2/CO) flame speed data available prior to this study and the region of interest (pressure, equivalence ratio and preheat temperature space) for modern gas turbines.

Since most syngas mixtures have significant diluent concentrations, it is also important to study effect of these diluents on flame speed. Presence of diluents in the reactant fuel mixtures could alter the flame propagation through flame temperature, chemical kinetics and some non-chemical effects. Particularly, large amounts of CO_2 dilution have been shown to have significance influence on flame propagation and flammability limits of CH_4 flames through non-gray radiation especially at elevated pressure [16,17]. Recently, Qiao *et al.* [18] studied the suppression effects of CO_2 and N_2 for hydrogen flames at atmospheric pressure and temperature. But there is no data available on H_2/CO mixtures diluted with either CO_2 or N_2 even at atmospheric pressure and room temperature conditions.

Clearly, there is a need to extend the range of available flame speed and strain sensitivity data for syngas mixtures, particularly at realistic engine pressures and reactant temperatures. Obtaining such measurements is the primary objective of this thesis work. In addition, the leading kinetic mechanisms relevant to syngas combustion such as (i) the optimized H_2/CO mechanism of Davis *et al*. [19], (ii) the comprehensive C_1 mechanism of Li *et al*. [20], and (iii) GRI-Mech 3.0 [21] have not been validated for flame speeds at elevated pressure and preheat conditions. Hence comparing these model predictions with the obtained measurements would help us to identify regions where the current models may need improvement. These considerations motivate the thesis objectives. An overview of the present work is given in the following section.

1.3 Overview of Present Work

The primary objective of this thesis work is to measure the laminar flame speeds and strain sensitivities of practical syngas fuel mixtures at realistic gas turbine conditions. To accomplish this goal two flame speed measurement techniques have been developed to facilitate flame speed measurement for lean syngas fuel mixtures at elevated pressure and preheat temperature. The limitations and various sources of uncertainties associated with each measurement technique are analyzed, and the results are validated with available literature data for the basic syngas fuel mixtures at limited operating conditions. Using these two measurement techniques, extensive flame speed and strain sensitivity information are obtained for various lean syngas mixtures. In particular the parameters and their range of variation considered are given by, 1) percentage of H_2 in H_2/CO fuel mixture: 5 to 95%, 2) preheat temperature: 300 to 700 K, 3) pressure: 1 to 15 atm, and 4) CO_2 and N_2 dilution: 0 to 70%.

The second objective of this thesis is to identify potential regions for improvement of the current kinetic models for syngas combustion by utilizing the above measurements. To this end, detailed numerical simulations of strained and unstrained laminar flames are performed with leading detailed kinetic models. The predicted flame speeds and strain sensitivities are compared with measurements, and the regions where the current models show significant deviations from the experimental data are identified. Further, sensitivity analysis is used to identify the most sensitive reactions under conditions where the largest discrepancies were observed. Based on this analysis and the reported uncertainties for the rate coefficients of all the most sensitive reactions, the possible reactions that are responsible for the discrepancy between the measurements and predictions are identified.

The general outline of the thesis is as follows. Chapter 2 provides the necessary background about syngas flame properties and dependence of laminar flame speed on various parameters such as pressure and preheat temperature. Also various flame speed measurement approaches reported in the literature are discussed briefly in this chapter. Chapter 3 describes the experimental facilities used in this study followed by details of the modeling approaches used to simulate laminar flames. Both measurements and modeling results of this study are presented in the following two chapters. First, the influence of preheat temperature for a range of H_2/CO ratios at atmospheric and elevated pressure conditions is discussed in Chapter 4. The influence of diluents (CO_2 and N_2) is covered in Chapter 5. Finally, Chapter 6 concludes the thesis with a summary and recommendations for further studies.

CHAPTER 2

BACKGROUND

This chapter provides a brief overview of laminar flame properties and flame speed measurements. In particular, the laminar flame properties of syngas mixtures are discussed in the first section, with an emphasis on laminar flame speed and its dependence on parameters such as pressure and preheat temperature. In the next section, the advantages and limitations of flame speed measurement approaches established in the literature are discussed, leading to the identification of suitable approaches to match with the objectives of this thesis.

2.1 Laminar Flame Properties of H_2/CO Mixtures

2.1.1 Adiabatic flame temperature

The first parameter of interest is adiabatic flame temperature (T_{ad}). It is defined as the equilibrium temperature of the products when the reactants are burned at constant pressure without any heat transfer to the surroundings. In flames, the reactants are converted to products essentially at constant pressure, thus the maximum temperature of the flame is typically close to the adiabatic flame temperature (in the absence of of non-unity Lewis number, differential diffusion and strain effects [22]). Flame temperature is an important parameter for a number of reasons; for example NO_x production is highly sensitive to temperature through the thermal (Zeldovich) mechanism, which tends to dominate NOx production beyond 1800 K. More to the point for the current study, the flame temperature can also have a significant influence on flame speed. Figure 2.1 compares the adiabatic flame temperatures for different pure fuel gases (CH_4, H_2 and CO)

with a typical syngas fuel mixture. The chosen syngas fuel composition is 35% H_2, 35% CO and 30% CO_2, as many syngas fuel sources produce mixtures with comparable amounts of H_2 and CO, and with significant levels of added diluents (CO_2, H_2O and N_2).

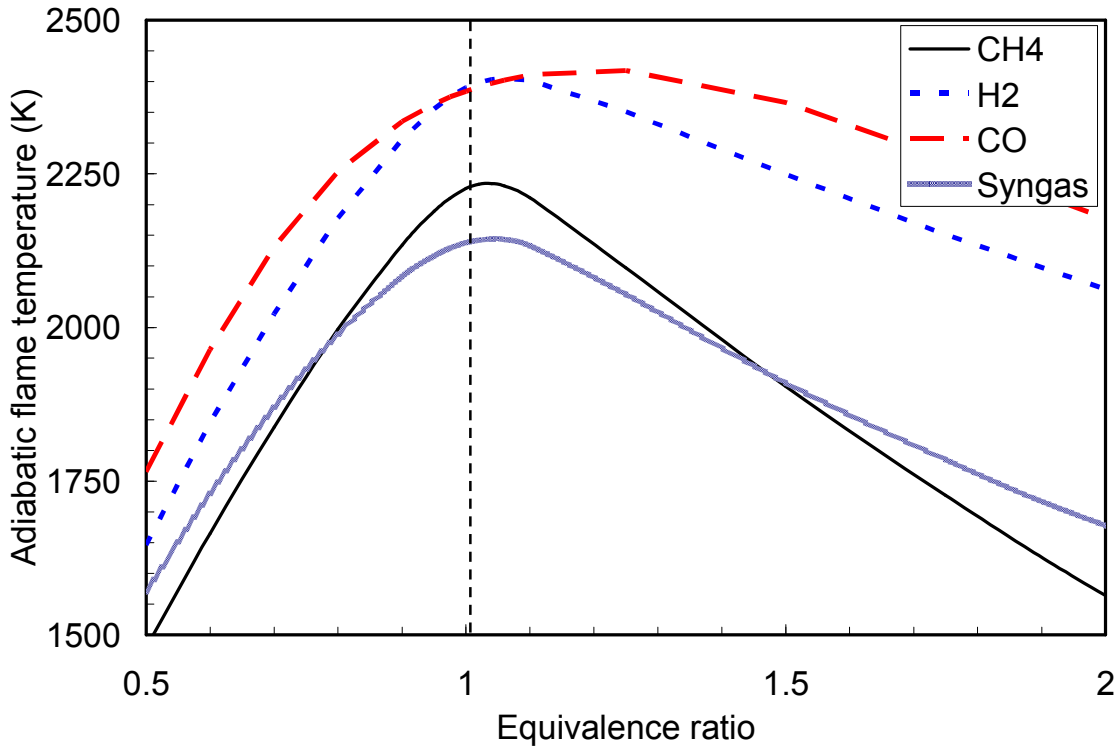

Figure 2.1. Adiabatic flame temperatures for CH_4, H_2, CO and typical syngas (35% H_2, 35% CO and 30% CO_2) fuels with air.

For all the fuels, the adiabatic flame temperature peaks around stoichiometric conditions (equivalence ratio Φ=1) as there is less excess fuel or oxidizer to absorb the heat release from combustion. Typically, the peak occurs at slightly fuel rich condition [23]. For example, the peak occurs at $\Phi \cong 1.04$ and $\Phi \cong 1.06$ for CH_4 and H_2, respectively.

Of the three pure fuels, CO has the highest flame temperature for a given equivalence ratio, while CH_4 has the lowest. At Φ=0.6, the CO flame temperature is around 300 K higher than for CH_4, and the differences are even greater on the rich side.

Methane-air mixtures have lower flame temperatures than CO and H_2, because CH_4 requires four times more oxidizer (on a molar basis) to achieve a stoichiometric mixture. For an undiluted oxidizer (e.g., pure O_2), the CH_4 flame temperatures are much closer to the other fuels. Though both CO and H_2 require the same amount of oxidizer for a given equivalence ratio, the CO flame temperature is slightly higher than for H_2 owing to the higher heating value of CO (on a molar basis). At Φ=0.6, the CO flame temperature is around 130 K more than hydrogen's. This difference is greatly reduced as the mixture nears stoichiometric conditions, since the higher temperatures there lead to reduced CO_2 levels, and therefore less heat release associated with the additional fuel.

The syngas flame temperature is lower than that for either H_2 or CO due to the significant amount of diluent in the syngas. For the 30% CO_2 dilution considered here, the flame temperature is similar to that for the CH_4 flame (less than ~100 K difference) over the range of practical equivalence ratios. Thus, we see that undiluted syngas mixtures would have higher temperatures than conventional methane (or natural gas) fuel, while syngas compositions with typical levels of dilution will have flame temperatures closer to those encountered in methane combustion.

2.1.2 Flame structure

Laminar flame speed is also influenced by the structure of a flame. The detailed flame structure of a one-dimensional, premixed flame can be obtained from simulations that involve the steady-state mass, species and energy conservation equation, with a comprehensive reaction mechanism for the fuel of interest. One example is Chemkin's freely propagating flame code (PREMIX), which includes a detailed package to evaluate the transport (diffusive) properties for complex gas mixtures. The PREMIX code

essentially solves for the mass burning rate ($\dot{m}'' = \rho_u s_L$), which is the eigenvalue of the problem, and thereby calculate the flame speed from the known unburned density. For all the syngas flame results presented in this chapter, the C_1 mechanism of Li *et al.* [20] is used.

The chemical structure of the syngas flame significantly changes with the amount of H_2 in the fuel mixture, owing to the completely different kinetic and transport properties of H_2 and CO. To elucidate this point, two lean syngas mixtures are chosen for analysis: one with very low H_2 content (5%) and the other with a high fraction of H_2 (95%). The simulations are performed for room temperature and pressure reactants.

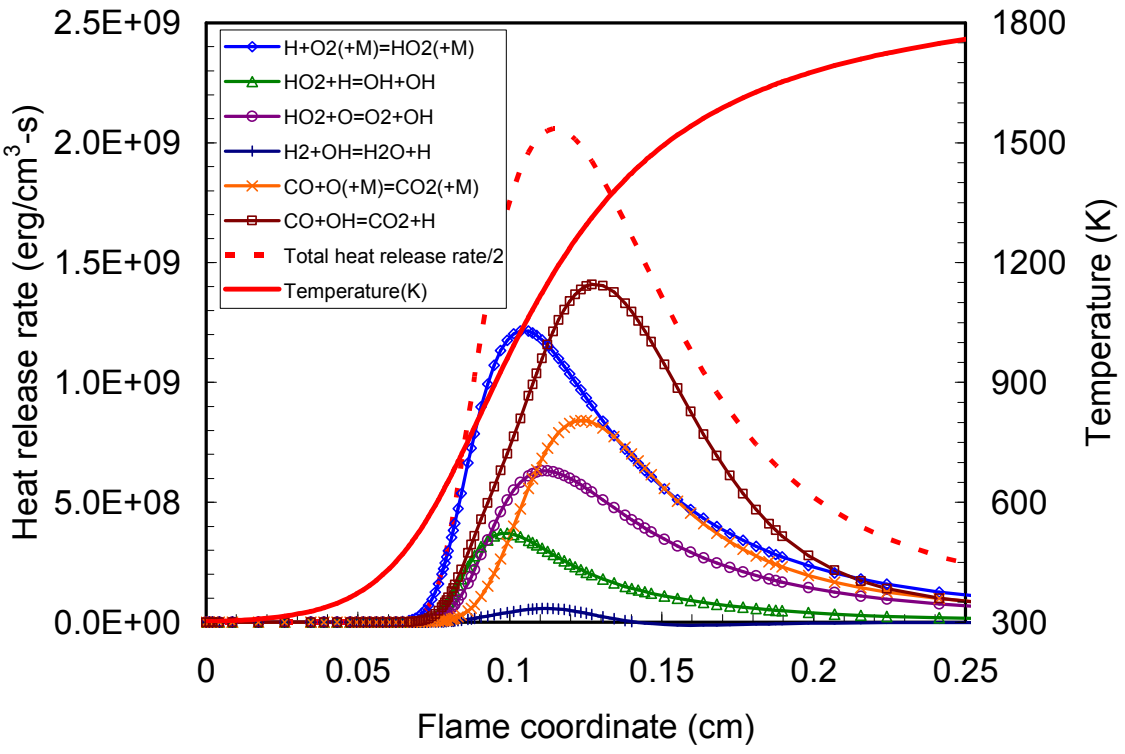

Figure 2.2. Chemical structure of a lean (Φ=0.6) H_2/CO fuel mixture with 5% of H_2 at normal temperature and pressure conditions.

Figure 2.2 shows the profiles of temperature and the heat release rate associated with key exothermic reactions along the flame coordinate for the low H_2 case. The main heat release reaction is $CO+OH=CO_2+H$. It is well known that in the absence of any hydrogen in the reactants (which can lead to OH production) that CO oxidation is rather slow. The heat release rate profile of this CO+OH reaction is very broad; it starts at a temperature of around 800 K, peaks around 1300 K, and continues until the final flame temperature is reached. Importantly, this reaction is also the main source for the significant amount of H atoms produced in the flame zone [11].

The H atoms produced in the flame zone diffuse back into the incoming reactant mixture, and react with O_2 to form HO_2 through the three-body radical termination reaction $H+O_2(+M)=HO_2(+M)$. As shown in Figure 2.2, this reaction is also one of the main heat release reactions in the leading edge of the flame. The HO_2, which is a relatively stable species at low temperatures, reacts with H and O atoms to produce a pool of OH radicals as the reactants move into the flame zone. These OH radicals attack CO and convert it to CO_2, thus completing the cycle. The other significant route for CO oxidation is through the reaction $CO+O(+M)=CO_2(+M)$. The importance of this reaction is drastically reduced as the amount of H_2 in the fuel mixture increases beyond 20%. The main H_2 oxidation reaction ($H_2+OH=H_2O+H$) contributes little directly to the overall heat release, yet it is still an important reaction as it competes for OH radicals with the main CO oxidation reaction in low H_2 content syngas flames.

Figure 2.3 presents the profiles of temperature and heat release rate for key exothermic reactions under lean conditions for a high H_2 content (95%) syngas fuel mixture. Since the equivalence ratio is the same as that used for the low H_2 simulation,

the flame temperature is only slightly lower. Not surprisingly with only 5% CO, the overall flame structure is very similar to that for pure H_2 [22]. The first notable difference between the low and high H_2 cases is that the overall thermal zone thickness (or the flame thickness) is significantly smaller for the high H_2 case. As the amount of H_2 increases, the flame thickness is expected to increase due to the increase in thermal diffusivity of the mixture. But as shown in Figure 2.2 and Figure 2.3, the increase in overall heat release rate with H_2 level (by factor of 8 between the two cases here) dominates, causing the overall decreases in flame thickness.

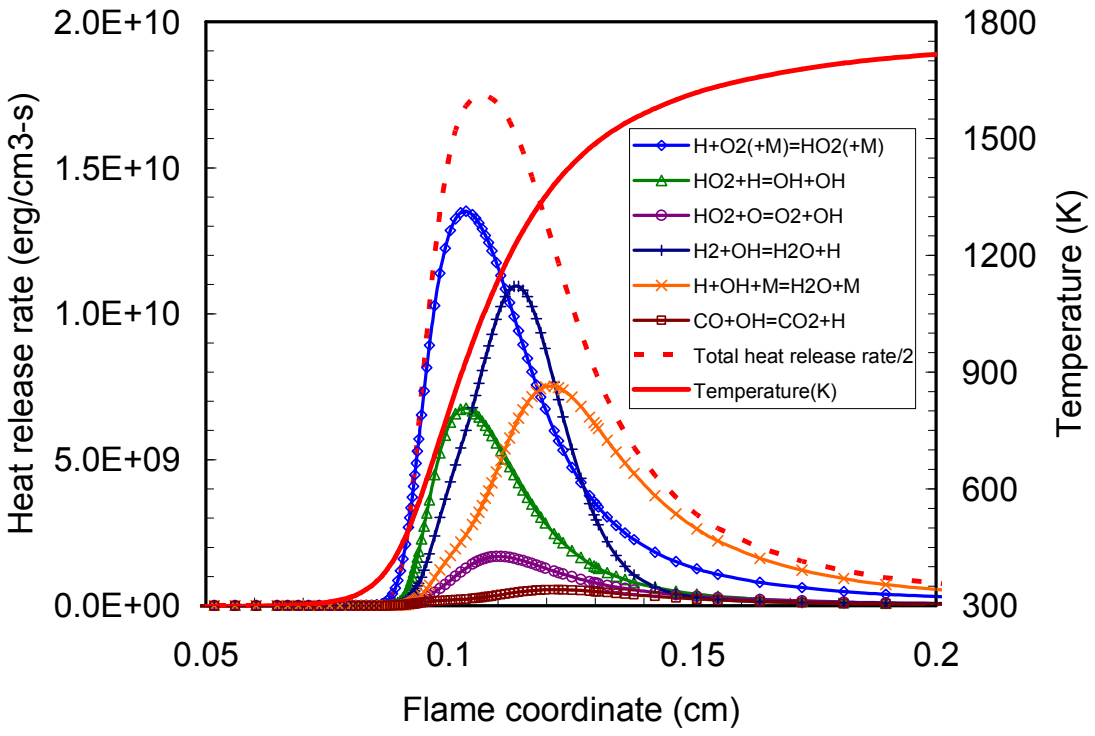

Figure 2.3. Chemical structure of a lean (Φ=0.6) H_2/CO fuel mixture with 95% of H_2 at normal temperature and pressure conditions.

Another important difference can be observed by comparing the temperature profiles with the overall heat release rate profiles. For the high H_2 case, the overall heat

release starts when the temperature is still very close to the initial reactant temperature. Looking at the contribution from individual exothermic reactions, this early rise in heat release is mainly due to the contribution of the H atom termination reaction $H+O_2(+M)=HO_2(+M)$. Also, this reaction is the dominant heat release reaction throughout most of the reaction zone, with a peak in its heat release rate when the temperature has risen to 900 K (it is surpassed by the H_2O formation reaction H+OH+M only after most of the heat release has occurred). Due to this significant amount of heat release in the early part of the flame, there is no preheat zone as such. This is in contrast to conventional CH_4-air flames, where the majority of the heat release occurs in the later regions of the flame, only after the temperature has risen significantly.

To understand the balance between different reactions, let us consider the production and destruction of H atoms. There is a significant amount of H atom production in the later stage of the flame, through the main H_2 oxidation reaction $H_2+OH=H_2O+H$. This reaction dominates H atom production, as opposed to the low H_2 case where $CO+OH=CO_2+H$ was the primary source of H. Similar to the low H_2 case, the produced H atoms diffuse back to the incoming (cold) reactants. There they react with O_2 to form HO_2, causing a sharp rise in HO_2 concentration in the early part of the flame. Recall that this reaction is highly exothermic and consumes H atoms. The HO_2 reacts further, with H atoms, and produces two OH radicals (i.e., $HO_2+H=OH+OH$), again consuming more H atoms in the early part of the flame. Then the produced pool of OH radicals attacks H_2 to form more H atoms ($H_2+OH=H_2O+H$) in the later portion of the flame. Hence the entire flame zone (which can be characterized as a reaction zone) can be split into H atom consumption (through $H+O_2(+M)=HO_2+M$ and $HO_2+H=OH+OH$) and

H production (via H_2+OH=H_2O+H) layers. The other important heat release reaction is H+OH(+M)=H_2O(+M), which mainly occurs in the later stage of reaction zone and which is rather slow.

2.1.3 Laminar flame speed

The laminar flame speed is traditionally defined as the velocity that a planar flame front travels relative to the unburned gas in a direction normal to the flame surface. From a simplified analysis of a flame based on a balance between heat release and diffusion [24], the flame speed can be modeled as,

$$S_L \approx \sqrt{\frac{\alpha \cdot RR}{\rho}}$$

where α is the thermal diffusivity, RR is the overall reaction rate, ρ is the unburned gas density. In this section, the influence of 1) H_2/CO ratio, 2) pressure, 3) preheat temperature and 4) dilution on the laminar flame speed of a typical syngas fuel mixture is briefly described.

2.1.3.1 H_2/CO ratio

Figure 2.4 illustrates the influence of H_2 level in the fuel mixture on the laminar flame speed. While the equivalence ratio, pressure and preheat temperature are held constant, the flame temperature also changes as discussed earlier, due to the small difference in heating value between H_2 and CO.

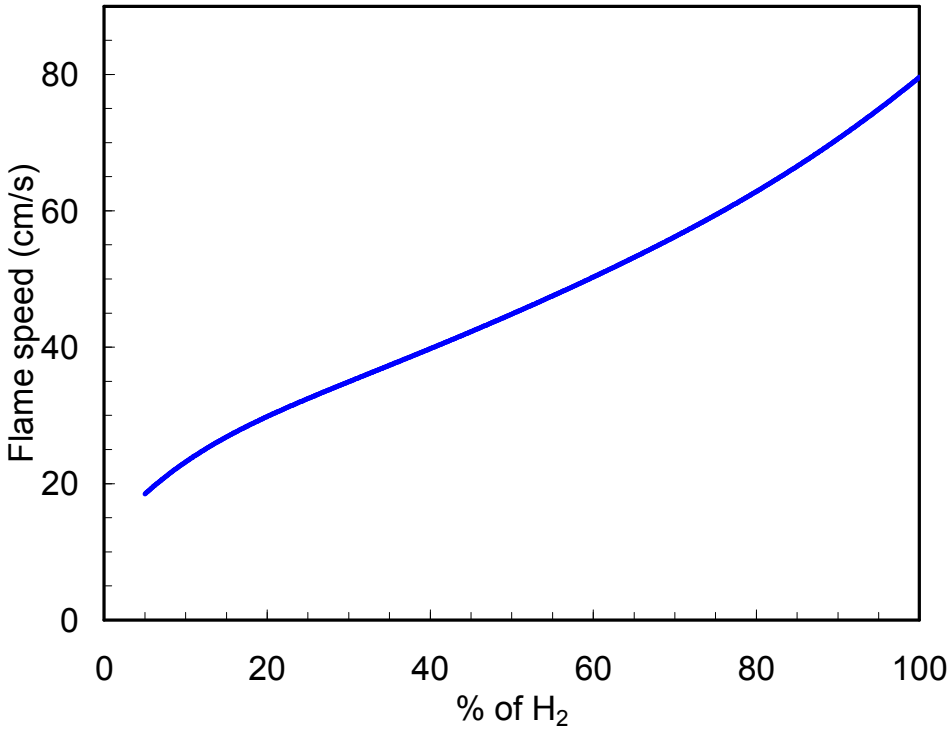

Figure 2.4. Laminar flame speeds for a range of H_2/CO fuel mixtures at a fixed equivalence ratio of 0.6, p=1 atm and T_u=300 K.

As shown in Figure 2.4, the flame speed increases as the relative amount of H_2 in the fuel goes up. This behavior is explained by the simple flame speed model presented above: (1) the overall reactivity of the fuel mixture increases with the amount of H_2, as illustrated in the flame structure section; and (2) the low molecular weight of hydrogen acts to increase the diffusivity of the reactant mixture.

Interestingly, the trend is slightly nonlinear especially for low H_2 amounts. The flame speed increases rapidly as the amount of H_2 increases from 5 to 20%. This is mainly due to the well known sensitivity of the CO oxidation rate to the presence of small amounts of hydrogen containing species. As discussed earlier, the main CO oxidation reaction shifts from slower CO+O(+M)=CO_2(+M) reaction to relatively faster

$CO+OH=CO_2+H$ reaction as the amount of H_2 increases, causing the rapid increase in flame speed. For 20-60% H_2, this sensitivity is reduced, and the flame speed increase with H_2 content is fairly linear. For further increases in the amount of H_2 beyond ~60%, there is slightly higher sensitivity of the flame speed to H_2 content.

2.1.3.2 Pressure

The influence of pressure on laminar flame speed is presented for a 50:50 H_2/CO fuel mixture at Φ=0.6 (Figure 2.5) and Φ=1.0 (Figure 2.6). The laminar flame speed decreases nearly logarithmically with pressure increase (as indicated by the curve fit in the figure). Typically, the increase in pressure is expected to increase the overall reaction rate (*RR*), and hence increase the laminar flame speed according to the standard model. On the other hand, the increased density of the reactant mixture with increase in pressure necessitates more thermal energy transfer from the reaction zone to raise the reactant temperature in the preheat zone. Since diffusivity is also inversely proportional to pressure, overall the increase in pressure reduces the flame speed. It should be noted here that the flame temperature is relatively insensitive to pressure (except at very low pressures, well below those of relevance to gas turbine combustion).

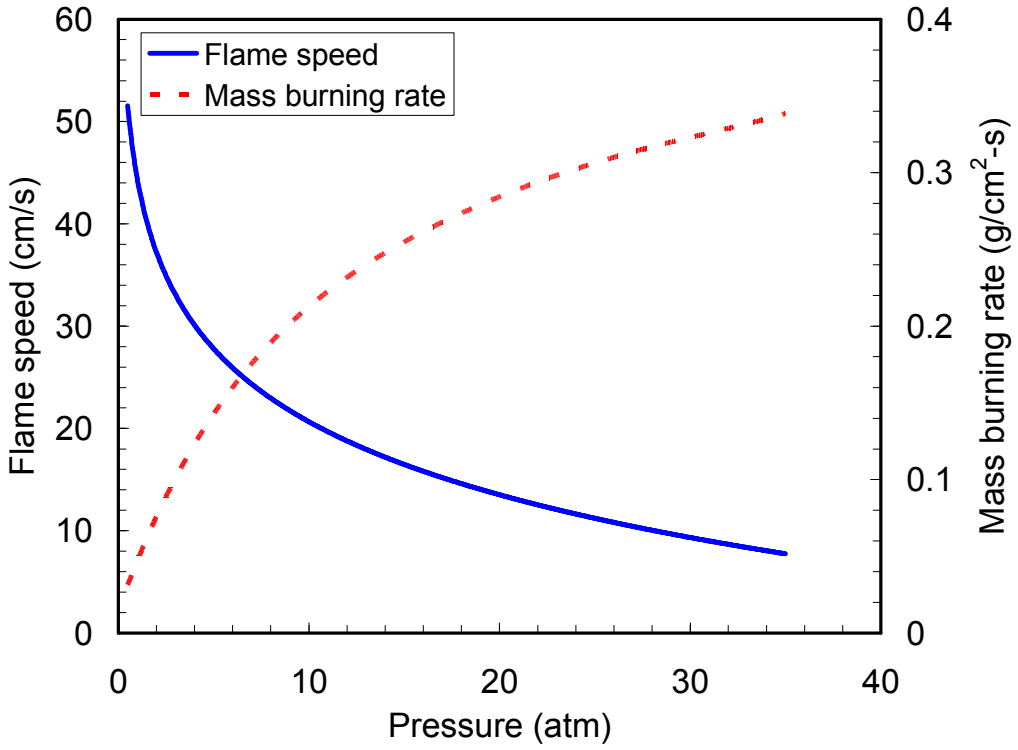

Figure 2.5. Laminar flame speed and mass burning rate as a function of pressure for 50:50 H_2/CO fuel mixture at Φ=0.6 and 300 K.

Also shown in Figure 2.5 and Figure 2.6 are the variation of mass burning rate (or mass flux=$\rho_u S_L$) with pressure. As opposed to the flame speed, the mass burning rate increases with pressure. The increase in density with pressure more than offsets the decrease in flame speed, leading to an increase in the mass burning rate. Interestingly the observed increase in mass burning rate is drastic at lower pressures (1-10 atm), and less pronounced at higher pressures (above 15 atm). Comparing Figure 2.5 and Figure 2.6, this nonlinear behavior is more pronounced for lean mixtures.

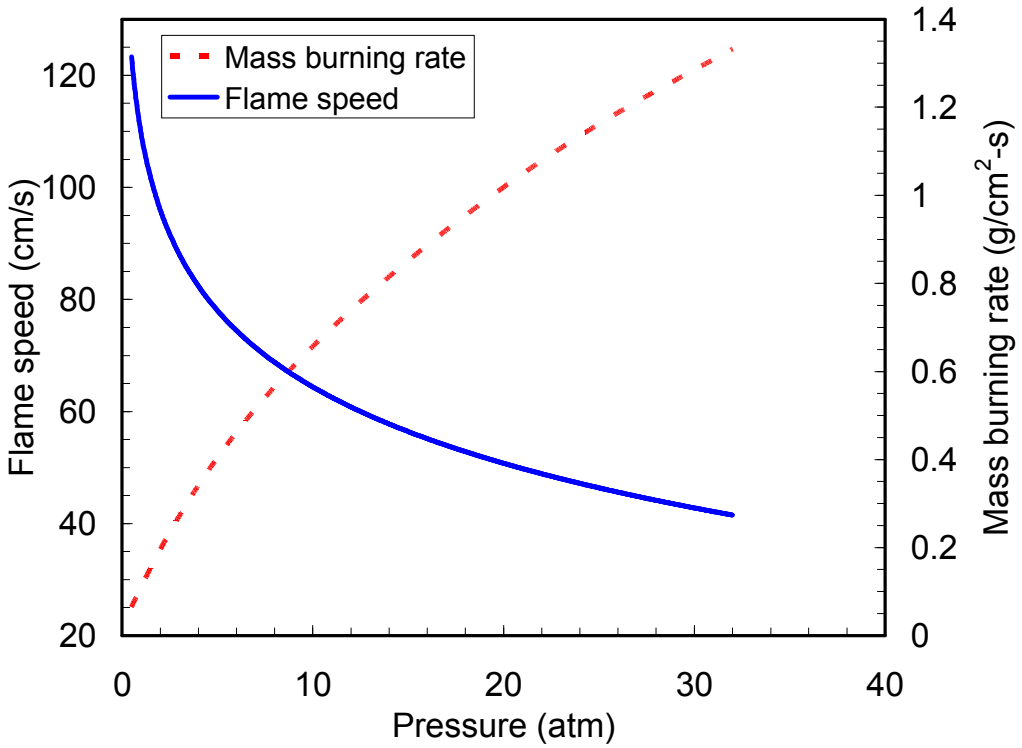

Figure 2.6. Laminar flame speed and mass burning rate as a function of pressure for 50:50 H_2/CO fuel mixture at Φ=1.0 and 300 K.

The other key aspect of pressure on flame propagation is that it emphasizes the relative importance chain branching and chain terminating reactions. For example, one of the main chain branching reaction in the H_2/O_2 system is $H+O_2=OH+O$, which is a temperature sensitive two-body reaction. Similarly, the chain termination three-body reaction $H+O_2+M=HO_2+M$ is temperature insensitive (with zero activation energy) [22]. Hence, a rise in pressure will tend to increase the relative rate of the H chain termination reaction compared to the chain branching step. This leads to a reduction of overall reaction rate, and hence hinders flame propagation. This effect can be quantified through calculating the reaction order (n) from simplified relations such as [25],

$$\dot{m}'' \approx \rho S_L \approx p^{\left(\frac{n}{2}\right)} \left(\frac{\lambda}{C_p}\right)^{\frac{1}{2}} \exp\left(-\frac{E_a}{2RT_{ad}}\right)$$

where $\dot{m}''$ is the mass burning rate, p is the pressure, n is the overall reaction order, λ is the thermal conductivity, C_p is the mixture specific heat, E_a is the overall activation energy and T_{ad} is the flame temperature. Neglecting any small change in λ, C_p and T_{ad} with pressure (due to compositional variations), the reaction order can be calculated to be,

$$n = 2\left(\frac{\partial \ln \dot{m}''}{\partial \ln p}\right)_{T_{ad}}.$$

The variation of calculated reaction order with pressure for the above two cases is shown in Figure 2.7. The calculated reaction order decreases monotonically with pressure from 1 to 30 atm. At any given pressure, the reaction order for the lean case is less than that for the stoichiometric case. This illuminates the influence of the H chain termination reaction. The reduction in H atoms affects flame propagation more for lean mixtures, hence the drastic reduction in mass burning rates for lean fuel mixtures. The calculated *n* value is always positive, which indicates that the mass burning rate will always increase with pressure for the typical medium H_2 content syngas mixture shown here. Negative values for *n* have been observed for lean, pure H_2 mixtures at ~20 atm, indicating a reduction in mass burning rate with pressure [22]. Hence it is possible that *n* can become negative for high H_2 mixtures. Moreover for both equivalence ratios, *n* tend towards two as the pressure decreases to subatmospheric levels. This again indicates the importance of the two body branching reaction over the three body terminating reaction at lower pressures.

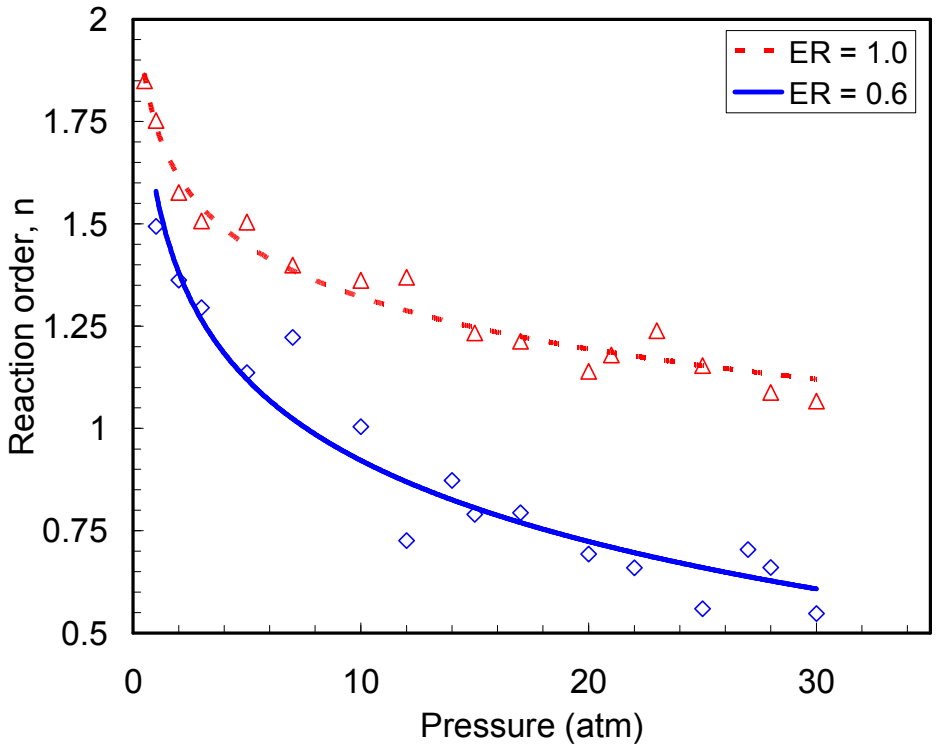

Figure 2.7. Variation of reaction order with pressure for 50:50 H_2/CO fuel mixture at two equivalence ratios. Symbols: numerical predictions, and lines: logarithmic fits.

2.1.3.3 Preheat temperature

The preheat temperature influences the laminar flame speed mainly through the changes in reaction rate and diffusive properties. At constant pressure, the functional dependence of laminar flame speed can be modeled by,

$$S_L \propto \left(\frac{\lambda}{C_p}\right)^{\frac{1}{2}} \exp\left(-\frac{Ea}{2RT_{ad}}\right)$$

An increase in preheat temperature also increases the adiabatic flame temperature. Since $\left(\frac{\lambda}{C_p}\right)$ only weakly increases with temperature, the main influence is through the

exponential dependence on adiabatic flame temperature. As shown in Figure 2.8, the laminar flame speed increases exponentially with preheat temperature for all three equivalence ratios for this 50% H_2 syngas mixture. As the preheat temperature increases from 300 to 700 K, the flame speed increase by 5 to 8 times. The rate of increase is more for lean mixtures than for stoichiometric mixtures.

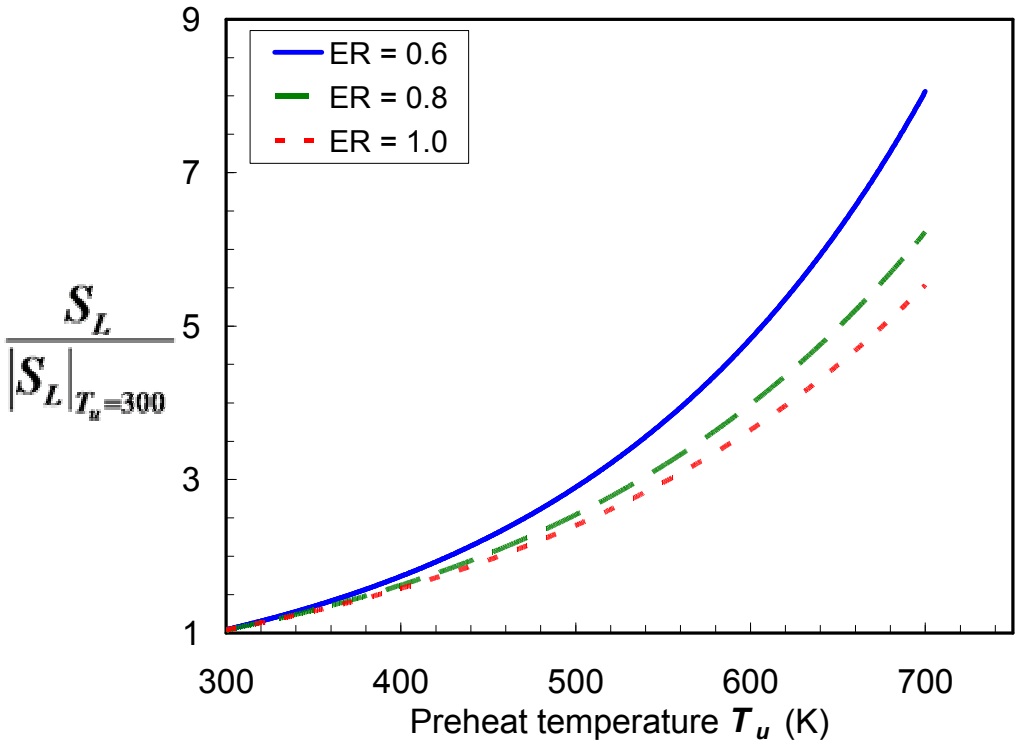

Figure 2.8. Normalized flame speeds as a function of preheat temperature for 50:50 H_2/CO fuel mixtures at three fixed equivalence ratios and T_u=300 K.

2.1.3.4 Diluents

As previously noted, syngas fuels have a large variability, not only in the combustible fuel content, but also in diluents such as CO_2, N_2 and H_2O. The presence of diluents in the fuel will impact the flame propagation in at least three ways, through changes in: 1) mixture specific heat and adiabatic flame temperature, 2) chemical kinetic

rates, and 3) radiative heat transfer. First, addition of diluents reduces the flame temperature and thus reduces the laminar flame speed through reduction in overall reaction rate. It also significantly reduces the flammability limits and extinction strain rate. This point has been emphasized in several studies on the effects of CO_2 dilution on CH_4 and H_2 flames [16,17,18,26].

Second, some of the diluents are not inert. For example, the chemical kinetic effects of CO_2 dilution can be manifested primarily through the main CO oxidation reaction $CO+OH=CO_2+H$. Higher CO_2 levels lead to enhanced back reaction rates and, hence, reduced CO oxidation and H atom production rates. This can potentially impede flame propagation. Chemical kinetic studies have emphasized this point by comparing the flame speeds of mixtures with CO_2 dilution, and a fictitious, chemically inert species with the same specific heat as CO_2. The results showed that CO_2 diluted flame speeds were lower [27]. This kinetic effect is expected to have profound influence on flame speeds for lean H_2/CO flames due to the importance of H atom concentration. As seen in the flame structure examples, H atoms control the main branching ($H+O_2=O+OH$) and termination ($H+O_2+M=HO_2+M$) reactions.

Third, addition of diluents can influence flame propagation through radiative heat transfer. For example, CO_2 and H_2O are effective absorbers and emitters of infrared radiation, unlike N_2 and O_2. The presence of significant amounts of CO_2 in the reactants would result in absorption of energy radiated from the hot products (e.g., CO_2 and H_2O). This enhancement of thermal energy transfer across the flame could aid in flame propagation and hence increase the laminar flame speed and extend the lean flammability

[28]. Conversely, the presence of an effective radiative emitter within the initial part of the reaction zone could lead to heat losses and reduced flame speeds.

2.2 Flame Speed Measurement Approaches

This section describes various flame speed measurement techniques as employed in the literature and their advantages and limitations. As defined earlier, the laminar flame speed is the velocity a planar flame front travels relative to the unburned gas in a direction normal to the flame surface. Though the definition is straightforward, in practice it is difficult to measure as the flame speed is strongly influenced either by flow non-uniformity (strain) or by flame motion or by both (stretch). The stretch (K) on the flame surface is defined as the Lagrangian time derivative of the logarithm of an infinitesimal flame area (A) and it can be expressed as,

$$K = \frac{1}{A}\frac{dA}{dt} = \nabla_t \cdot v_{s,t} + (V_f \cdot n)(\nabla \cdot n).$$

where $v_{s,t}$ is tangential velocity along the flame surface and V_f is the flame front velocity in laboratory coordinates [31]. The first term on the right hand side is the hydrodynamic strain due to the nonuniformity of the flow along the flame surface, and the second term is the stretch due to the motion of the curved flame. Since it is nearly impossible to get a planar, adiabatic flame in a uniform velocity field, it is extremely challenging to make a direct measurement of the one-dimensional, unstretched, laminar flame speed. Hence some assumptions have to be made in its measurement either by neglecting the effect of stretch or by systematically subtracting its influence on the measured flame speed. There are three leading approaches in the literature for laminar

flame speed measurements: (1) the Bunsen flame approach, (2) the spherically expanding flame approach, and (3) the stagnation flame approach.

2.2.1 Bunsen flame approach

This approach typically uses a 2-d or axisymmetric conical premixed flame, stabilized on the lip of a slot burner or a straight cylindrical tube, respectively. This conical flame is affected by hydrodynamic strain (tangential velocity gradient along the flame surface) and pure curvature (at the flame tip and azimuthal curvature for 3D conical flame), and their combined influence on local flame speed depends on the Markstein length of the reactant mixture [31]. The main disadvantage of this approach is that it neglects the influence of the stretch on the measured flame speed.* There are two popular methods to deduce the flame speed from these conical flames: (1) flame area method, and (2) flame angle method.

2.2.1.1 Flame area method

The average flame speed (S) calculated in this method is an area weighted flame speed over the entire flame surface. Considering the overall mass balance, the average flame speed is calculated by dividing the volume flow rate of the mixture with the surface area of the flame.

$$\dot{m} = \rho S A \text{ or } S = \frac{\dot{Q}}{A}$$

*While the rim stabilized conical flame is not truly adiabatic, because of heat losses to the burner rim (as well as some radiation losses), the effect should be small as the heat loss is confined primarily to the base of the flame. Also, the effect of rim heat loss should be independent of burner size as the flame volume from which heat is lost is proportional to the rim area.

where $\dot{m}$ and $\dot{Q}$ are the measured mass and volume flow rates of reactants through the burner, and ρ and A are the unburned density and conical flame surface area at appropriately chosen location.

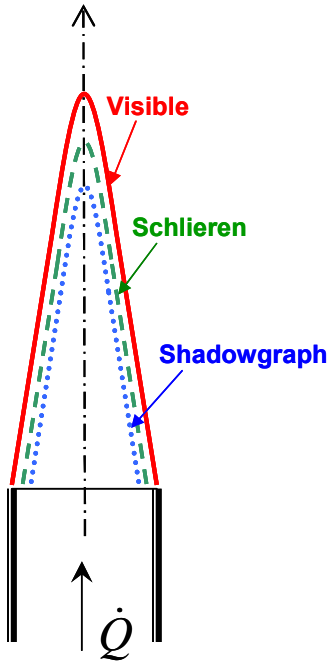

Figure 2.9. Bunsen flame with three standard optical accessible flame edges.

The choice of location is a concern as it gives a wide range of flame surface area and hence measured flame speed. Traditionally, there are three flame edges used for flame area calculation: (1) schlieren (first derivative of density), (2) inner edge of shadowgraph (second derivative of density), and (3) visible (chemiluminescence) edge. From the definition of the unburned laminar flame speed, the apparent flame area should be the unburned flame area, which is just upstream of the preheat zone of the flame. Hence, the inner edge of shadowgraph images or schlieren edges have been preferred over the visible (chemiluminescence) for flame area calculation as they are closer to the unburned boundary. Specifically, the inner edge of the shadowgraph image of the flame has been assumed to give the best result of all three as it is the closest to the unburned

surface of the flame. It should be noted that the flame cone can act as a lens in the shadowgraph, which raises the uncertainty in the measured flame area [24]. It is important to point out, however, that the use of the unburned flame area does not result in a measurement of the 1-d *unstretched* unburned flame speed, as the unburned surface is strongly affected by curvature and strain.

2.2.1.2 Flame angle method

In this method, the angle suspended by the flame edge to the unburned incoming flow velocity in the shoulder region of the conical flame is measured and the flame speed is calculated by, $S_u = U \sin\alpha$ where U is the unburned gas velocity and α is the half cone angle as shown in Figure 2.10 [24].

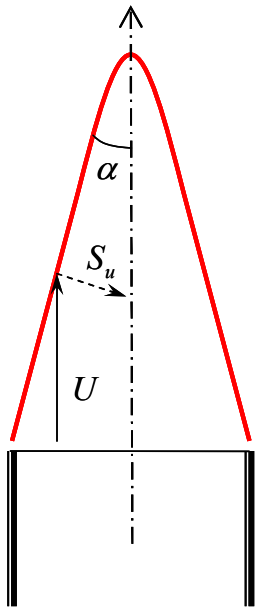

Figure 2.10. Definition of the unburned flame speed based on the half cone angle.

A conical flame stabilized on a contoured nozzle is preferred over straight cylindrical tube burner for the following reason. The exit velocity profile of a long cylindrical tube is parabolic and hence the flame angle (α) to the incoming flow varies

along the flame height. Whereas, a contoured nozzle produces a nearly uniform exit velocity profile, which gives a fairly straight edge along the shoulder of the flame to determine the half cone angle more accurately. The main drawback of this method, apart from the measurements not corrected for stretch, that there is a huge uncertainty even if there is a small divergence in the streamline approaching the flame.

2.2.2 Spherically expanding flame method

A freely expanding spherical flame in a nominally constant pressure vessel is used for stretch corrected flame speed measurement as shown in Figure 2.11 [11,13,15]. This spherical flame is a positively stretched flame as the flame area increases with time. The stretch (K) imposed on the flame is due to the flame motion and can be calculated from $K = (V_f \cdot n)(\nabla \cdot n) = \frac{2}{R_f}\frac{dR_f}{dt}$ where V_f is the flame front velocity $\left(V_f = \frac{dR_f}{dt} \right)$ and R_f is the radius of the flame front at time *t*. The products inside the spherical flame are at rest in the laboratory frame of reference. Since the product are not moving (on average), the velocity of the flame propagation (V_f) is nothing but the burned flame speed (S_b). From continuity and assuming that the flame is quasi-steady, the unburned flame speed (S_u) is calculated from $S_u = S_b(\rho_b / \rho_u)$.

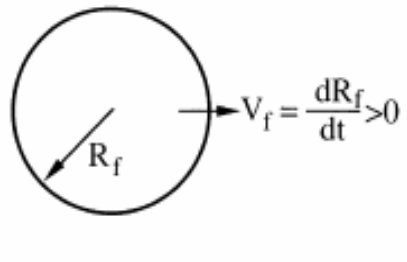

Figure 2.11. Schematic of freely expanding spherical flame.

The unburned flame speeds (S_u) and the corresponding stretch rates (K) imposed on the flame are calculated from the measured flame radius at each time instant. At lower stretch rates, it is typical to find a linear relationship between the flame speed and the imposed stretch rate, i.e., $S_u = S_u^0 - L_M \kappa$, where S_u^0 is the linearly extrapolated measured flame speeds to zero stretch rate and L_M is the Markstein length or stretch sensitivity. Thus this method measures the stretch corrected unburned flame speed and also the stretch sensitivity of the fuel mixtures.

The main drawbacks of this method are: (1) the distortion of the flame shape due to buoyancy, especially for slow burning flames; (2) the heat loss to the electrodes used to ignite the flame, especially during the initial stage of flame development; and (3) the development of intrinsic instabilities over the flame surface at elevated pressure, especially at higher flame radius or, in other words, lower stretch rates. The real advantage of this method is that it is well suited for measurements at elevated pressure as there is no bulk flow and hence associated flow instabilities.

2.2.3 Stagnation flame approach

A steady 1-D strained laminar flame stabilized in a well-defined stagnation flow field is used for measurements in this approach [10]. The stagnation flow field is achieved either by impinging two identical nozzle-generated flows or by impinging a generated flow with a solid wall. The stretch imposed on the flame is due to the non-uniformity (divergence) of the upstream flow or the hydrodynamic strain, which is represented by $K = \nabla_t \cdot v_{s,t}$. The flame speed and the imposed strain rate on the flame are determined from the axial velocity profiles across the flame.

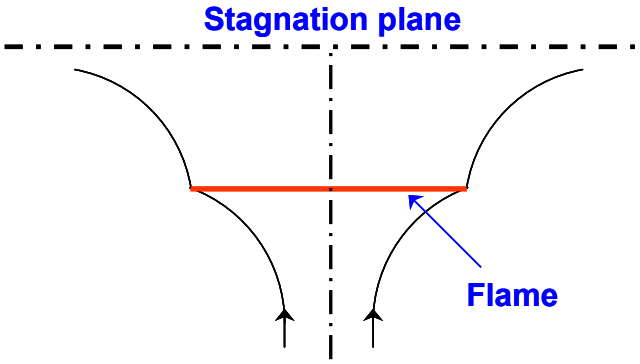

Figure 2.12. Schematic of the stagnation flow field with flame.

Typically the axial velocity decreases from the nozzle exit due to the presence of the stagnation plane, and it reaches a minimum before the flame. As the flow enters the flame, due to preheating and thereby thermal expansion, the axial velocity increases and reaches a maximum just after the peak of the heat release. After the heat release, the axial velocity decreases to zero at the stagnation plane. Commonly, the minimum velocity before the preheat zone is considered as the reference strained unburned flame speed (S_u), and the maximum gradient of the axial velocity ahead of the minimum velocity location is taken as the imposed strain rate (K). The influence of strain on the flame speed S_u is subtracted by evaluating the flame speeds at various strain rates and taking advantage of the (typically) linear relationship between the flame speed and the imposed strain rate, i.e., $S_u = S_u^0 - L_M \kappa$, especially at lower strain rates. The strained flame speed linearly extrapolated to zero strain rate is used to represent the unstrained flame speed (S_u^0), while the slope of the linear fit (L_M) represent the Markstein length or strain sensitivity of the mixture. Like the spherically expanding flame method, this method measures the stretch corrected unburned flame speed and also the strain sensitivity of the fuel mixtures.

Of these three approaches, the stretch corrected spherical bomb or stagnation flame techniques should, in the absence of other issues, be more accurate for lean H_2/CO fuel mixtures, which are expected to be stretch sensitive. The major drawbacks of these stretch corrected approaches, however, are their complexity and practicality for measurements under adverse conditions. Also, they are quite time consuming compared to the simpler Bunsen flame approach. For experiments intended to measure flame speeds over a wide range of conditions, the simplicity of the Bunsen flame approach is highly advantageous.

For stretch corrected measurements of lean mixtures at high preheat temperatures, the stagnation flame approach is preferable to the spherical flame method. It is difficult to produce a stationary combustion bomb with a uniform reactant temperature profile. Heat transfer to or from the vessel walls will tend to produce a nonuniform profile, while using "stirring" methods to solve this problem impart motion to the reactants, voiding an important requirement for the bomb method. On the other hand, the inflowing premixed gases in the stagnation flame can more easily be set to the desired uniform temperature. Also for lean fuel mixtures with significant amounts of H_2, the flame is likely to develop spontaneous wrinkles due to the nonequidiffusive nature of the fuel mixtures (thermo-diffusive instability) [11,13,15]. These wrinkles can be suppressed by applying a sufficiently strong positive stretch in the stagnation flame approach. In the spherically expanding flame, however, the stretch imposed on the flame is not controllable, and hence as the flame expands (in other words, as the imposed stretch decreases), it is affected by both thermo-diffusive and hydrodynamic instabilities.

For these reasons, a modified Bunsen approach (with a chemiluminescence-based determination of flame area) is utilized in this work to determine flame speeds across a wide range of conditions. The stagnation flame approach is used to obtain stretch corrected measurements at limited conditions identified as "significant" by the Bunsen results. A detailed description of the Bunsen and stagnation flame approaches as employed here, and the associated experimental facilities are presented in the next chapter.

CHAPTER 3

MEASUREMENT AND MODELING APPROACHES

The measurement approaches employed in the present work are described in detail in the first section of this chapter, followed by a brief description about the modeling efforts and the leading kinetic models considered for improvement in this study. Finally, various sources of uncertainties associated with the measured flame speeds are discussed.

3.1 Measurement Approaches

The goal of this work is to measure the flame speed for a wide range of syngas fuel mixtures at various conditions. Two measurement approaches are employed to achieve this goal: a quick and simple (1) Bunsen flame approach is utilized to determine flame speeds across the wide range of conditions, while a stretch corrected (2) stagnation flame approach is utilized to determine flame speeds and strain sensitivities at limited conditions identified as "significant" by the Bunsen results. A detailed description of the Bunsen and stagnation flame approaches as employed here, and the associated experimental facilities are presented in the following sections.

3.1.1 Bunsen flame approach

The Bunsen approach uses a conical premixed flame, stabilized on the lip of a contoured nozzle or a straight cylindrical tube. As described in the previous chapter, this flame is affected by strain and curvature and the average flame speed is calculated by dividing the volume flow rate of the mixture with the surface area of the flame. From the

definition of the unburned laminar flame speed, it is natural to think that the appropriate flame area should be the unburned flame area, just upstream of the preheat zone of the flame. Though the unburned flame area can be measured with the schlieren technique, the measured flame speed would still not be the 1-d, *unstretched*, unburned flame speed as the unburned surface is strongly affected by curvature and stretch. However, as detailed below, use of the reaction zone area can provide a more accurate measure of the unstretched (unburned) 1-d flame speed.

Sun *et al*. [29] derived the sensitivity of the unburned and reaction zone (defined as the peak of the heat release) flame speeds (S_u and S_b, respectively) for a curved flame traveling in a non-uniform flow field with a generalized integral analysis that includes thermal expansion in the preheat zone and neglects higher order terms. Generally the flame speed is affected by flame movement ($\dot{R}$), strain (κ) and pure curvature (γ). For a stationary flame, they showed that the burned flame speed at the reaction zone is only affected by strain, while the unburned flame speed is affected by both strain and pure curvature effects. Their analysis produces the following expressions for the unburned (S_u) and reaction zone (S_b) flame speeds relative to their 1-d values (S_u^0 and S_b^0),

$$\frac{S_u}{S_u^0} = 1 + \frac{Ze}{2}\left(\frac{1}{Le} - 1\right)\frac{\alpha^0 \kappa \delta_T^0}{S_u^0} + \gamma \delta_T^0$$

$$\frac{S_b}{S_b^0} = 1 + \left[\frac{Ze}{2}\left(\frac{1}{Le} - 1\right) - \frac{1}{Le}\right]\frac{\alpha^0 \kappa \delta_T^0}{S_u^0}$$

where Ze is the Zeldovich number; α is a factor that accounts for thermal expansion; $\gamma = \nabla_t \cdot n$ is the curvature of the flame front; $\kappa = \nabla_t \cdot \left[\frac{u_t}{u}\right]$ is the strain rate; and δ_T is the flame thickness. Since S_b is affected only by flame strain, the effect of strong

azimuthal curvature in our conical flame case should not influence the flame speed at the reaction zone. Considering the effect of flame strain on S_b, Choi *et al*. [30] have shown that the magnitude of the strain rate measured at the reaction zone in the shoulder region of the conical flame is much less compared to that at the tip, and its effect on the reaction zone speed is minimal. All the flames reported here are stabilized with the highest possible velocity, such that the heights of the flames are large compared to the burner diameter. This reduces the ratio of strain affected flame tip area to the flame shoulder area. Hence considering both curvature and strain effects, it can be concluded that the measured flame speeds at the reaction zone for the conical flame should be very close to the 1-d reaction zone flame speed. Hence the mass balance for the conical flame can be shown as,

$$S_b^0 \approx S_b = \frac{\dot{m}}{\rho_b A_b}$$

where ρ_b is the density and A_b is the surface area at the reaction zone. From a 1-d flame mass balance,

$$S_b^0 = \frac{\rho_u}{\rho_b} S_u^0$$

and this expression for S_b^0 can be substituted into the former expression to produce,

$$S_u^0 \approx \frac{\dot{m}}{\rho_u A_b} = \frac{\dot{Q}}{A_b}$$

where $\dot{Q}$ is the volumetric flow rate of the unburned mixture. Since chemiluminescence is primarily produced in the heat release zone of the flame, the surface area measured from a chemiluminescence image can approximate A_b. Hence it can be seen that for a

conical flame, the flame speed calculated by dividing the volumetric flow rate of the mixture with the luminous cone surface area should closely approximate the unstretched (one-dimensional) *unburned* laminar flame speed. The experimental facilities used for obtaining the flame images at atmospheric pressure and elevated pressure conditions are detailed in the following section and the validation of this approach is presented in the first section of the results chapter.

3.1.1.1 Experimental facility

3.1.1.1.1 Atmospheric pressure

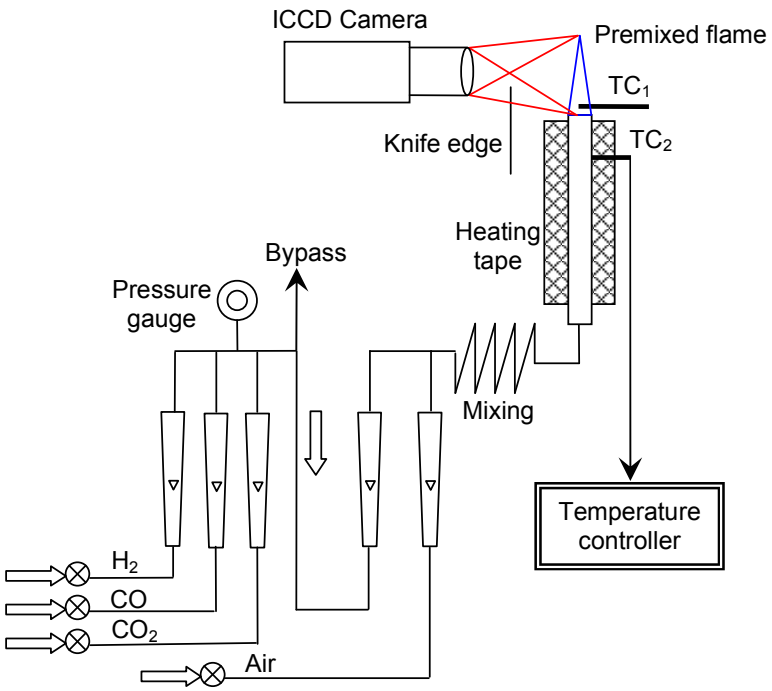

Figure 3.1. Schematic of the Bunsen flame experimental setup used for flame speed measurement at atmospheric pressure (TC=thermocouple). Mixing is achieved through long flow lines.

Figure 3.1 is a schematic of the experimental facility used for the laminar flame speed measurements at atmospheric pressure. The desired fuel composition is first

prepared using a bank of calibrated rotameters, one for each gas. After mixing thoroughly, the fuel is split into two flows: the desired flowrate of fuel passes through another rotameter (calibrated for the particular fuel composition), while the remainder is flared in a diffusion flame. Finally, the required quantity of air is added, and the mixture goes to the burner. This arrangement allows simple control over the equivalence ratio (Φ) and average velocity through the burner while maintaining the desired fuel composition.

For the atmospheric pressure studies, the burners are simply straight cylindrical stainless steel tubes, with various inner diameter (D) ranging from 4.5 to 18 mm. The length of each tube is at least $50D$ in order to ensure that the flow is laminar and that the exit velocity profile is fully developed. The burner diameter is chosen to ensure that the flow remains laminar (Reynolds number, $Re_D < 2000$) and that the average velocity is at least five times greater than the estimated laminar flame speed. The reactants are preheated by electrical resistance tape wrapped around the burner. Once the desired reactant temperature is achieved (as determined by a type-K thermocouple, TC_1, temporarily placed at the center of the burner exit), the surface temperature of the burner is monitored by a second thermocouple, TC_2, and held constant by a temperature controller. The mixture temperature at the exit of the burner has a nearly uniform radial profile ($\Delta T \approx 3$-5 K). Digital images of the flame emission are captured with a 12-bit intensified CCD camera (576 × 384 pixels) and a 105 mm, f/4.5 UV camera lens. The camera system is sensitive in the ultraviolet and visible regions (~220-650 nm), and hence is capable of capturing both OH^* and CO_2^* chemiluminescence from the flame reaction zone.

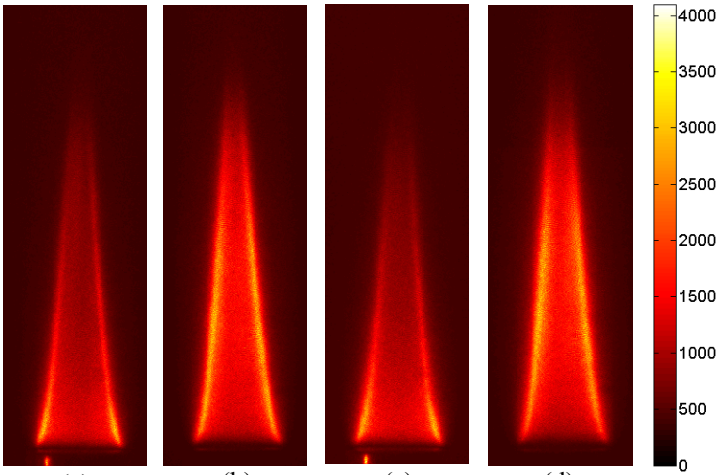

Figure 3.2. Images of flame emission for various fuels and conditions: (a) H_2:CO=95:5, Φ=0.61 without knife edge, (b) same as (a) but with knife edge, (c) H_2:CO=95:5 and 20% CO_2, Φ=0.62 without knife edge, (d) same as (c) with knife edge. The color scale represents the intensity variation of the 12 bit flame images.

Figure 3.2 shows some typical images of the flame radiation. The majority of the flame emission comes from the flame edge, i.e., chemiluminescence from the reaction zone. The less intense region in the central portion of the image is due primarily to chemiluminescence from the front and back edges of the flame. The intensity of the flame edge varies along the flame height, mainly due to two causes. First, the integrated flame area decreases along the flame height, which causes the measured flame radiation intensity to decrease. Second, the reactant mixtures studied are lean and contain a considerable amount of hydrogen. Thus, the Lewis number (*Le*) of these mixtures is expected to be below one due to the high diffusivity of hydrogen. Since negative strain on the flame surface increases downstream along the conical Bunsen flames, the burning intensity for *Le*<1 flames is reduced [31]. This reduction in burning intensity can reduce the radiation intensity along the flame height. Moreover for very lean mixtures, a high

negative strain at the flame tip can extinguish the flame locally, leading to tip opening phenomenon [31].

As described above, flame speed calculation in this approach depends on locating the flame reaction zone in order to determine the reaction zone area. Thus large variations in intensity with height can be problematic. The imaging system includes an unusual feature, a horizontal knife edge (see Figure 3.1) placed in front of the lens in order to vary the collection solid angle along the flame height. Figure 3.2a and Figure 3.2c show the flame emission from high hydrogen content, lean flames acquired without the knife edge and with a 3 ms exposure time. Locating the flame reaction zone in these images is clearly difficult. The vertical location of this knife edge can be adjusted so as to reduce the amount of light coming from the flame base while the amount of light coming from the flame tip remains unchanged. Then by increasing the exposure time (~25 ms), the tip of the flame is made visible, without saturating the image at the flame base. The result is seen in Figure 3.2b and Figure 3.2d. The flame tip is clearly more visible, and thus the flame area can be calculated more accurately. These images also show that if flame extinction happens, due to high negative strain, it only occurs at very small flame radius (high curvature). Thus the reaction zone area is only weakly affected.

3.1.1.1.2 Elevated pressure

The schematic of the experimental setup used for flame speed measurement at elevated pressure is shown in Figure 3.3a. The most notable difference from the atmospheric pressure facility (see Figure 3.1) is the burner geometry; it is now a smoothly contoured nozzle with high contraction ratio instead of a simple straight tube.

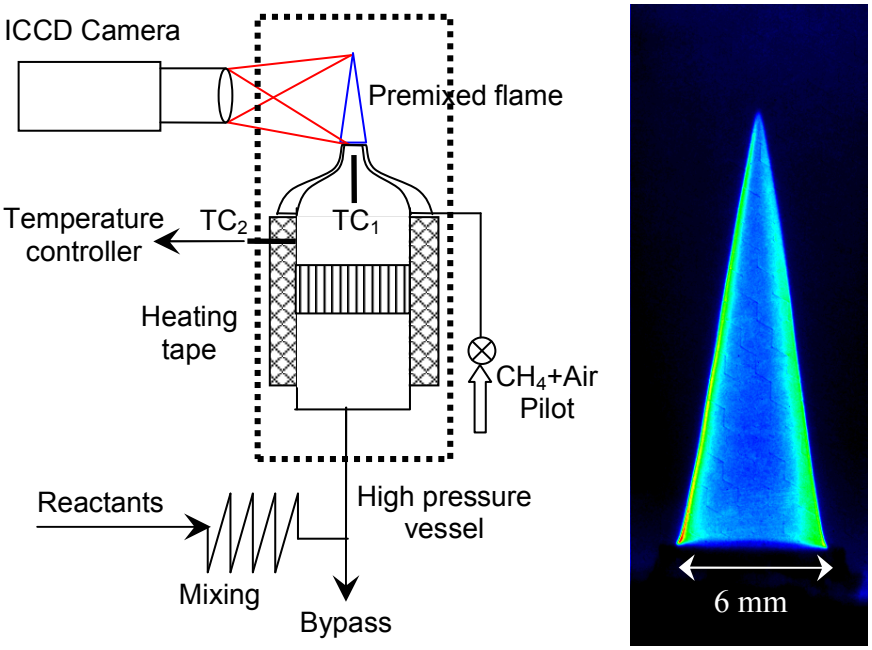

Figure 3.3. (a) Schematic high pressure Bunsen flame experimental setup (TC=thermocouple). Mixing is achieved through long flow lines. (b) Typical image of flame emission at 15 atm and 600 K preheat temperature (80:20 H_2/CO fuel mixture, 10:90 O_2:He oxidizer).

As the pressure increases, the desired Reynolds number (based on the tube diameter) of the jet flow increases much beyond the nominal limit (Re~2000) for a steady laminar flow with straight tubes (even with the smallest diameter burner diameter *D*~4.5mm). The high contraction ratio, contoured nozzle, however, ensures steady laminar flow even at much higher Reynolds number (based on the burner exit diameter *D*). The exit diameters of the burners used in this study are 9 and 6 mm, with corresponding contraction ratios of 72 and 161. Another striking difference from the atmospheric pressure facility is that the contoured nozzle burner also has a sintered plate-stabilized pilot flame around the rim of the nozzle exit to stabilize the main jet flame. This becomes necessary as the static stability (flash back and blow off) of the jet flame

stabilized on a contoured nozzle is limited to a narrow range of operating velocities. This is mainly due to the fact that the velocity gradient near the wall is higher and not easily controllable compared to that of straight tubes.

The reactant mixture, with desired composition and flow rate, is prepared in a similar fashion to the atmospheric pressure facility. After mixing thoroughly, the reactant mixture is sent through a plenum, where it is preheated by electrical resistance tape wrapped around the plenum. Ceramic flow straighteners are installed in the plenum to remove any unsteadiness in the incoming flow. The contoured nozzle is attached at the end of the plenum. The reactant temperature is monitored by a type-K thermocouple, TC_1, placed at the center of the burner, one inch upstream of the exit. Once the desired reactant temperature is achieved, the surface temperature of the plenum is monitored by a second thermocouple, TC_2, and held constant by a temperature controller. The entire system is placed in a N_2 ventilated high pressure vessel, designed to withstand pressures of 30 atm with optical access for the purpose of chemiluminescence imaging of the flame and velocity measurement using Laser Doppler Velocimetry (LDV). Digital images of the flame emission are captured with a 16-bit intensified CCD camera (1024×256 pixels) and a 105 mm, f/4.5 UV camera lens. Figure 3.3b shows a sample image of the recorded flame emission at an elevated pressure and reactant temperature condition for a typical fuel mixture.

Laminar flame speed measurements for lean H_2/CO fuel mixtures at elevated pressure need special attention as these flames develops spontaneous wrinkles on the flame surface. This wrinkle formation is mainly attributable to hydrodynamic and thermo-diffusive instabilities, which become prominent at high pressure conditions,

mainly due to the reduced flame thickness. Figure 3.4a clearly shows the presence of these wrinkles (folds on the surface of the flame) due to hydrodynamic instabilities on a conical Bunsen flame of 50:50 H_2/CO fuel mixture at elevated pressure temperature conditions.

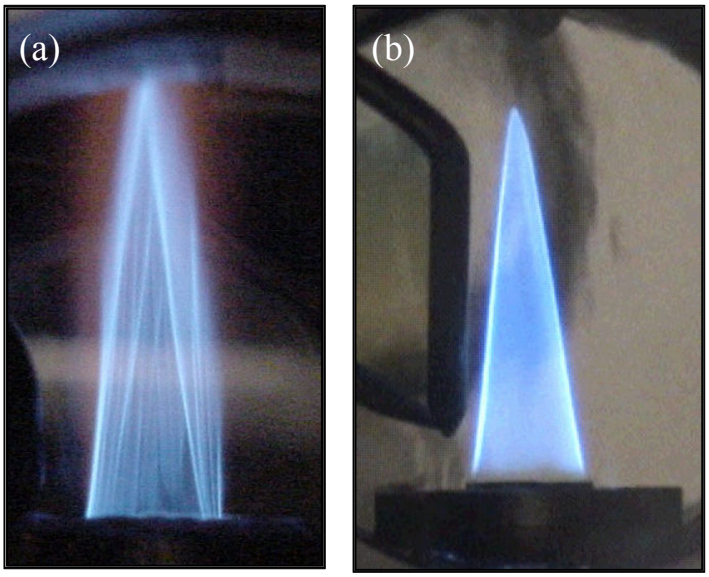

Figure 3.4. A sample flame images of 50:50 H_2/CO fuel mixture at Φ=0.6, p=10 atm, and T≅600 K with (a) standard air, and (b) 10:90 O_2/He mixture.

As proposed in a previous study [32], replacing N_2 in the oxidizer (air) with helium (He) greatly reduces the flame's propensity to wrinkle. This is mainly due to the fact that He has a higher diffusivity compared to N_2; thus replacing N_2 with He improves the thermal and mass diffusivity of the reactant fuel mixture, increasing the flame thickness and Lewis number (*Le*). This in turn greatly suppresses the formation of hydrodynamic and thermo-diffusive instabilities. This is evident as shown in an image of a flame with a O_2:He (1:9) "air" mixture in Figure 3.4b for the same fuel mixture and test condition as in Figure 3.4a. It should also be noted that replacing N_2 with He does affect the flame temperature and the flame speed, but it does not affect the fundamental

chemistry [32]. In order to have flame speeds comparable to those obtained with standard air, but with lower flame temperatures, an O_2/He mixture with a 1:9 volumetric ratio was chosen for all the test conditions considered in this study.

3.1.1.2 Flame speed calculation

As detailed earlier, the laminar flame speed is calculated by dividing the volumetric flow rate by the reaction zone area (A_b) of the flame. An edge detection program was developed to determine A_b from the chemiluminescence images. Since these Bunsen flames are essentially axisymmetric, each flame image is split in half along the burner axis. The edge detection program detects the reaction zone edge by locating the maximum derivative of the flame intensity along the radius of the flame. For the high pressure flames, the minimum (i.e., largest negative) derivative of the flame intensity is considered due to its higher signal to noise ratio. It should be noted here that the difference in location between the minimum and maximum derivate is rather small due to reduced flame thickness (and hence, the chemiluminescence zone thickness) at elevated pressure conditions. The flame area is then found by revolving the detected edge along the axis of the burner. The same procedure is repeated for the other half of the flame image. For each experimental condition, 25 images are typically recorded, and the reported flames speeds are based on the average of the 50 A_b values (25 images × 2 half-flames). The validation of this measurement approach is presented in Chapter 4 for methane and two syngas fuels at both atmospheric and elevated pressure conditions.

3.1.2 Stagnation flame approach

The stagnation flame approach is a well-established method for stretch-corrected flame speed measurements [33]. A steady 1-D strained laminar flame stabilized in a well-defined stagnation flow field is used for the measurements. The flame speed and the imposed strain rate on the flame are determined from measured velocity profiles across the flame. The details of the experimental facility and the demonstration of the method are discussed in the following sections.

3.1.2.1 Experimental facility

A general schematic of the stagnation flow burner is shown in Figure 3.5. In this approach, the stagnation flow field is achieved with combination of a contoured nozzle and a solid surface (stagnation plug) placed above the exit of the nozzle. This configuration is advantages over the commonly employed opposed jet flow configuration for the following reasons: (1) the use of a solid wall leads to more stable flames, (2) problems related to heating of the upper burner are eliminated, and (3) use of a single jet greatly simplifies burner operation.

The reactant mixture with desired composition, flow rate and preheat temperature are prepared in a similar fashion to the high pressure Bunsen flame studies discussed earlier. In addition, similar to the high pressure Bunsen facility, burner is essentially the same contoured nozzle with high contraction ratio. These high contraction ratio nozzles, apart from maintaining steady laminar flow even at high Reynolds number based on the burner exit diameter, create a uniform velocity profile at the burner exit to ensure uniform flame stretch throughout the flame area. Various nozzles with exit diameters (D) of 6, 9 and 12.5 mm are employed to produce a stable flame, with higher flame speed mixtures

requiring the smaller nozzle. The exiting fuel/air mixture is surrounded by a small N_2 coflow, in order to reduce the shear layer development along the periphery of the jet. Care was also taken to reduce the size of the wake region created due to the finite thickness of the contoured nozzle at the burner exit.

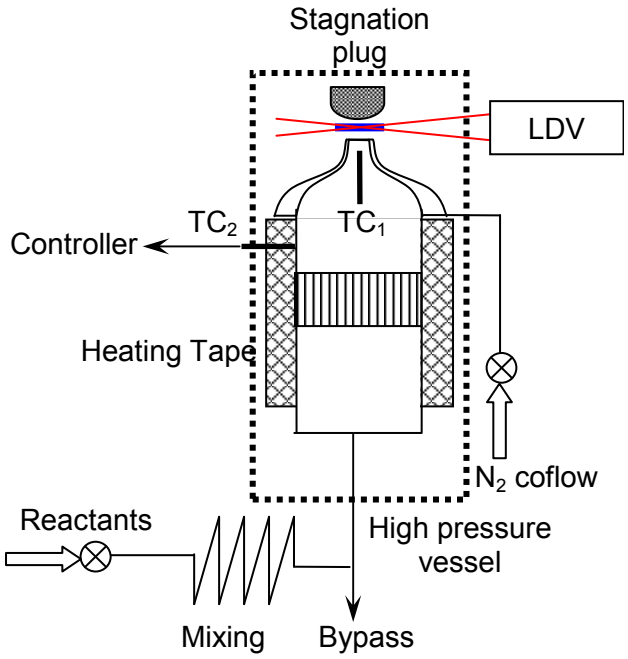

Figure 3.5. Schematic of the experimental setup (TC=thermocouple).

Flow stagnation is achieved with a rounded plug placed at a distance *L* above the contoured nozzle. The plug is produced from a stainless steel rod (38 mm diameter). The end of the rod is first formed into a hemisphere and then machined to produce a flat surface with 12.5 mm diameter. The rounded plug, compared to a flat plate, provides a more steady stagnation flow field due to its aerodynamic nature, i.e, the flow flows the contour of the rounded plug more easily, and hence greatly improves the flame stability especially at high pressure or high flame speed conditions (e.g., reactants at elevated preheat temperature). Moreover at the high flame speed conditions, providing the N_2 coflow is not sufficient to inhibit the unsteady shear layer development. This leads to

uniform shedding of vortices along the periphery of the diverging stagnation flow which makes the flame unsteady. In order to avoid the formation of these vortices, a burner stabilized stagnation flame, as shown in Figure 3.6, is used for measurements (only for highly preheated reactants). This flame configuration is achieved by cutting off the N_2 coflow completely. Detailed flow field measurements have been performed to confirm the 1-d nature of the center flat stagnation flame.

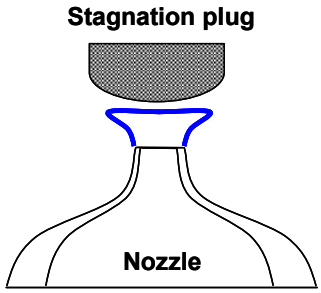

Figure 3.6. Schematic of the burner stabilized stagnation flame.

The distance (L) between the burner exit and stagnation plug is adjusted depending on the burning velocity. For high burning velocities, a lower L/D leads to a stable stagnation flame. In the current measurements, L/D ranges from 0.5 to 1 (it should be noted that this corresponds to L/D=1-2 for the commonly employed counterflow flame configuration). These L/D values are sufficiently large that the effect of finite domain on the measured flame speed can be considered small [39].

The use of a solid wall as a stagnation plane, as opposed to the counterflow configuration with adiabatic twin flames, is generally considered to have an insignificant effect on the measured unburned flame speed, provided that the flame is stabilized sufficiently away from the stagnation plane [33]. The effects of the solid wall are mainly downstream heat loss from the flame products to the wall and zero radial velocity

gradient at the wall. A detailed numerical analysis of the influence of these effects on the unburned strained flame speed is reported in the measurement uncertainty section for a typical fuel mixture and test conditions considered in this study.

The axial and radial velocities along the stagnation streamline are measured with a Laser Doppler Velocimetry (LDV) system. The fuel mixture is seeded with alumina (Al_2O_3) particles. The nominal size of these particles is chosen to be 1-2 μm in order to minimize thermophoretic effects [34]. The radial profile of axial velocity and the centerline axial velocity gradient were measured close to the nozzle exit to establish the boundary conditions at the nozzle exit for the simulations. The measurements show less than 15% variation of the axial velocity along the radial direction. Also, the axial velocity gradient along the centerline approaches zero at the nozzle exit. This confirms that the outflow from the high contraction ratio nozzle is nearly a plug flow, as expected.

3.1.2.2 Method demonstration

To illustrate this method, the measured axial velocity along the stagnation stream line for a typical stagnation flame is shown in Figure 3.7. The axial velocity decreases from the exit of the nozzle and reaches a minimum where the preheat zone starts. After reaching a local minimum, the axial velocity increases sharply inside the flame and then decreases to zero at the wall.

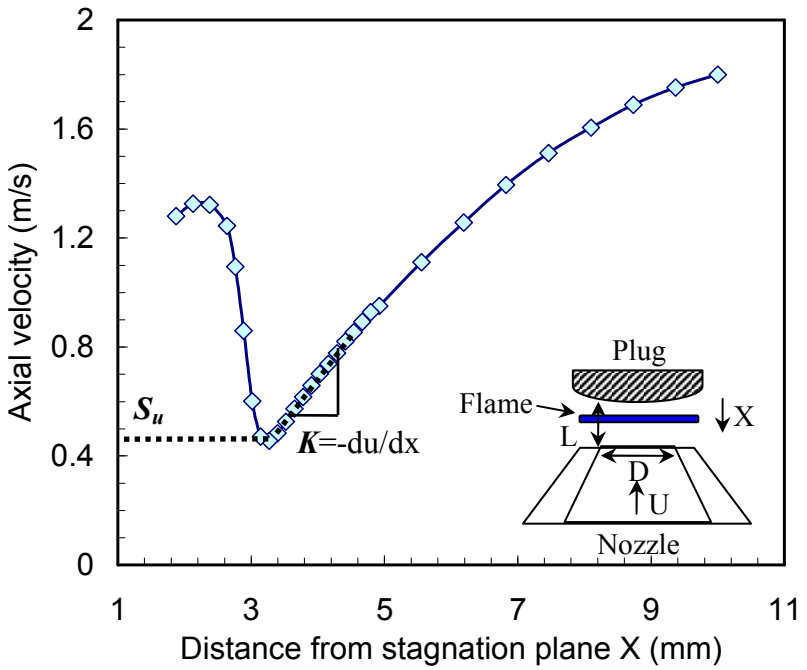

Figure 3.7. Typical measured axial velocity along the stagnation streamline. Figure insert shows layout of nozzle generated wall stagnation flame.

Based on the standard approach [35], the minimum velocity before the preheat zone is considered as the reference strained unburned flame speed (S_u), and the maximum gradient of the axial velocity (as determined from the velocity measurements) ahead of the minimum velocity location is taken as the imposed strain rate (K) (see Figure 3.7). The imposed strain rate is controlled by changing the nozzle exit velocity. As the nozzle exit velocity increases, the strain rate increases, and the flame moves closer to the stagnation surface. For each fuel mixture, the strain rates and corresponding strained flame speeds are measured for a range of nozzle exit velocities. The flame speeds were measured across a range of strain rates, with the lowest attained strain rates limited either by flashback or flame stability (unsteadiness).

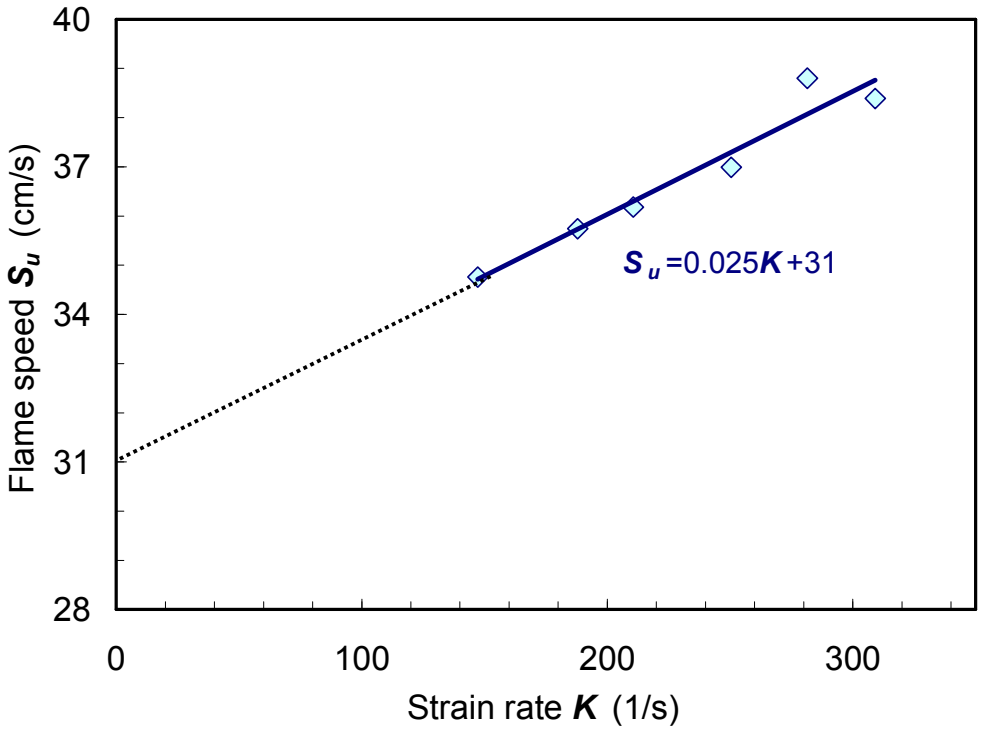

Figure 3.8. Variation of the measured flame speed with strain rate for H_2:CO:CO_2 40:40:20 fuel mixture at Φ=0.59, p=1atm and T≅300K.

For example the variation of the measured flame speed for a H_2:CO:CO_2 40:40:20 fuel mixture at Φ=0.59, p=1atm and T_u=300K is shown in Figure 3.8. It is clear that the measured flame speed increases linearly with imposed strain rate. The linearly extrapolated measured flame speeds to zero strain rate have been commonly used to represent the unstrained flame speed (S_u^0), while the slope of this linear fit represents the mixture unburned strain sensitivity. For example in the case shown in the figure, the extrapolated unstrained flame speed is 31 cm/s while the unburned strain sensitivity is 0.025 cm.

Using the above two measurement approaches, extensive flame speed and strain sensitivity information were obtained for typical syngas mixtures at conditions relevant to gas turbine engines. Various parameters such as fuel composition, dilution levels, equivalence ratios, pressure and preheat temperature considered in this thesis work are shown in the Table 3.1.

Table 3.1. List of fuel mixtures and test conditions considered for the flame speed measurements.

Fuel (H_2:CO)	Dilution	Approach*	Φ	P (atm)	T_u (K)
5:95; 50:50	0	B	0.6-1.0	1	300-700
95:5	CO_2 20%	B	0.6-1.0	1	300-700
50:50	CO_2 20%	S	0.6-0.8	1	300
50:50	CO_2 0 and 40%	S	0.6-0.8	1	600-700
100:0	0	S	0.3-0.5	1	700
100:0	$N_2 \approx 70\%$	S	0.8-1.6	1	700
5:95 to 20:80	0	S	0.6	5	300
50:50	0	B	0.6-1.2	10	300
50:50	0	B	0.5-0.8	10	600
20:80 to 80:20	0	B	0.6	15	600
20:80 to 80:20	0	B	0.8	15	300
50:50 to 90:10	CO_2 40%	B	0.75	15	600

*B - Bunsen flame approach; S - Stagnation flame approach

3.2 Modeling Approaches

The experimental results are compared to predictions of standard one-dimensional flame models employing various leading kinetic models. The unstrained laminar flame speeds are calculated with the Chemkin PREMIX algorithm and compared with Bunsen flame measurements. Similarly, the strained flames are simulated with the Chemkin OPPDIFF code and compared with stagnation flame measurements in the same range of strain rates. In the strained flame simulations, the distance between the nozzle and stagnation plane (L) was matched to the experimental value, since it can have a significant effect on the predicted strained flame speed. The plug flow boundary condition, which is a close representation of the measured nozzle data, is used at the nozzle exit. Sensitivity of the measurements to uncertainties in nozzle velocity boundary conditions (plug or potential) are investigated through detailed numerical simulations and shown to be small in the measurement uncertainty section.

The predicted flame speed and strain rate are determined from the stagnation simulation with the same definitions that were applied to the experimental data (minimum axial velocity for flame speed and maximum preflame axial velocity gradient for strain). In all the flame simulations, the converged solution was obtained for a large number of grid points by considering the gradient and curvature to be 0.1. Multi-component diffusion and Soret effects (thermal diffusion) are included in both PREMIX and OPPDIFF simulations, as they have significant influence on the calculated flame speeds, especially for high H_2 content flames.

Four reaction mechanisms are considered in this study: (1) GRI Mech 3.0 [21], (2) the H_2/CO mechanism of Davis *et al*. [19], (3) the C_1 mechanism of Li *et al*. [20], and

(4) the H_2 mechanism by Li *et al*. [36]. The first three reaction mechanisms are relevant to syngas combustion while the fourth one is a H_2 model, considered only for pure H_2 and N_2 diluted H_2 fuels. The GRI mechanism has been tested and validated extensively for methane and natural gas combustion over a wide range of pressure and temperature conditions. It is also widely used in academia and industry. It consists of 325 elementary chemical reactions with associated rate coefficients and thermochemical properties for the 53 species involved. The second reaction mechanism was developed and optimized specifically for H_2/CO combustion. It consists of 14 species and 30 reactions, and incorporates recent updates for rate parameters and third body efficiencies of a few key reactions. It also includes modifications of thermodynamic and transport properties for species relevant to high temperature H_2 and CO oxidation. The third choice is a hierarchically developed detailed kinetic mechanism for oxyhydrogen and C_1 species (CO, CH_2O and CH_3OH). It consists of 85 elementary reactions and 21 species with associated rate coefficients and thermochemical properties. The fourth mechanism is an updated comprehensive kinetic model for hydrogen combustion. It consists of 19 elementary reactions and 11 species with associated rate coefficients and thermochemical properties.

3.3 Measurement Uncertainties

In this section, the uncertainties in all the measured quantities associated with the flame speed calculation for both the Bunsen and stagnation flame approaches are outlined. The uncertainties related with the flow metering and reactant preheating are discussed first, as it is common for both approaches.

The flow metering system is a bank of rotameters, each for one gas. These rotameters are calibrated with a bubble flow meter or wet test meter to ± 1% accuracy for each gas and pressure condition, i.e., correction factors are not used either for molecular weight or density. The combined standard uncertainty of any measured quantity is estimated by "root-sum-of-squares" (RSS) method. For example, the standard uncertainty (or standard deviation) on the equivalence ratio is estimated to be $\pm\sqrt{3}$ % or $\pm\sqrt{4}$ % for two or three component fuel mixtures (e.g., for two component fuel mixture, it is two fuels and an oxidizer - hence, the total is the sum of three uncertainties). Similarly the uncertainty on the total volumetric flow rate is estimated to be in the range of $\pm\sqrt{3}$ to $\pm\sqrt{5}$ %, as there are three to five different gases in the reactants.

With high preheat systems, it is important to consider the possible uncertainty on the measured flame speed due to the chemical changes occurring while the reactants are in the plenum. This is particularly important at elevated pressure conditions as the highly preheated reactants are approaching the third explosion limit. As discussed in the experimental facility section, the cold reactants enter the plenum and are preheated by the plenum wall, which is maintained at a slightly higher temperature (~100-150 K) than the desired reactant temperature (measured close to the exit of the nozzle). The residence time of the reactants in the plenum is less than three seconds. A detailed numerical analysis was conducted with a combination of plug flow followed by a PREMIX calculation for a typical fuel mixture (H_2/CO 50:50 at equivalence ratio of 0.6) and test conditions (p=15 atm; T_u=600 K) considered in this study. In order to get a conservative estimate, the plug flow temperature is assumed to be 775 K; this is much higher than the bulk reactant temperature and somewhat higher than the maximum temperature

experienced by flow near the plenum wall. For a 3 s residence time, there is no significant change in the flame speed, while for 5 and 7 s residence times, the flame speed decreases by 1 and 6%, respectively. The reduced flame speeds are associated with partial oxidation of the reactants in the plenum. It is also interesting to note that the induction (ignition delay) time of this mixture at 775 K preheat temperature is 7.6 s. Hence, we conclude that any chemical reactions in the plenum do not have a significant influence on the measured flame speeds.

3.3.1 Bunsen flame approach

As described earlier for the Bunsen method, the laminar flame speed is calculated by dividing the volumetric flow rate of the reactants by the flame reaction zone area. Hence, the main uncertainties are in the flow metering system and flame area calculation. The uncertainty on the total volumetric flow rate is estimated to be $\pm\sqrt{5}\,\%$ for five component (maximum considered here) reactant mixture. The flame area is calculated from the chemiluminescence images of the flame. For each experimental condition, typically 25 images are recorded, and the reported flame speeds are based on the average of the 50 A_b values (25 images × 2 half-flames). The maximum deviation of the measured flame area (for a single image) from the average of all the images is always less than $\pm\,5\%$ and the standard deviation is approximately $\pm\,3\%$. Thus the precision in the measured *mean flame area*, based on a 95% confidence level is roughly ± 1%, calculated from the relation $\left(\pm\frac{\sigma}{\sqrt{N}} * CLF\right)$, where σ is the standard deviation of the area measurements, N is the number of measurements used to calculate the mean, and CLF

(confidence level factor) is assumed to be 1.96 for 95% confidence (assuming a Gaussian probability distribution).

Hence, the maximum combined standard uncertainty on the measured flame speed is $\pm\sqrt{5+1}\,\%$ or $\pm 2.5\%$. It should be noted here that the above estimated uncertainty does not include systematic (or bias) errors stemming from the assumptions (discussed in the measurement approach section) regarding the influence of curvature and strain on the flame speed at the reaction zone.

3.3.2 Stagnation flame approach

In this approach, the measured axial velocity across the flame is used for flame speed determination. At each axial location along the stagnation stream line 10,000 measurements were acquired. The uncertainty in the strained flame speed measurement can be estimated from the root-mean-square fluctuation of the measured axial velocity at the location where the average axial velocity is a minimum (definition of the strained unburned flame speed). A typical rms fluctuation at the minimum velocity location is about 2-4%. Hence, the maximum uncertainty in the minmum axial velocity is calculated to be much less than $\pm 1\%\left(\pm\frac{4}{\sqrt{10000}} * CLF\right)$ for 95% confidence. Since this is too small to be indicated on plots, all the strained flame speeds are reported here with the corresponding rms fluctuations. Apart from this random error, there are some systematic uncertainties on the measured strained flame speeds, due to the disparity in experimental and modeling boundary conditions at both stagnation and nozzle exit planes, which are discussed in detail in the following sections. Moreover, the systematic uncertainty on the

calculated unstrained flame speed associated with a linear strain rate extrapolation is also discussed.

3.3.2.1 Significance of wall boundary condition

For all the strained flame speed predictions, the Chemkin opposed flow code was used with two premixed flames on either side of the stagnation plane; the simulation is adiabatic. In the experiments, however, a solid wall replaces one of the premixed jets, which makes the system nonadiabatic due to the loss of heat from the product gases to the solid wall. This could potentially reduce the unburned strained flame speeds. Moreover in the opposed flame (counter flow flame) case, the radial velocity gradient at the stagnation plane is finite (due to a slip condition), while for the single jet case it is zero at the plug wall (due to a no slip condition). This zero radial velocity gradient changes the strain rate distribution in the product zone, which could change the unburned flame speed. In order to investigate the effects of both heat loss and no-slip condition at the wall, a detailed numerical analysis was conducted on a wall stagnation flame configuration, and the results were compared with that of the counter flow flame case.

The wall stagnation flame was simulated with the Chemkin opposed flow code, but with modified boundary conditions. For the opposed flow code there are two nozzles separated by distance L. The boundary conditions at each nozzle exit are the same: $T = T_i$, $F = \rho u/2$, $G = \rho v/r$, and for the species, the sum of convection and diffusion is equal to the total inflow mass flux. Here, F and G are the parameters defining axial (u) and radial (v) velocities respectively, and they are function of x only. To simulate the wall stagnation flame, one of the nozzle boundary conditions is changed as follows: the axial velocity is zero ($F=0$), the temperature is $T=T_{wall}$, the radial velocity gradient is zero (G

= *0*), and for the species the diffusive velocity is zero. All of these boundary conditions can be applied in the opposed flow code by considering the top nozzle as a solid wall and specifying $u=0$ and $T=T_{wall}$. The other two boundary conditions for the radial velocity gradient and the species are automatically satisfied. The distance between the nozzles has to be reduced from L to $L/2$. Figure 3.9 shows the variation of the temperature and radial velocity gradient along the axial direction for both counter flow flame (CFF) and wall stagnation flame (WSF) for the same mixture and single-jet flowrate. In this example, L=0.6 cm and the axial velocity at the nozzle exit is 1.2 m/s. The temperature of the wall is 900 K (for the wall stagnation flame).

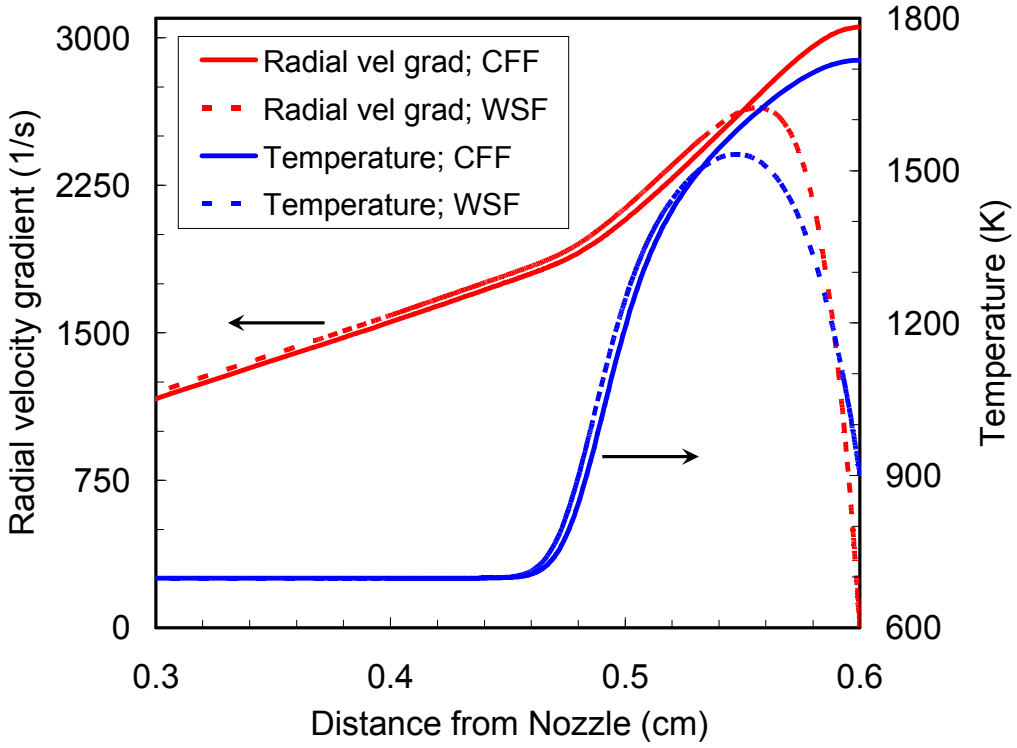

Figure 3.9. Numerical simulation of counter flow flame (CFF) and wall stagnation flame (WSF) for H_2 with N_2 diluted air (O_2:N_2 1:9) at Φ=0.8 and 700 K preheat temperature.

For both cases, the flame is located ~0.46 cm from the nozzle exit. The temperature for the CFF case increases and reaches a maximum (1717 K) at the stagnation plane. For the WSF case, the temperature rise is nearly identical in the preheat zone, but it reaches a lower maximum (1531 K) somewhere in the reaction zone, afterwards decreasing due to heat loss to the wall (and reaching the specified 900 K at the wall stagnation plane). The radial velocity gradient, in a similar fashion to the temperature, increases and reaches maximum at the stagnation plane for the CFF case. For the WSF case, it increases and then decreases to zero at the wall in order to satisfy the no-slip condition at the stagnation plane. Thus there is a significant change in strain rate distribution in the product zone close to the wall. Moreover the wall stagnation flame is slightly displaced further from the stagnation surface compared to the counter flow (twin flame) case.

Numerical simulations of CFF and WSF were carried out for H_2 with N_2 diluted air (O_2:N_2 1:9) at Φ=0.8 and 700 K preheat temperature. This fuel composition is chosen for detailed investigation because it is expected to be more sensitive to heat loss for two reasons: 1) the flame is located closer to the wall (within about two flame thicknesses) compared to the other cases reported here, and 2) the temperature and velocity rise across the (weaker) flame are smaller. Figure 3.10 shows the strained flame speed predicted with GRI Mech over a range of strain rates for both the CFF and WSF. For the WSF, simulations were performed for two wall temperatures (900 and 1700 K). The heat loss will clearly be very small for T_{wall}=1700 K, because the temperature at the stagnation plane for the CFF case is nearly the same value. Hence the effect of no-slip boundary condition at the wall should dominate for this simulation. For the T_{wall} = 900 K case,

however, the amount of heat loss is much greater and hence the effect of both heat loss and no-slip boundary condition can be studied.

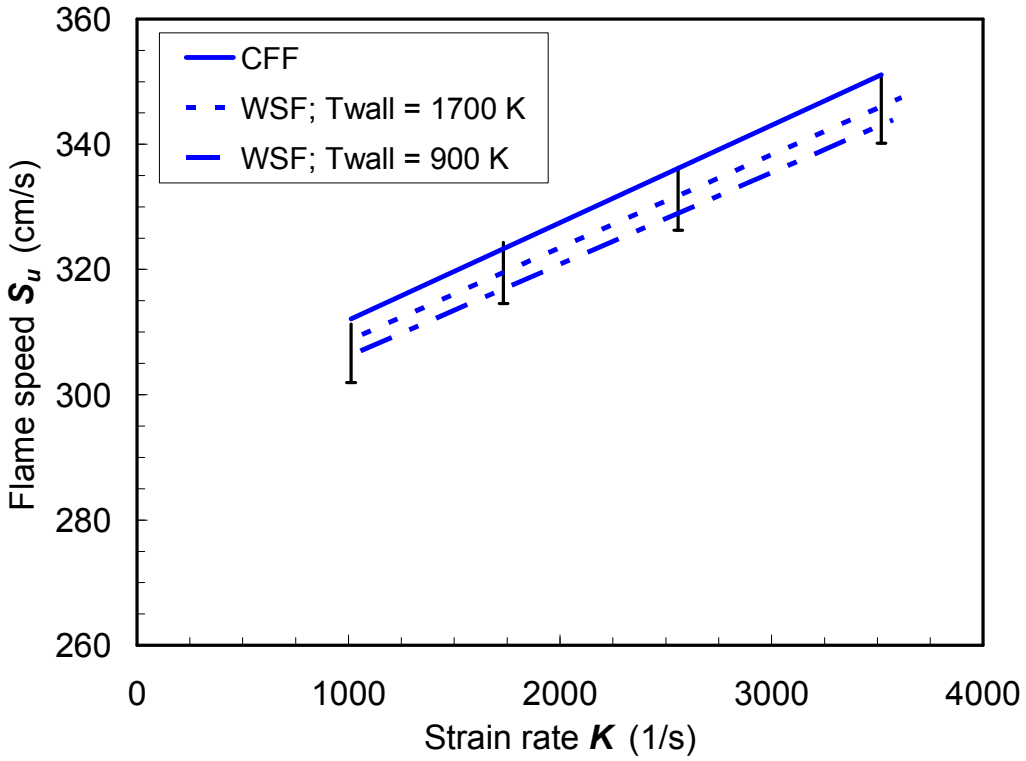

Figure 3.10. Model predicted strained flame speeds for CFF and WSF with two different wall temperatures. The fuel mixture is H_2 with N_2 diluted air (O_2:N_2 1:9) at Φ=0.8 and 700 K preheat temperature. The vertical bars indicate 3% deviation from CFF.

The predicted strained flame speeds increase linearly for all three cases over the range of strain rates simulated. Moreover the predicted strain sensitivities are almost the same for all three cases. Comparing the strained flame speeds, the WSF predictions are always (slightly) lower than the CFF predictions. The WSF predictions with T_{wall}=1700 K under predict the CFF by less than 2%. Since the temperatures at the stagnation plane are nearly the same for both cases, the zero radial velocity gradient at the wall is seen to slightly reduce the strained flame speed. When the wall temperature is

reduced further, the predicted strained flame speed decreases a bit more. For T_{wall}=900 K, the predicted flame speeds are now below the CFF results by less than 3% throughout the strain rate range tested. Even though the flame (product) temperature is lower for the WSF due to greater downstream heat loss, the unburned strained flame speed is not significantly altered (even when the flame is located within two flame thicknesses from the wall).

3.3.2.2 Significance of nozzle boundary condition

The predicted strained flame speeds were calculated using the Chemkin opposed flow code with plug flow boundary conditions at the nozzle exit. Since the experiments employed a high contraction ratio nozzle, the nozzle exit flow is close to plug flow. However due to non-ideal behavior at the nozzle exit (wall boundary layer and pressure gradient induced by the stagnation condition), the exit velocity profile does slightly deviate from the plug flow boundary condition. This could potentially change the minimum axial velocity (identified as the strained flame speed) between the experiments and simulations for the same imposed strain rate (defined as the maximum gradient in the reactants). For large deviations from plug flow, one would expect the inflow boundary condition to approach a potential flow. Therefore, detailed numerical simulations were performed for plug and potential flow boundary conditions for the fuel mixtures and experimental conditions (Φ, L and strain rates) reported here.

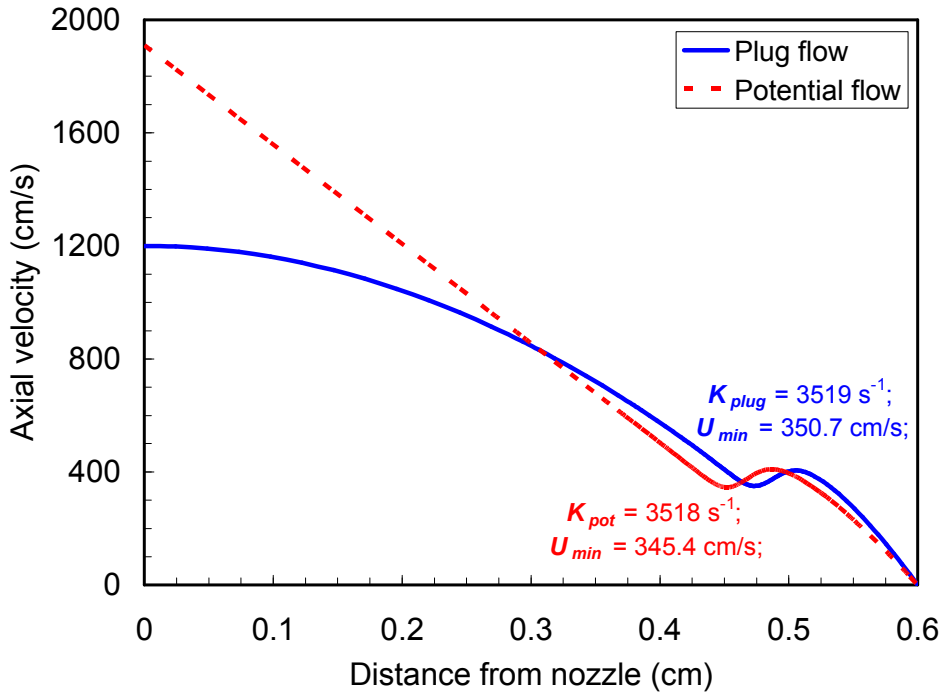

Figure 3.11. Numerical simulation of stagnation flame with plug and potential flow boundary conditions for the same strain rates. The fuel mixture is H_2 with N_2 diluted air (O_2:N_2 1:9) at Φ=0.8 and 700 K preheat temperature.

Figure 3.11 shows the variation of the axial velocity for both boundary conditions at identical strain rates. While the flame location for the potential flow is closer to the nozzle than for the plug flow, the minimum velocity before the flame is not affected significantly by the change in boundary condition. The minimum velocity for the potential flow case is 351 cm/s, while it is 345 cm/s for the plug flow boundary condition (less than a 1.5% effect). Similar analyses were performed for a range of strain rates for mixtures of H_2 with N_2 diluted air at Φ=0.8 and 700 K preheat temperature (Figure 3.12).

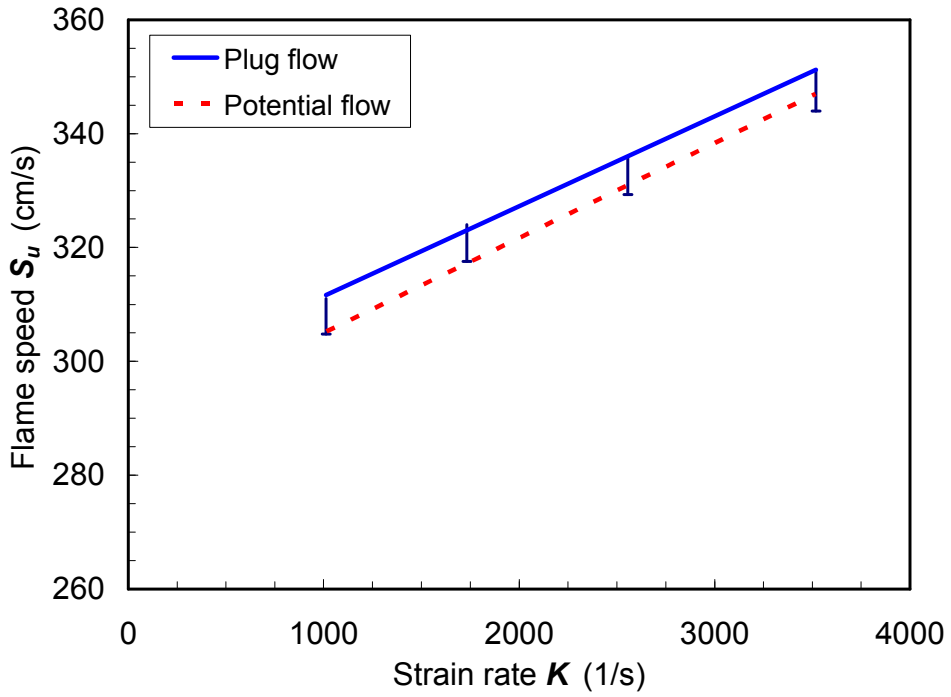

Figure 3.12. Model predicted strained flame speeds with plug and potential flow boundary conditions. The vertical bars indicate 2% deviation.

The predicted flame speed with potential flow boundary conditions is less than that of the plug flow boundary conditions for all the strain rates, but the difference between the two is within 2%. This indicates that the minimum velocity axial velocity is not very sensitive to the boundary conditions (for the same applied strain rate defined by the maximum velocity gradient ahead of the flame). Hence the small deviations from plug flow that might be expected in the experimental nozzle boundary condition can be neglected.

3.3.2.3 Extrapolation uncertainty

Another important issue to be addressed here is that there is some uncertainty in the way the unstrained flame speed is calculated in the stagnation flame technique. Ideally the strained flame speeds (from OPPDIFF) extrapolated to zero strain rate should

equal the unstrained flame speeds predicted in the PREMIX simulation. However the linearly extrapolated flame speed is always higher than that of the true unstrained flame speed by as much as 10%. For example, Figure 3.13 shows that the OPPDIFF predicted linearly extrapolated unstrained flame speed (340 cm/s) is higher (~8%) than the PREMIX predicted true unstrained flame speed (316 cm/s) for the 50:50 H_2:CO fuel mixture at Φ=0.6 and 700 K preheat temperature. In addition, this discrepancy grows with increasing flame thickness, which can be attributed to the finite domain effect [39] (both in the experiment and computation) though large *L*/*D* values are employed.

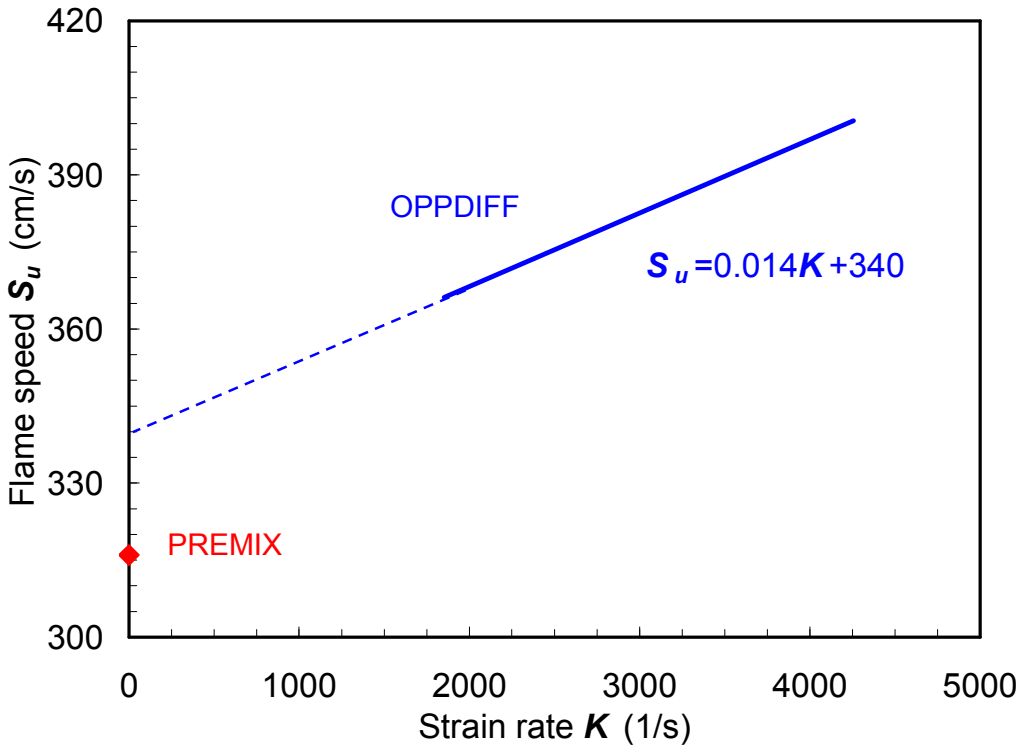

Figure 3.13. Comparison between the extrapolated flame speed (OPPDIFF) and the true unstrained flame speed (PREMIX) for 50:50 H_2:CO fuel mixture at Φ=0.6, T≅700K, and p=1atm. Both simulations are performed with GRI Mech 3.0.

This discrepancy between the unstretched and extrapolated values may simply be a result of the somewhat arbitrary definition of the unburned strained flame speed as the minimum velocity point in the approaching velocity profile. Numeric studies suggest that a more appropriate definition for the unburned strained flame speed would be the approaching axial velocity extrapolated to the barycenter of the reaction zone [37]. This definition significantly improves the agreement between the linearly extrapolated and unstrained flame speed. Since it is difficult to experimentally identify and determine the required barycenter of the reaction zone, the more common minimum velocity point approach [35] is employed here.

Due to this significant uncertainty in extrapolating the stagnation flame data to zero strain, this technique is used to verify the measured "unstrained" flame speeds only at conditions where there is a large discrepancy between the PREMIX and Bunsen flame data. Moreover, it is more conservative to compare the strained flame speed measurements (without extrapolation) to the corresponding strained flame speed predictions in the same strain rate range. Hence, the strained flame speed measurements are primarily compared with the corresponding strained flame speed predictions in the same strain rate range (and using the same definition of flame speed).

CHAPTER 4

INFLUENCE OF PREHEAT TEMPERATURE

One of the prime objectives of the present work is to measure the laminar flame speeds for a range of syngas composition with varying levels of preheating (i.e., different unburned gas/preheat temperatures) under lean conditions. Two measurement approaches were employed; a modified Bunsen approach based on reaction zone area imaging and the stagnation flame approach for stretch corrected measurements. Measurements were obtained for a range of preheat temperatures at both atmospheric and elevated pressure conditions. All the measurements are compared with numerical predictions based on leading kinetic models in order verify their ability to predict the variation of laminar flame with preheat temperature. Before presenting the measurements and modeling results, the validation results for the modified Bunsen flame approach at room temperature is presented in the first section of this chapter. Then, the influence of preheat temperature at atmospheric and elevated pressure is presented in the following sections. Finally, results from a sensitivity analysis are presented that highlight important reactions and their influence on the overall uncertainty of the model predictions. Short conclusions are provided at the end of each section and highlighted by underlining the text.

4.1 Validation – Bunsen flame approach

In our modified Bunsen flame approach, it was shown in the previous chapter that the flame speed calculated by dividing the volumetric flow rate of the mixture with the luminous cone surface area should closely approximate the *unstretched* (one-

dimensional) *unburned* laminar flame speed. To validate this approach, experiments were conducted for methane and two syngas fuel compositions previously measured with stretch corrected, counter-flow and spherically expanding flame methods at both atmospheric and elevated pressure conditions.

4.1.1 Atmospheric pressure

Experiments were conducted for CH_4-air mixture for a range of equivalence ratios. The appropriate burner diameter used for these experiments was 18 mm. Figure 4.1 shows measured flame speeds along with the results from previous measurements using counter flow flames. The flame speeds measured with the current Bunsen flame approach agree with literature values obtained in counter-flow flames, especially for lean conditions of interest in the current study. The current measurements slightly under predict the most up-to-date literature values on the rich side.

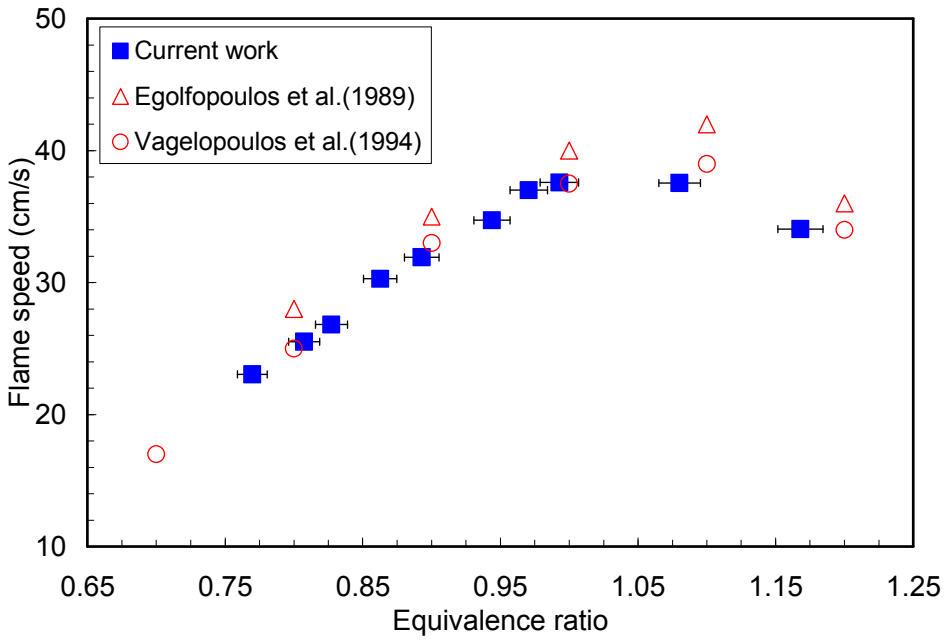

Figure 4.1. Measured laminar flame speeds in Bunsen flame for CH_4 flames at p=1atm and $T_u \cong 300K$, including previous counter-flow flame experiments [38,39].

Experiments were also conducted for two H_2:CO fuel compositions (50:50 and 5:95 by volume). The burner diameters used for these two compositions were 4.5 and 13.6 mm, and the equivalence ratio was varied from 0.6 to 1. As seen in Figure 4.2, the measured flame speeds for the 50:50 H_2:CO fuel mixture are in good agreement with values obtained from the stretch-corrected, spherically expanding flames throughout the lean equivalence ratio range tested. For example, the reported stoichiometric flame speed [11] for the 50:50 mixture is 115 cm/s; the present measurement is 112 cm/s (a 2.6% difference). This agreement is at least as good as the spread in the data reported by different investigators. The 5:95 results are also in close agreement, though with slightly greater differences (<10%) near stoichiometric mixtures.

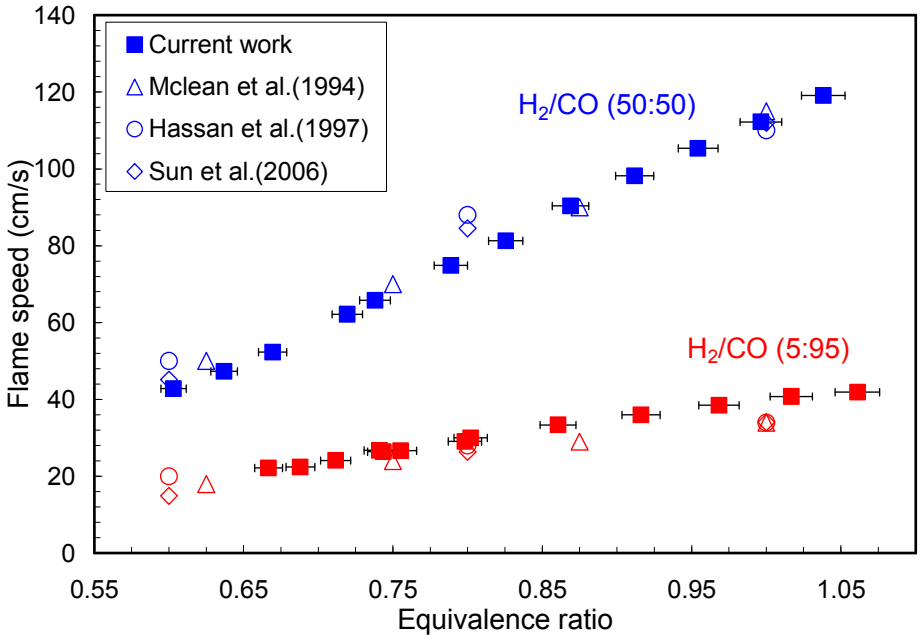

Figure 4.2. Measured laminar flame speeds in Bunsen flame for H_2:CO 50:50 and 5:95 compositions at p=1atm and T≅300K, including previous spherical flame experiments [11,14,15].

4.1.2 Elevated pressure

Experiments were conducted for a 50:50 H_2/CO fuel mixture at 10 atm. To match the previous study's conditions, a O_2:He mixture (1:7 by volume) was used as the oxidizer, rather than standard air, in order to suppress the hydrodynamic and thermo-diffusive instabilities that become prominent at elevated pressure conditions for H_2/CO fuel mixtures. Figure 4.3 shows the comparison between the current and previous measurements for a range of equivalence ratios (0.6 to 1.2). The measurements with the current approach are again in good agreement (<10%) with the previously obtained, stretch-corrected values over most of the range of equivalence ratios tested.

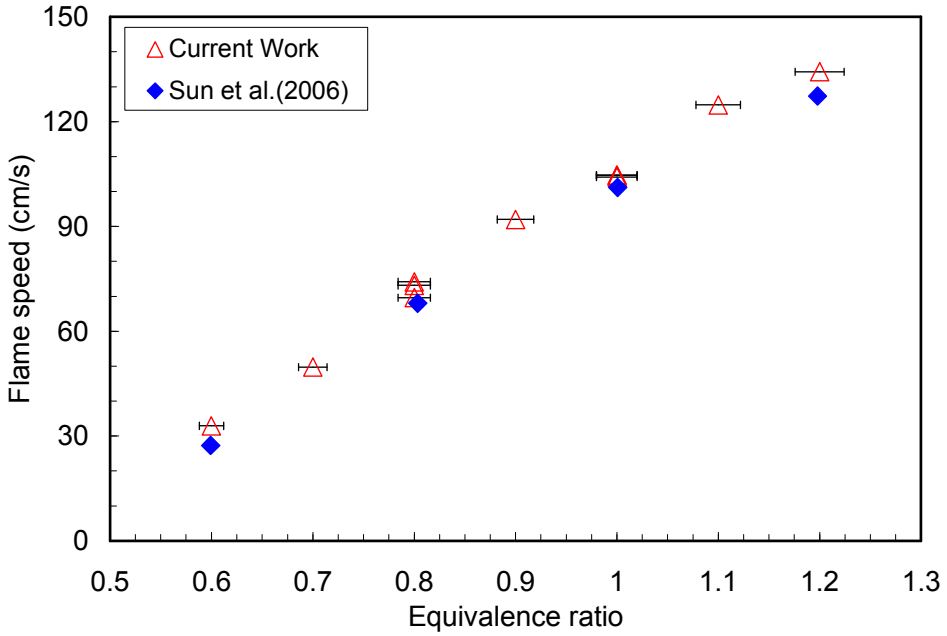

Figure 4.3. Comparison of measured laminar flame speeds obtained with conical flame and spherical flame [15] approaches for a 50:50 H_2/CO fuel mixture (O_2:He 1:7 oxidizer) at p=10 atm and T_u=300K.

Overall, these comparisons indicate that the systematic errors associated with this modified Bunsen flame approach based on reaction-zone-area are small, and the

technique should be reasonably accurate for a range of lean H_2/CO fuel mixtures and operating conditions. Hence this approach is used for measurements at a wide range of conditions due to its simplicity, while the stagnation flame approach is utilized to determine flame speeds and strain sensitivities at limited conditions.

4.2 Atmospheric pressure results

The effects of reactant preheat temperature at atmospheric pressure are examined for three H_2:CO compositions: 95:5, 50:50 and 5:95 ratios by volume. These compositions were chosen in order to cover a broad range of syngas mixture variations, and to aid in validation (or improvement) of syngas flame speed models.

4.2.1 Room temperature flame speeds

Laminar flame speeds were measured using the Bunsen flame approach for the three compositions at room temperature and a range of lean equivalence ratios (0.6-1.0). A burner diameter of 4.5 mm was used for the 95:5 and 50:50 mixtures, and 13.6mm for the 5:95 case. The measurements are shown in Figure 4.4. The horizontal error bars on the measured data indicate the systematic uncertainty in the equivalence ratio associated with the flow metering uncertainties. In general, the measured flame speed increases with the amount of H_2 in the fuel mixture, with the 95:5 mixture having flame speeds roughly four or five times higher than the 5:95 mixture. Also, as expected, flame speeds increase (nearly linearly) as the mixture becomes richer.

The flame speeds predicted by the two models (GRI Mech 3.0 and the Davis *et al*. H_2/CO mechanism) are also included in Figure 4.4. Comparing the measurements with the model predictions, remarkable agreement (~5% or less discrepancy) is observed for

the medium H_2 content (50:50 H_2:CO) fuel mixture over the complete (lean) equivalence ratio range tested. At very lean conditions, the GRI Mech 3.0 predictions are slightly lower than the measurements, while the H_2/CO mechanism predictions are slightly higher. Both models slightly underpredict the data at near stoichiometric conditions, though the difference is likely less than the uncertainty in the measurement approach. Similarly for the low H_2 content (5:95 H_2:CO) fuel mixture, both models predictions are essentially the same and they are in good agreement (within 5-7%) with measurements for all the lean conditions tested.

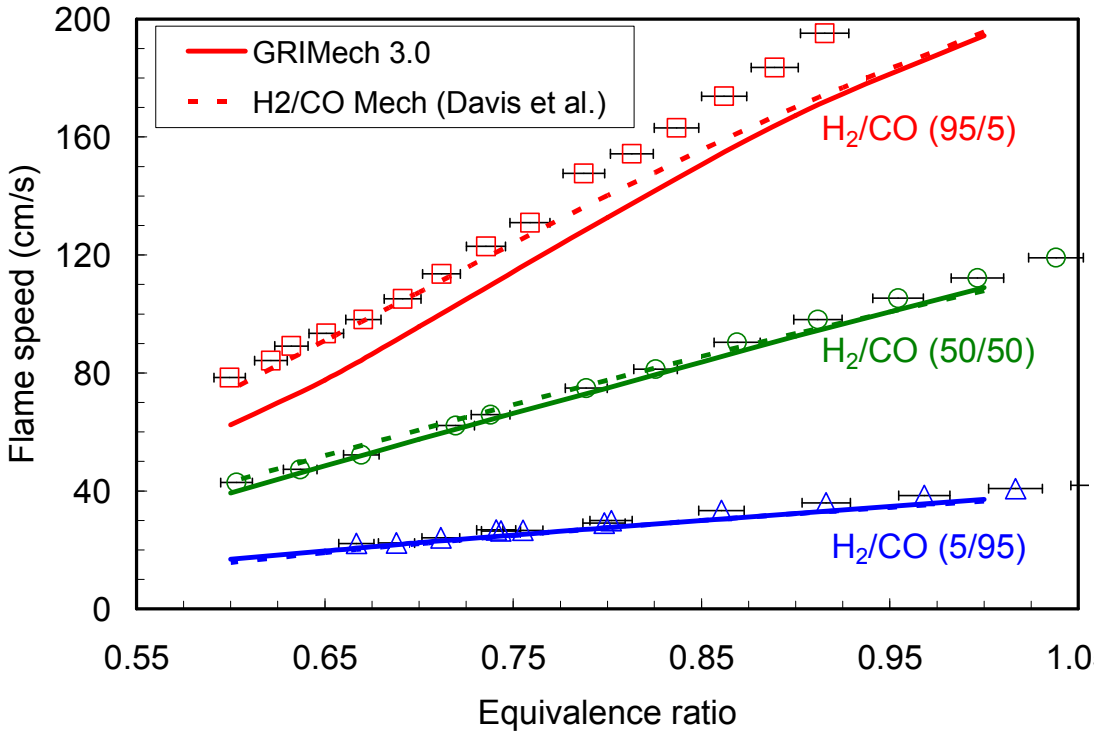

Figure 4.4. Measured and models predicted laminar flame speeds for three H_2:CO compositions at p=1atm and T_u≅300K; Bunsen flame measurements (symbols) and PREMIX predictions (lines).

As opposed to the excellent predictive ability of the models observed for medium and low H_2 content fuel mixtures, significant differences are observed for the high H_2

content (95:5 H_2:CO) fuel. The GRI Mech 3.0 predictions are consistently lower than the measured flame speeds. The discrepancy between the GRI predictions and measurements is about 12% near stoichiometric conditions and increases to 20% as the equivalence ratio decreases to 0.6. The H_2/CO mechanism predictions are similar to those with the GRI mechanism near stoichiometric conditions, but unlike GRI, the deviation from the measurements decreases as the equivalence ratio is reduced. At the leanest conditions studied (Φ=0.6-0.75), the agreement between the H_2/CO mechanism predictions and measurements is excellent (within 3-4%). Hence, the laminar flame speed predictions with the H_2/CO mechanism, which was optimized for various H_2/CO mixtures including pure hydrogen, are considerably more accurate than those with GRI Mech 3.0 for high H_2 content fuel mixtures.

Overall we find that for *room temperature and atmospheric pressure reactants*, both models provide reasonably accurate predictions of laminar flame speed for low and medium H_2 content fuel mixtures. For high H_2 content fuel mixture at lean equivalence ratios, the H_2/CO mechanism predictions are in better agreement with measurements.

To explore the temperature dependence of the flame speed, experiments were carried out for lean mixtures with the same three H_2:CO ratios over a range of reactant preheat temperatures from 400 to 700 K. As the unburned reactant temperature increases, the flame speed should increase due to increased chemical rates, and thermal and mass diffusivities. This increase in flame speed requires the burners to be operated at higher average flow velocities (compared to the room temperature case). Fortunately, the increase in the unburned reactant temperature also increases the viscosity of the unburned mixture, which allows the flow to remains laminar even at the higher operating velocities.

Hence, the same diameter burners used for the room temperature cases were used for the preheated cases.

4.2.2 Medium H_2 content fuels with preheat

The influence of preheat temperature for the 50:50 H_2:CO composition is shown in Figure 4.5. The measured and predicted flame speeds increase rapidly with the unburned gas temperature for any given equivalence ratio. Similar to the room temperature reactant results, the predictions from both GRI Mech 3.0 and the H_2/CO mechanism are in good agreement (within ~5%) with the measured flame speeds up to a preheat temperature of about 500 K throughout the lean equivalence ratios tested. For further increases in preheat temperature, the discrepancy between the measured and predicted flame speeds increases.

For the 600 K preheat temperature, both model predictions are consistently higher than the measured flame speeds. While the models are close (~5%) to measurements near stoichiometric conditions, they over predict the measurements as much as 15% near the leanest condition tested (Φ~0.6), with the GRI predictions being closer to the experimental data. For the highest preheat case (700 K), the simulations with GRI Mech 3.0 over predict the measured flame speeds by as much as 15% for near stoichiometric mixtures and 30% at the leanest conditions tested. The H_2/CO mechanism predictions are very similar to those found with GRI Mech 3.0 except at the leanest Φ, where the H_2/CO mechanism predictions are higher than the GRI predictions by 5%. Thus the H_2/CO mechanism has an even larger over prediction (~35%) for this 50:50 H_2:CO mixture at 700 K preheat temperature.

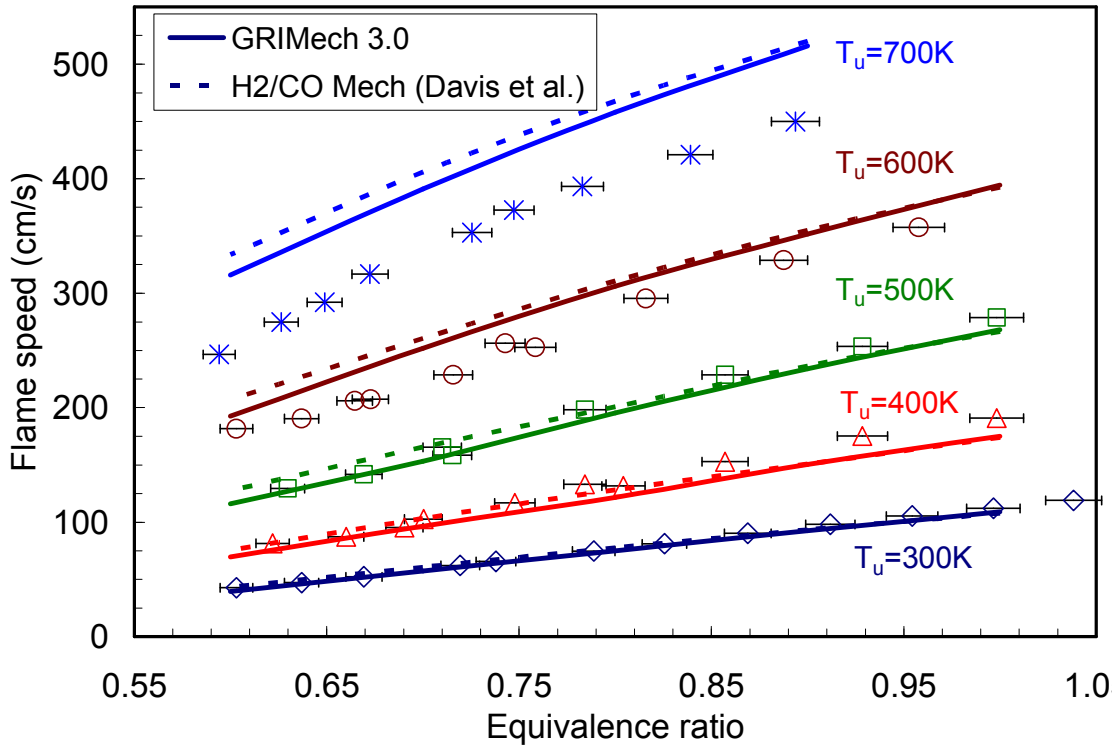

Figure 4.5. Laminar flame speed for fuels with 50:50 H_2:CO composition for various preheat temperatures at p=1atm; Bunsen flame measurements (symbols) and PREMIX predictions (lines).

To validate the results obtained with the Bunsen flame approach, the stagnation flame technique was also used to determine (strained) flame speeds for the 50:50 H_2:CO mixture at high preheat (700K) and at two equivalence ratios (0.6 and 0.8), where large discrepancies were observed between the Bunsen measurements and model predictions. Due to the very high flame speeds for these mixtures and the need for high hydrodynamic strain rate to produce a stable flame, a small nozzle diameter (6.25 mm) with L/D=0.8 was used. As seen in Figure 4.6, the measured strained flame speeds increase linearly with imposed strain rate for both equivalence ratio cases. It is important to note that the flame at Φ=0.6 is more strain sensitive than the Φ=0.8 case. This trend is expected

because of the increased flame thickness and the reduction in the concentration of highly diffusive deficient species (H_2) as the equivalence ratio is decreased.

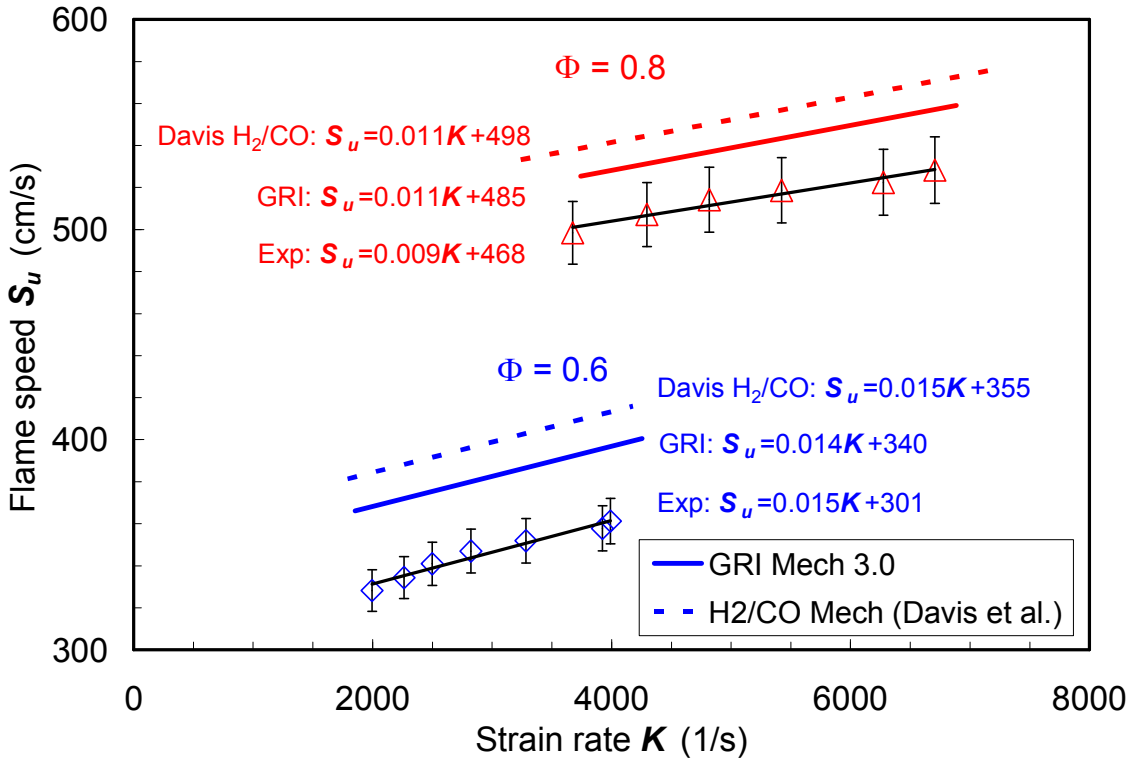

Figure 4.6. Strained laminar flame speeds for lean mixtures with 50:50 H_2:CO fuel composition at p=1atm and T=700K; stagnation flame measurements (symbols and linear fit) and OPPDIF predictions (lines).

Also shown in Figure 4.6 are the predicted strained flame speeds in the same strain range employed in the experiments for both equivalence ratios. While the predicted and measured strain sensitivities are quite similar (roughly -0.010 cm for Φ=0.8 and -0.015 cm for Φ=0.6), the strained flame speeds predicted with both mechanisms are consistently higher than the measurements for both Φ. This trend agrees with the Bunsen flame results (Figure 4.5). The GRI Mech 3.0 calculated strained flame speeds over predict the measurements by 12%, while the H_2/CO mechanism over predicts the

measurements by 17% at Φ=0.6. The predictions improve at Φ=0.8, with the GRI results over predicting the measurements by 7%, and the H_2/CO mechanism by 9%. This also agrees with the Bunsen flame results; the relative discrepancy between the measured and predicted flame speeds increase as the equivalence ratio decreases for the high preheat, 50:50 H_2:CO case. Though, the amount of over prediction is lower for the stagnation flame measurements.

In summary, flame speeds measured with two very distinct experimental techniques show that leading chemical mechanisms have difficulty predicting the temperature dependence of the flame speed for medium H_2 content syngas fuels. Specifically, the model predictions predict flame speeds that increase too rapidly with preheat temperature, especially at fuel lean conditions.

In addition it is interesting to note that the unstrained flame speeds based on linearly extrapolating the stagnation flame data to zero strain are noticeably higher than the flame speeds measured with the Bunsen flame method. For example at Φ=0.6, the unstrained flame speed obtained from the stagnation data (Figure 4.6) is 301 cm/s, which is ~20% higher than the corresponding flame speed from the Bunsen data (250 cm/s, Figure 4.5). As noted previously, however, linearly extrapolating strained flame speeds is known to over predict the true unstrained flame speed (see Figure 3.13). This occurs in the model predictions as well as the experiments. For example for the same Φ=0.6 case, the GRI predicted linearly extrapolated unstrained flame speed (340 cm/s, Figure 4.6) is higher by ~8% than the unstrained flame speed (316 cm/s, Figure 4.5) predicted with PREMIX (a similar level of discrepancy is observed for the H_2/CO mechanism).

Hence for a more appropriate comparison between the two measurement approaches, we can estimate the systematic error associated with extrapolating to zero strain from the modeling results (~8% at Φ=0.6). Correcting the measured extrapolated value of 301 cm/s for the Φ=0.6, 700 K case yields an unstrained flame speed of ~280 cm/s, which is within ~10% of the value obtained with the Bunsen approach. This further supports the accuracy of the conical Bunsen flame approach developed as part of this effort (i.e., using the reaction zone to determine the flame area). Similar agreement between the two measurements techniques is observed for the Φ=0.8 case as well. The consistently lower flame speeds obtained from the Bunsen measurements may result from the increased flame thickness (and possibly chemiluminescence zone thickness) associated with high preheat temperature. This would lead to a bias in determining the reaction zone flame area for the Bunsen approach that would cause a measurement lower than the true flame speed.

4.2.3 Low H_2 content fuels with preheat

Figure 4.7 shows the influence of preheat temperature on flame speed for the low hydrogen content fuel mixture (5:95 H_2:CO). As was the case for the room temperature reactants, the predictions from the GRI and H_2/CO mechanisms are essentially the same at each preheat temperature, and the measured flame speeds are higher than the predictions. The models predictions are in good agreement (~10%) with measurements for preheat temperature up to 400 K throughout the lean mixtures tested, though the agreement is slightly better at the leanest conditions. For preheat temperature above 500 K, the discrepancy between the measurements and predictions increases to 10-15%. Further, the agreement between the measurements and predictions again improves as the

equivalence ratio drops. Because preheating improves flame stability, measurements were possible for even leaner (Φ<0.6) mixtures at high reactant temperatures (for the same burner diameter).

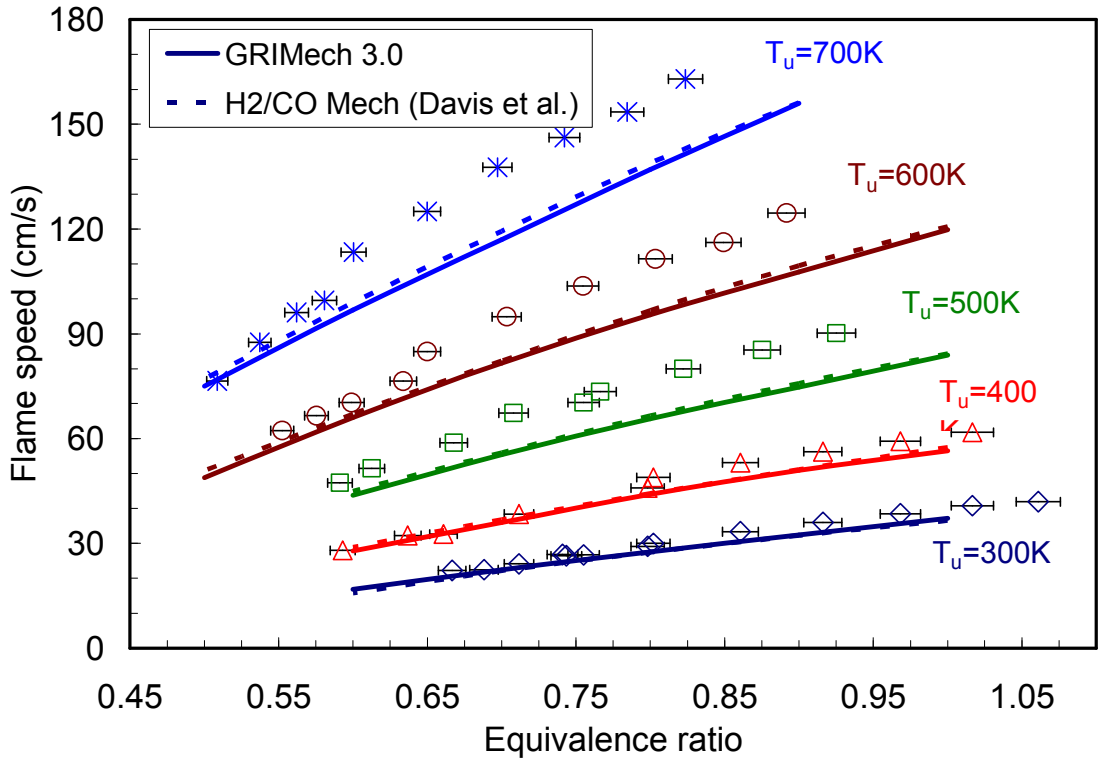

Figure 4.7. Laminar flame speed for fuels with 5:95 H_2:CO composition for various preheat temperatures at p=1atm; Bunsen flame measurements (symbols) and PREMIX predictions (lines).

Since, the measurements are in reasonable agreement with the predictions from both mechanisms for the various preheat temperatures, especially at the very lean conditions, stagnation flame measurements were not conducted for this fuel mixture. Also the systematic errors associated with the Bunsen flame approach are expected to be even less for this case compared to the 50:50 mixture. This follows from two reasons: 1) the fuel mixture is expected to be less stretch sensitive due to the low H_2 levels in the fuel

mixture, and 2) a larger burner diameter (13.6 mm) was employed, which reduces the influence of curvature on the measured flame speeds.

In summary, the predicted flame speeds are in good agreement with the measurements at very lean conditions at all temperatures. As the reactants approach more stiochiometric conditions, however, the models always tend to somewhat under predict the measurements. In general, however, the models are reasonably able to capture the dependence of the flame speed on preheat temperature.

4.2.4 High H_2 content fuels with preheat

Results for the high hydrogen content fuel (95:5 H_2:CO) are shown in Figure 4.8. As the flame speeds are extremely high (>8 m/s) for this mixture with preheating, the velocities needed to stabilize the flames are also high. To reduce the exit velocities and maintain laminar conditions, the fuel stream was diluted with 20% CO_2, thereby reducing the flame speeds. As will be made more clear in the next chapter, small amounts of CO_2 do not significantly change the agreement between the measurements and model predictions. Hence, though this fuel mixture is diluted with 20% CO_2, the results presented here mainly highlight the influences of the reactant preheat temperature.

As shown in Figure 4.8, the computed flame speeds from the two mechanisms are nearly the same at near stoichiometric conditions for all the preheat temperatures. However for lean conditions, the GRI predictions are lower than those from the H_2/CO mechanism, by as much as 30% at very lean equivalence ratios. As in the room temperature (300 K) case, the predictions with the H_2/CO mechanism are in good agreement with the experiments (within 10%) for 400 K throughout the tested

equivalence ratio range. The GRI Mech predictions, on the other hand, are lower than the measurements by as much as 30% at fuel lean conditions.

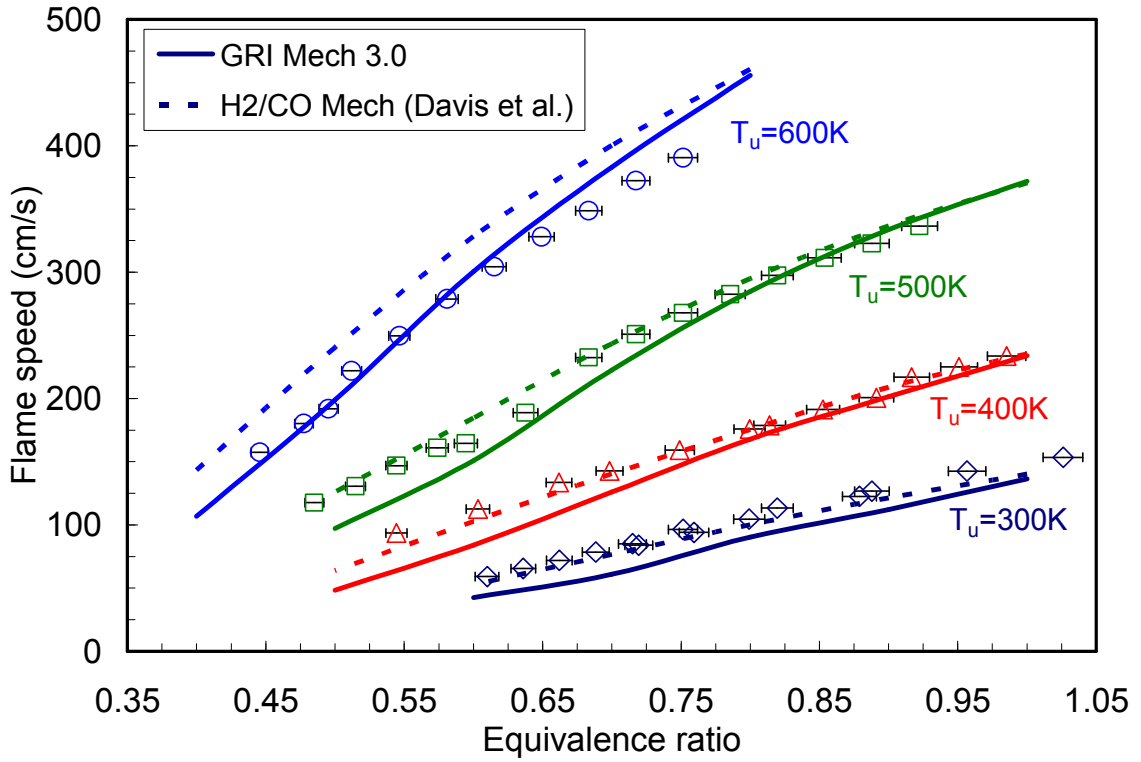

Figure 4.8. Laminar flame speed for fuels with 95:5 H_2:CO composition with 20% CO_2 dilution for various preheat temperatures at p=1atm; Bunsen flame measurements (symbols) and PREMIX predictions (lines).

As the preheat temperature increases to 500 K and above, the agreement between the GRI predictions and measurements improves, whereas the H_2/CO mechanism begins to over predict the measurements especially at fuel lean conditions. For example, at 600 K preheat, the H_2/CO mechanism over predicts the measurements by as much as 20% at Φ=0.45 while the GRI results are now better able to reproduce the measurements. Given the poorer prediction with the GRI mechanism at lower temperatures, the improved agreement at high preheat temperatures may simply be fortuitous.

In summary for high H_2 content fuel mixtures, the predicted flame speeds from both models increase with preheat temperature faster than the measured flame speeds, especially at very lean conditions. This trend is identical to the behavior observed for medium H_2 content fuel mixtures.

4.2.4.1 Pure H_2 at elevated preheat temperature

In order to verify this observed trend with the Bunsen flame measurements for high H_2 fuel mixtures, strained flame measurements at high preheat were also performed. Specifically, stagnation flame data were acquired for pure H_2 fuels at very lean equivalence ratios. As the enhanced temperature dependence of the model predicted flame speeds is mainly observed for medium and high H_2 content fuel mixtures, it is likely that the sources of error is in the H_2 oxidation rather than the CO oxidation model. Hence for better understanding, a recently updated comprehensive kinetic model for hydrogen combustion (the H_2 mechanism of Li *et al*. [36]) has been included in the analysis.

Strained flame speeds for highly preheated H_2-air mixtures were measured for very lean conditions (Φ=0.3 and 0.5). The 6.25 mm diameter burner diameter was used with a stagnation surface spacing of L/D=0.8. The measured and predicted strained flame speeds for various strain rates at Φ=0.3 and 700 K preheat temperature are shown in Figure 4.9. As seen in the medium H_2 results, the strained flame speeds increase linearly as the imposed strain rate increases. The H_2/CO and H_2 mechanisms over predict the measurements by 10% and 16%, respectively, for the investigated strain rate range, while the GRI mechanism predictions fall below the measurements by about 6%.

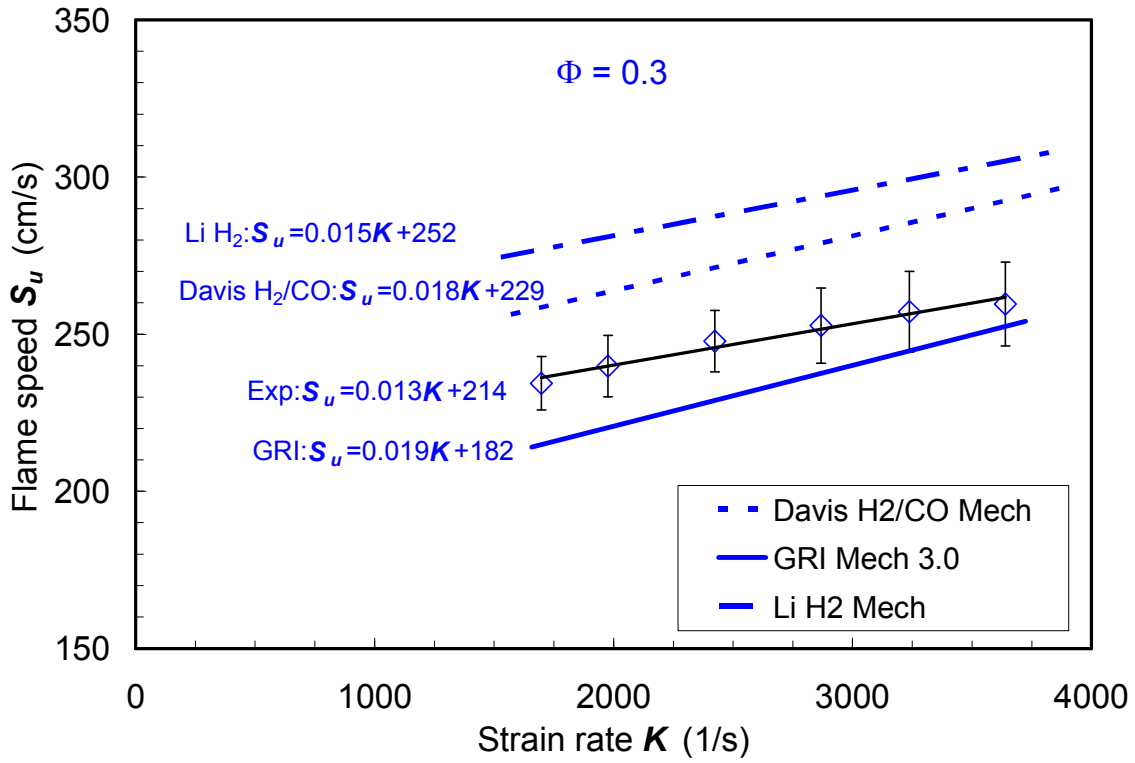

Figure 4.9. Strained laminar flame speeds for mixture of H_2 with air at Φ=0.3 and 700 K preheat temperature; stagnation flame measurements (symbols and linear fit) and OPPDIF predictions (lines).

These discrepancies should be compared to the estimated uncertainties in the measurements and modeling. The measurement precision, as indicated by the error bars in Figure 4.9, is within ~3% for most of the measurements. As described in the previous chapter, uncertainties in the wall and nozzle boundary conditions between the experiments and the 1-d simulations could lower the model results by no more than ~2-3%. Thus the differences between the numerical and experimental results are larger than the combined uncertainty of ~4%. Yet the differences are not too large (mostly within ±10-15%), so it can be concluded that the model predictions are in reasonable agreement with the measurements. The predicted strain sensitivities (the negative of the slopes in the

equations of Figure 4.9) from all the models are similar (-0.015 to -0.019 cm), and they are in reasonable agreement with the measured strain sensitivity (-0.013 cm), though somewhat higher (by 15-50%).

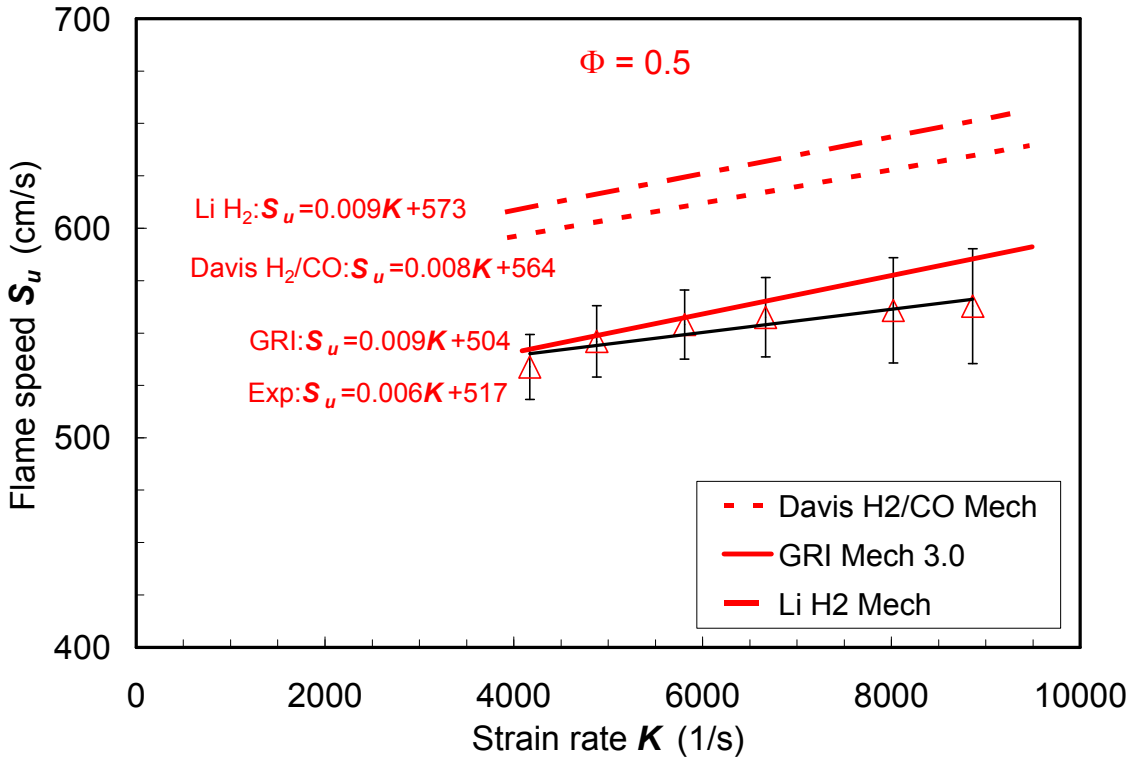

Figure 4.10. Strained laminar flame speeds for mixture of H_2 with air at Φ=0.5 and 700 K preheat temperature; stagnation flame measurements (symbols and linear fit) and OPPDIF predictions (lines).

The measured and predicted flame speeds for various strain rates at Φ=0.5 are shown in Figure 4.10. The unstrained flame speed from the linearly extrapolated measurements is 517 cm/s, and the measured strain sensitivity is -0.006 cm. Comparing to the Φ=0.3 case, the unstrained flame speed increases, and the strain sensitivity decreases, as expected for the richer mixture. Similar to the medium H_2 content data (see Figure 4.6), the decrease in the strain sensitivity is attributed to the decrease in the flame

thickness and also the increase in the concentration of the highly diffusive deficient species (H_2) as the equivalence ratio increases.

The strained flame speeds predicted by the GRI mechanism are now in excellent agreement with the measurements. As with the leaner mixture, the H_2/CO and H_2 mechanisms over predict the measured flame speeds, by 12% and 15% respectively, about the same amounts as in the Φ=0.3 case. The predicted strain sensitivities are even closer to one another in this case (-0.08 and -0.09 cm) and are again somewhat higher (by 30-50%) than the measured strain sensitivity (-0.06 cm).

Overall the agreement between the measurements and the predictions is good for the lean H_2 mixtures at *elevated* preheat temperature, with the GRI mechanism appearing to provide results that are in somewhat better agreement than the other two mechanisms. The flame speed results from the H_2 and H_2/CO mechanisms over predict the measurements, though the H_2 mechanism tends to over predict the measured flame speeds slightly more. It should be noted here that this result is very similar to the observations from the Bunsen flame measurements (see Figure 4.8). Specifically that at elevated preheat temperature and lean conditions, the predictions from GRI are in better agreement with measurements while the H_2/CO mechanism over predict the measured flame speeds.

4.2.4.2 Pure H_2 at room temperature

To elucidate the effect of preheat temperature on these observed discrepancies between the experiments and modeling, it is important to consider the models' performance at low preheat temperature. To this end, the predicted unstrained laminar flame speeds (from PREMIX) at room temperature are compared with measured,

unstretched laminar flame speeds from Egolfopoulos *et al.* [40] for pure H_2 at essentially the same equivalence ratios considered in the high preheat results presented above. In their work, the unstretched laminar flame speed is calculated by linear extrapolation of the measured strained flame speeds determined in a counter-flow flame arrangement.

The ratio of the predicted unstrained flame speeds to the measured (linearly extrapolated) values, for all three models, are shown in Figure 4.11 for both elevated preheat temperature (700 K) and room temperature reactants (300 K). For the elevated preheat temperature, the models only slightly under or over predict the measurements. Hence the predicted/measured flame speed ratio is close to unity. On the other hand, Figure 4.11 reveals that all three models significantly under predict the experimental results for the room temperature reactants.

The H_2 mechanism, which was the farthest from the data at high preheat, now produces results that are closest to the measured room temperature flame speeds (15% too low at Φ=0.5). The GRI mechanism, which produced predictions closest to the high temperature flame speeds, has the greatest discrepancy at room temperature, under predicting the measurements by 35% at Φ=0.5. In addition, the amount of under prediction increases as the mixture becomes leaner for all three models. For example, the H_2/CO mechanism under predicts the measurements by 20% at Φ=0.5 and 60% as the equivalence ratio decreases to 0.35. From comparing the low and high temperature results, it is evident that the predicted flame speeds increase with preheat temperature faster than the measured values, and the good agreement with the measurements at 700 K is somewhat fortuitous.

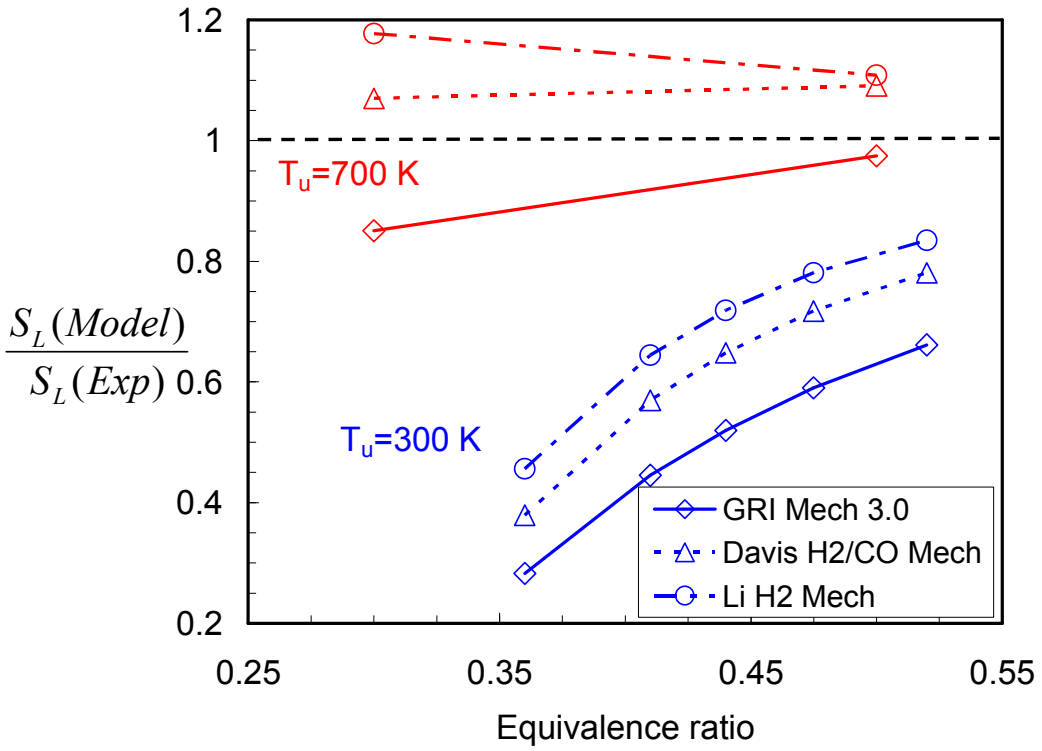

Figure 4.11. Ratios of the models predicted (PREMIX) and measured unstrained laminar flame speeds for lean mixtures of H_2 with standard air at 300 K and 700 K preheat temperatures.

Thus the atmospheric pressure results indicate that the predictive capability of the current models is poor at very lean equivalence ratios for medium and high H_2 content mixtures. In particular, the models over predict the temperature dependence of the measured flame speed as verified by two independent measurement approaches. Next, we examine the influence of pressure on this observed higher temperature dependence.

4.3 Elevated pressure results

As discussed in the previous chapter, flame speed measurements at elevated pressure were performed with O_2:He mixture as the oxidizer to suppress the hydrodynamic and thermo-diffusive instabilities that become prominent at elevated

pressure conditions especially for lean H_2/CO fuel mixtures. In order to have flame speeds comparable to those obtained with standard air, but with lower flame temperatures, an O_2/He mixture with a 1:9 volumetric ratio was chosen for all the test conditions considered in this study.

Since the GRI mechanism was not optimized for reactant mixtures containing He, the C_1 mechanism of Li *et al.* is considered together with H_2/CO mechanism of Davis *et al.* for elevated pressure conditions. Like the GRI and H_2/CO mechanisms, the C_1 mechanism also over predicts the temperature dependence of the measured flame speeds for medium and high H_2 content fuel mixtures at atmospheric pressure, in fact with a slightly higher degree of over prediction than the other two models. To demonstrate this, atmospheric pressure results for the 50:50 H_2:CO fuel mixture at various preheat temperatures are presented again in Figure 4.12, but now compared to the predictions from the C1 mechanism.

Similar to the GRI and H_2/CO mechanisms predictions (see Figure 4.5), the C1 mechanism predictions are in good agreement (within ~10%) up to a preheat temperature of about 500 K. For further increase in preheat temperature, the discrepancy between the measured and predicted flame speeds increases rapidly. Recall that the H_2/CO mechanism over predicts the measured flame speeds by ~15% at the 600 K preheat temperature for lean mixtures below Φ~0.7; the C_1 mechanism over predicts the measurements even more (by 20-25%) for the same conditions. As the preheat temperature increases further to 700 K, the C_1 mechanism over predict the measured flame speeds by as much as 20% near stoichiometric conditions and by 40% at the leanest conditions tested, while the H_2/CO mechanism over predictions were 15% (stoichiometric) and 35% (leanest mixture)

higher at those respective conditions. Thus, the C_1 mechanism is also found to over predict the temperature dependence of the measured flame speed at atmospheric pressure and fuel lean conditions.

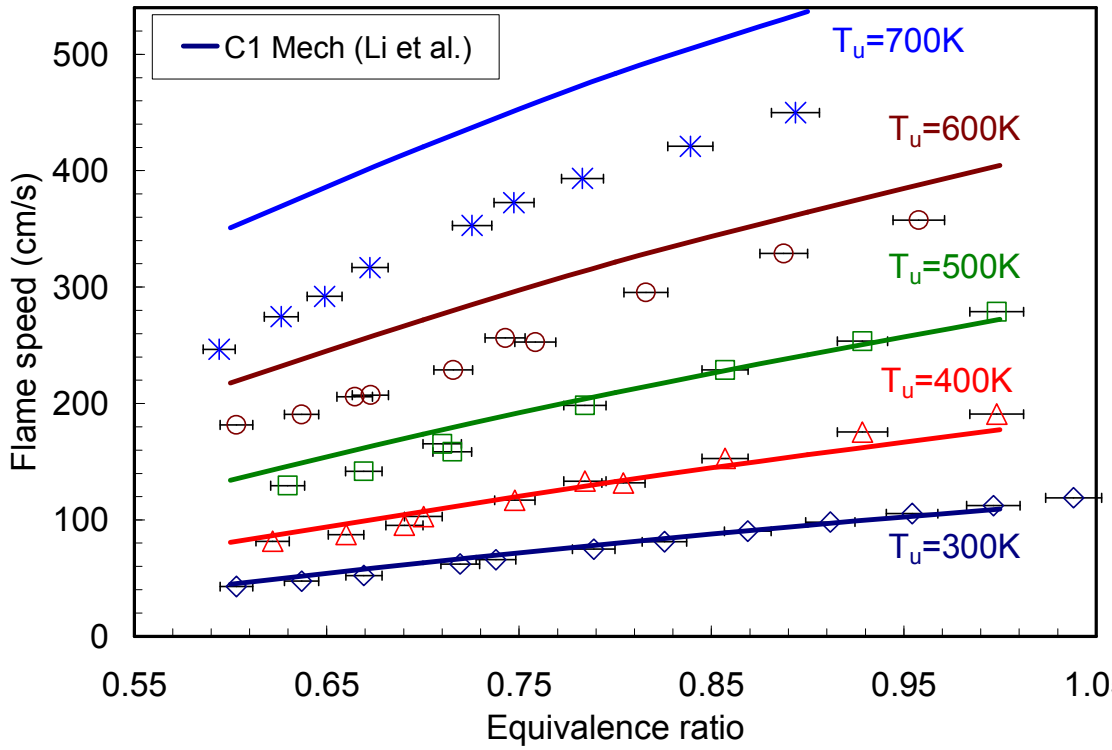

Figure 4.12. Laminar flame speed for fuels with 50:50 H_2:CO composition for various preheat temperatures at p=1 atm; Bunsen flame measurements (symbols) and PREMIX predictions (lines).

A slightly different approach was adopted for selecting the mixture composition for elevated pressure conditions. Since the focus of the present study is lean fuel mixtures, the equivalence ratio was kept constant while changing the H_2/CO ratio from 20:80 to 80:20. As noted in Chapter 2, varying the H_2/CO ratio at a fixed equivalence ratio does not change the flame temperature much (~ within 100 K), since H_2 and CO produce similar amounts of heat release. In order to elucidate the effect of preheat temperature at elevated pressures, experiments were conducted for room temperature

(300 K) and elevated preheat temperature reactants (600 K) over a wide range of H_2/CO ratios (20-80% H_2) at 15 atm. The equivalence ratio was adjusted at each preheat temperatures in order to achieve nearly the same adiabatic flame temperature in order to isolate the effect of preheat temperature.

4.3.1 Elevated preheat temperature

The first set of results, as presented in Figure 4.13, were conducted at high preheat temperature (600 K) and a fixed equivalence ratio of 0.6. The adiabatic flame temperature varies only slightly as the amount of H_2 changes from 20 to 80% (~1850 to 1780 K).

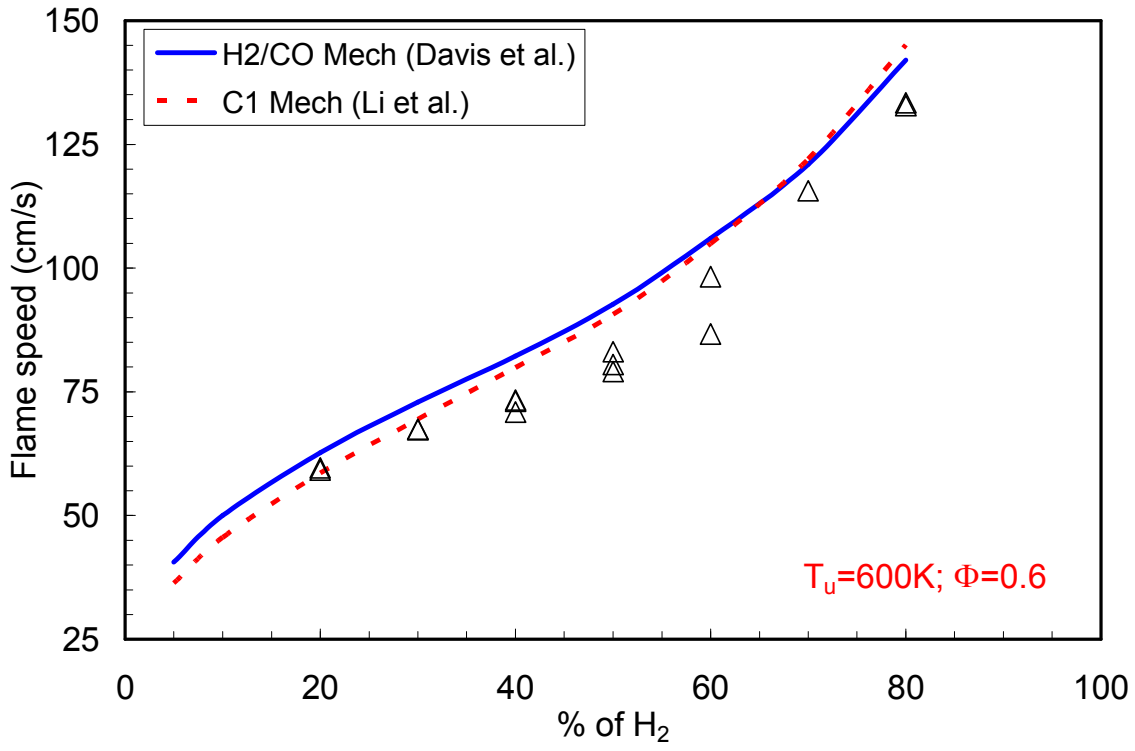

Figure 4.13. Laminar flame speeds for a range of H_2/CO fuel mixtures (O_2:He 1:9 oxidizer) at a fixed equivalence ratio of 0.6, p=15 atm and T_u=600 K; Bunsen flame measurements (symbols) and PREMIX predictions (lines).

The measured and model predicted flame speeds increase rapidly with the amount of H_2 in the fuel mixture, especially as the amount of H_2 increases above 50%. Both models predict essentially the same flame speeds for mixtures with more than 50% H_2, but the H_2/CO mechanism predictions are slightly (~10%) higher compared to the C_1 mechanism's as the amount of H_2 in the fuel mixture drops to 10%. The models consistently over predict the measured flame speeds; the C_1 mechanism predictions are in better agreement (~5%) with the measurements for low H_2 content (up to 30%). As the amount of H_2 increases to medium levels (40-60%), the discrepancy between the models and measurements increases, with the models over predicting the measurements by 10-15%. For further increases in H_2 content (above 70%), the model predictions are again in good agreement with the data. The small discrepancy (less than 10%) between any two measurements at a given amount of H_2 in the fuel mixture is due to the change in: 1) the burner diameter, or 2) the average velocity of the reactants at the exit of the nozzle, which alters the curvature and strain on the flame surface and hence the measured flame speed slightly.

4.3.2 Room temperature (no preheat)

To examine the temperature dependence of the laminar flame speed, experiments were also conducted for room temperature reactants at a fixed equivalence ratio of 0.8. The equivalence ratio was increased from the preheated case (Φ=0.6), in order keep the flame temperatures similar for both cases. The variation in the adiabatic flame temperature as the amount of H_2 changes from 20 to 80% is 1890 to 1810 K (compared to an average flame temperature of 1820 K for the preheated data presented in Figure 4.13).

The measured and predicted flame speeds are presented in Figure 4.14 as a function of H_2 content in the fuel mixture.

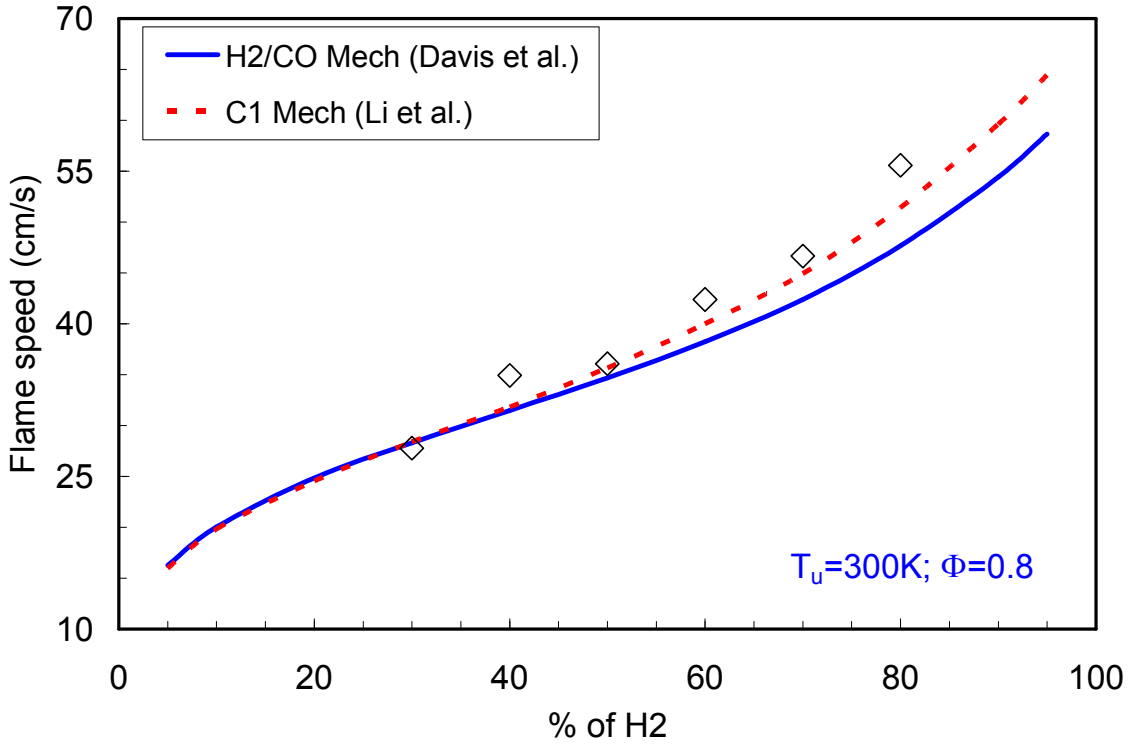

Figure 4.14. Laminar flame speeds for a range of H_2/CO fuel mixtures (O_2:He 1:9 oxidizer) at a fixed equivalence ratio of 0.8, p=15 atm and T_u=300 K; Bunsen flame measurements (symbols) and PREMIX predictions (lines).

Unlike the preheated case, both models predict essentially the same flame speeds for H_2 content *below* 50%, while the H_2/CO mechanism predicts slightly (~10%) *lower* flame speeds than the C_1 mechanism for H_2 content above 50%. Comparing the model predictions with the measurements, we find that the model predictions tend to *underpredict* the measurements (except for low H_2 content mixtures) – this is the opposite trend found for the 600 K preheat temperature. The C_1 mechanism predictions are generally closer to the measured flame speeds (within ~5% for 30-70% H_2), while the H_2/CO mechanism predictions under predict the measurements by about 10%. As the

amount of H_2 in the fuel mixture increases to 80%, the amount of under prediction increases to 10% for the C_1 mechanism and 15% for the H_2/CO mechanism.

Thus we find that for low amounts of H_2 in the fuel mixture (below ~30%), the models predictions are in good agreement with the measurements at both preheat temperatures. As the amounts of H_2 increases to medium levels (~40-60%), the models are able to reasonably predict the low preheat temperature flame speeds, but over predict the measurements at elevated preheat temperature. This trend is very similar to the atmospheric results presented in (Figure 4.5). For the high H_2 content fuels (>70% H_2), the models *under* predict the measurements at low preheat temperature, and slightly *over* predict the measurements at elevated preheat temperature. Again this trend is consistent with the previous atmospheric pressure studies for the high H_2 content fuels (Figure 4.8).

Hence, it is clear from Figure 4.13 and Figure 4.14 that there is a higher temperature dependence of the predicted flame speeds compared to the measured values for medium and high H_2 content fuel mixtures. The enhanced temperature dependence is, however, less pronounced at high pressure compared to atmospheric pressure (see Figure 4.5 and Figure 4.8).

Possible sources of this discrepancy are errors in the rate constant expressions used for one or more reactions in the mechanism, or errors in the thermophysical and transport properties of various species. It is unlikely that the problem likes in the thermophysical and transport properties, since their temperature dependence is known to a relatively high accuracy. Thus the most likely cause for the observed discrepancies should be the uncertainty in the reaction rate parameters of one or more reactions.

4.4 Sensitivity analysis

To identify the relevant reactions that are possibly responsible for the observed higher temperature dependence, sensitivity analysis was performed using the Chemkin package at conditions where larger discrepancies are observed. Sensitivity analysis provides the first order sensitivity coefficient of the predicted flame speed with respect to variations in the magnitude of the pre-exponential rate constant. Chemkin reports the normalized sensitivity coefficient (s_i) for each i^{th} reaction which is defined as,

$$s_i = \frac{A_i \partial S_u}{S_u \partial A_i}$$

where A_i is the pre-exponential factor of the i^{th} reaction and S_u is the calculated unburned flame speed.

4.4.1 Medium H_2 content fuels

Sensitivity analysis was performed for a 50:50 H_2/CO fuel mixtures at atmospheric pressure for two conditions: 1) room temperature (~300 K) reactants at an equivalence ratio of 0.8, where the measurements are in good agreement with models predicted flame speeds; and 2) elevated preheat temperature (~700 K) reactants at an equivalence ratio of 0.6, where the models significantly over predict the measured flame speed. The two equivalence ratios were chosen to keep the flame temperature nearly constant at ~2200 K. The C_1 mechanism of Li *et al*. is considered for this analysis and the calculated normalized sensitivity for all the important reactions (with normalized sensitivity in $O(0.1)$) are presented in Figure 4.15.

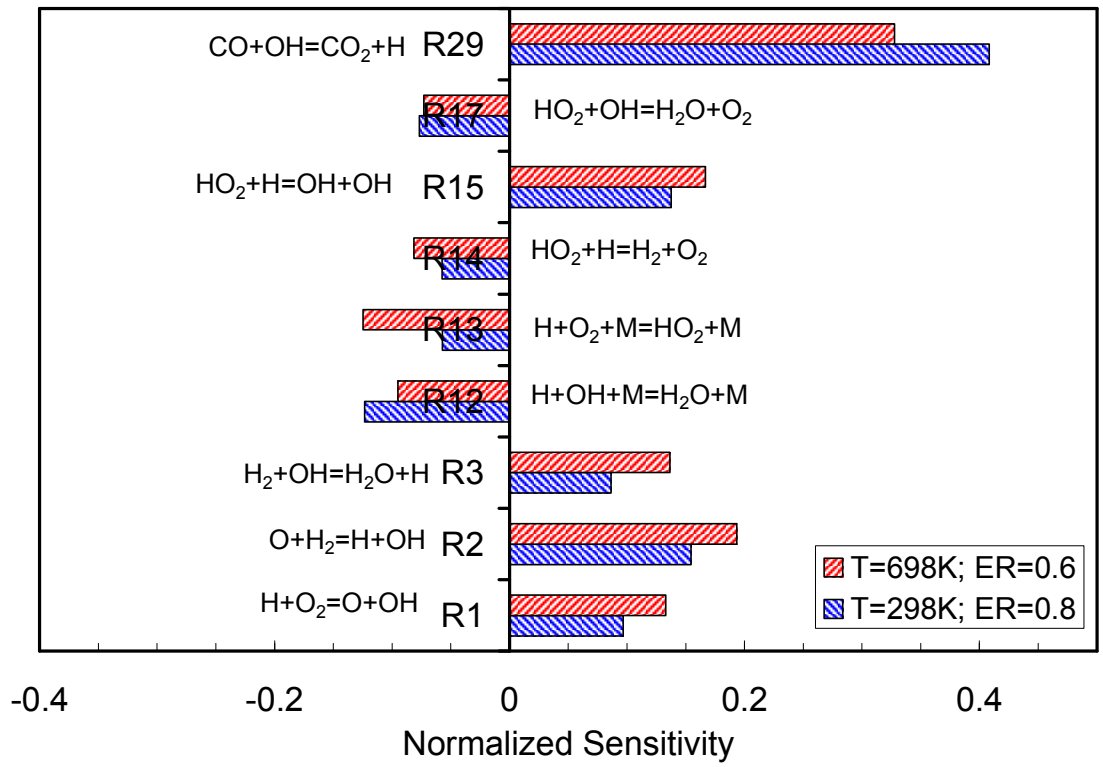

Figure 4.15. Normalized sensitivity coefficients of the laminar flame speed to the pre-exponential rate constants. The fuel mixture is 50:50 H_2/CO and the oxidizer is standard air.

A positive sensitivity coefficient indicates that the flame speed increases with an increase in the rate constant. As expected, the chain branching reactions (R1, R2 and R15) are positively sensitive to the flame speed, while the chain termination reactions (R12, R13, R14 and R17) are negatively sensitive. It is interesting to note that the only sensitive reaction in CO chemistry is the main CO oxidation reaction (R29). Though it has the highest sensitivity, this may not be the cause for the observed higher temperature dependence as the predictive capability of the models is good for predominantly CO content fuel mixtures for a range of preheat temperatures and pressure. As the observed, higher temperature dependence of the modeled flame speeds is mainly for medium and high H_2 content fuel mixture, it is more likely that the source of error is in the H_2

oxidation model. In general, the magnitude of the sensitivity coefficient of most of the H_2 oxidation reactions increases as the preheat temperature increases. More importantly, the magnitude of the normalized sensitivity of the chain termination reaction (R13) $H+O_2+M \leftrightarrow HO_2+M$ doubles as the preheat temperature increases. In the flame structure of H_2 flames (figure from Chapter 2), this reaction is one of the two major heat release reactions in the H radical consumption layer (i.e., the early part of the flame, with temperatures normally ranging from 300 to 1200 K). The other major heat release reaction in the H consumption layer is the HO_2 destruction reaction (R15) $HO_2+H \leftrightarrow OH+OH$, which is also found to be very sensitive for flame speed prediction (see Figure 4.15). As these two reactions depend on the H radical concentration, they are directly linked with the dominant H production reaction (R3) $H_2+OH \leftrightarrow H_2O+H$, which is also the main heat release reaction in the H production layer and important to flame speed prediction. To elucidate the effect of preheat temperature on these reactions, the reaction rates of the three reactions are plotted against the local flame temperature (Figure 4.16) for both room temperature and elevated preheat temperature reactants.

For room temperature reactants, the distinct zones of H consumption (where R13 and R15 dominates) and H production (where R3 dominates) can be seen distinctly. In the H consumption region, the formation of HO_2 through R13 starts as early as 400 K, followed by HO_2 destruction through R15. This is a very important reaction as it produces two OH radical, which enhances the H production through R3 in the H production zone in the temperature region range of 900 K to 1300K. The H radicals produced through R3 diffuse to the low temperature region (H consumption zone) to form HO_2 through R13 and complete the cycle. Thus, for flames with significant amount

of H_2, reactions occur at almost all temperatures and a significant amount of heat release can occur even very early in the flame structure. Moreover, the H consumption zone can be thought of as a preheat zone, and the H production zone as a reaction zone for conventional high activation energy flames.

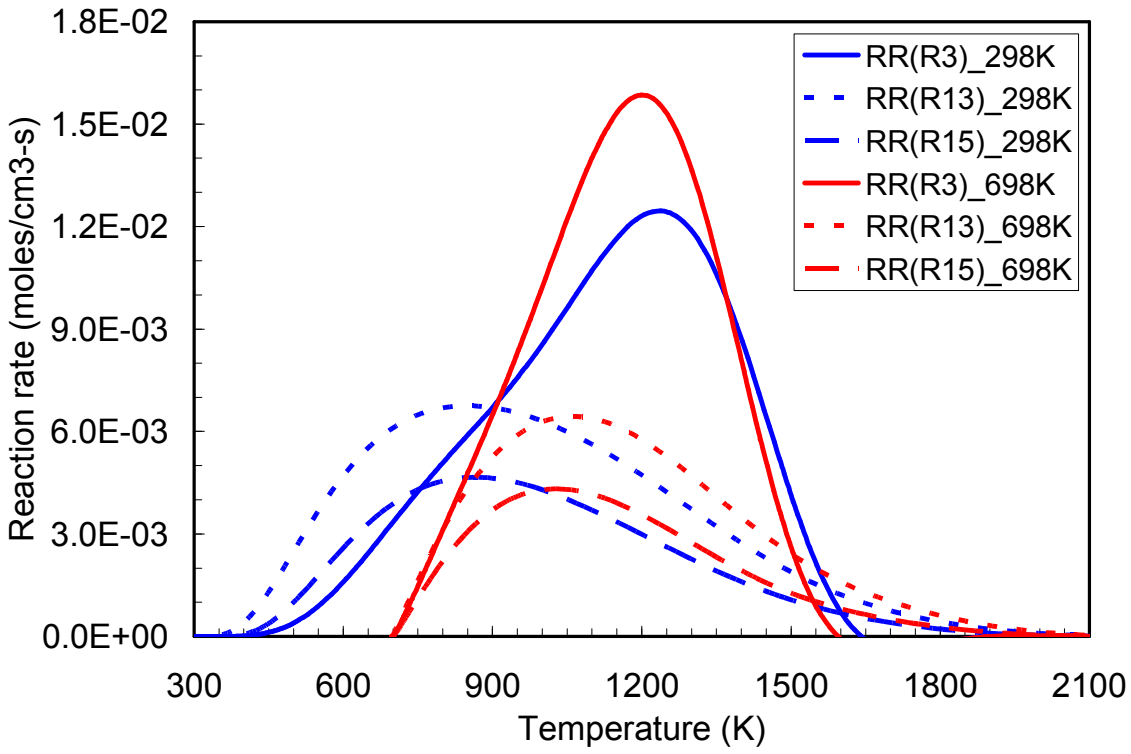

Figure 4.16. Variation of the reaction rates for R3, R13 and R15 reactions in the H production and consumption layers for preheated and room temperature reactants. The fuel mixture is 50:50 H_2/CO and the oxidizer is standard air.

As the preheat temperature increases to 700K, as shown in the Figure 4.16, the balance between the H production and consumption zones is affected. The H consumption layer moved to higher temperature and coincides with the H production layer. It should be recalled here that all the models are optimized only for room temperature reactants, and hence the changes in early part of the flame was not modeled rigorously. Any errors in modeling the rates of these reactions in the intermediate

temperature range (~800K to 1200K) could lead to increasing problems as the preheat temperature increases. Correspondingly the sensitivity analysis predicts higher dependence of the flame speed on these reactions as the preheat temperature increases.

The predicted sensitivity coefficients determined above can be combined with the estimated uncertainties in reaction rates to calculate the combined uncertainty of the model predictions for flame speed. The combined fractional uncertainty on the computed flame speed is defined as the root-sum-squares of the contribution from individual reactions and it is given by [41],

$$\frac{\sigma_{S_u}}{S_u} = \left[\sum \left(s_i \frac{\sigma_{A_i}}{A_i} \right)^2 \right]^{\frac{1}{2}}$$

where σ_{S_u} is the uncertainty in the computed flame speed and σ_{A_i} is the reported uncertainty in the i^{th} reaction rate constant's pre-exponential factor.

As discussed earlier, R3, R13 and R15 are identified as the key reactions at elevated preheat temperatures, and it is interesting to calculate the combined uncertainty on the computed flame speed only due to the uncertainties in the rate constants of these three reactions. The reported fractional uncertainties, (i.e., $\frac{\sigma_{A_i}}{A_i}$) for R3, R13 and R15 are 30, 20 and 100%, respectively [19]. Using the normalized sensitivity coefficients reported in Figure 4.15, the estimated combined uncertainty on flame speed at elevated preheat temperature is ±17% when considering only reactions R3, R13 and R15. If all the high sensitive reactions reported in Figure 4.15 are included, then the estimated combined uncertainty on flame speed increases to ±23%. Also, the main contribution among these reactions is from the HO_2 consumption reaction (R15) because of its higher sensitivity

and uncertainty in the rate constant. For comparison, the discrepancy between the measured and predicted flame speeds was 15-30% for the medium H_2 content, atmospheric pressure case. Hence this analysis shows that the models could better match the experiments at elevated preheat temperature by adjusting the rate coefficients within their uncertainty limits, mainly of the three key reactions (R3, R13 and R15).

4.4.2 High H_2 content fuels

A similar analysis was performed for pure H_2 at very lean conditions and two reactant preheat temperatures (300K and 700K), where the models were seen to predict flame speeds with higher temperature dependence than observed in the experiments (see Figure 4.11). The equivalence ratios for the room temperature and elevated preheat temperature reactants were chosen to be 0.45 and 0.3, respectively, in order to keep the same flame temperature (~1540 K) and hence isolate the effect of preheat. The predicted sensitivity coefficients of the important reactions (with normalized sensitivity $O(0.1)$) are presented in Figure 4.17.

As seen for the medium H_2 content fuel mixture, the sensitivity coefficients of all the reactions increase with the preheat temperature. More importantly, the critical reactions in the H consumption (R13 and R15) and production layers (R3) have larger sensitivity coefficients than for the medium H_2 case (see Figure 4.15). This shows that these three reactions are increasingly important as the amount of H_2 increases in the fuel mixture especially at elevated preheat temperatures (see Figure 4.17).

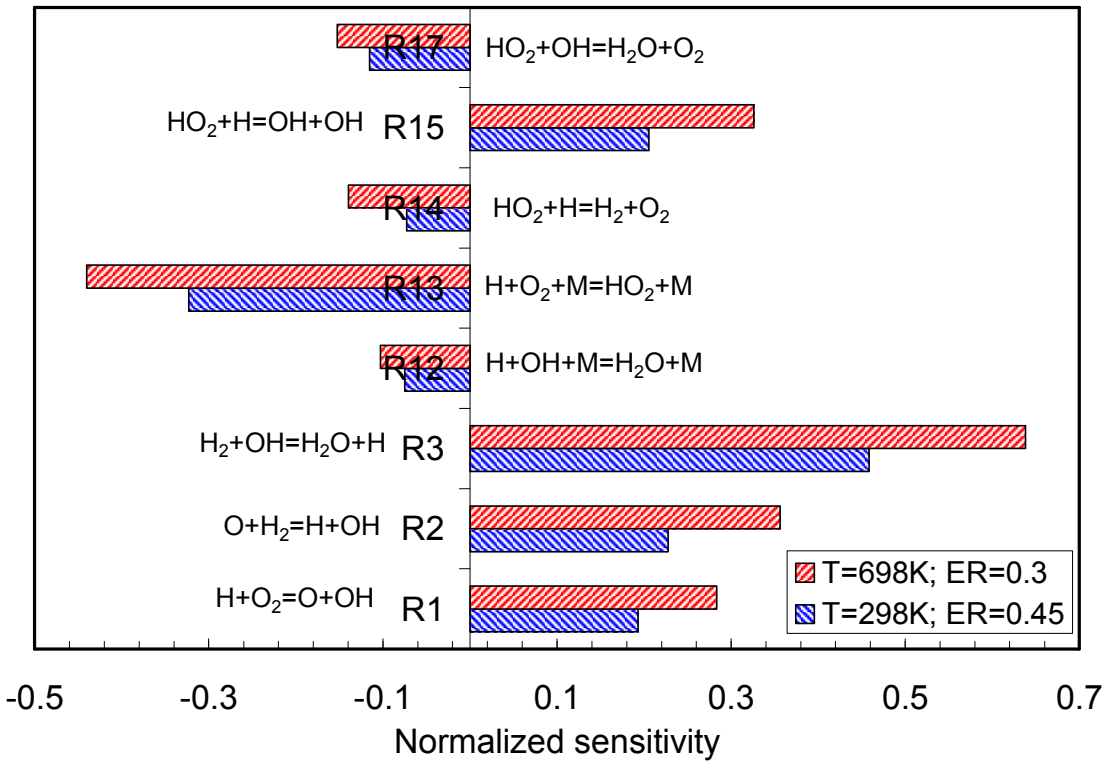

Figure 4.17. Normalized sensitivity coefficients of the laminar flame speed to the pre-exponential rate constants. The fuel H_2 and the oxidizer is standard air.

The combined fractional uncertainty of the flame speed for this case is calculated based on the uncertainties of the rate constants and the calculated sensitivity coefficients as detailed earlier. The combined uncertainty on the flame speed at elevated preheat temperature is about ±40% (using only reactions R3, R13 and R15), which is twice that of the calculated uncertainty for the medium H_2 content fuel. The combined uncertainty on the flame speed including all the sensitive reactions at elevated preheat temperature is nearly the same (about ±45%).

Thus this analysis clearly shows that the uncertainty involved with model predictions progressively increases with reactant preheat temperature, as well as with the amount of H_2 in the fuel mixtures. Since the predicted combined uncertainty on the

model predicted flame speeds is of the same order as the observed discrepancies between the measurements and model predictions, the observed discrepancies can be attributed to errors in the reaction rate constants, primarily for reactions R3, R13 and R15.

In this study, the sensitivity analysis considered changes in the pre-exponential factor alone (as is done with many optimized models, including the H_2/CO mechanism considered in this study). However, the temperature dependent parameters (e.g., activation energy) should be considered as the problem seems to be in the intermediate temperature range (~800-1200 K) for these key reactions.

CHAPTER 5

INFLUENCE OF DILUENTS

Understanding the influences of diluents on flame propagation is important as syngas fuel mixtures often contain large amounts of diluents such as CO_2, N_2 and H_2O. The presence of significant amounts of diluents in the reactant mixtures alters the flame propagation characteristics through chemical and non-chemical effects. One of the main objectives of this thesis is to examine the influence of CO_2 and N_2 addition on the laminar flame speeds and strain sensitivities for a range of syngas fuel mixtures. Experiments were conducted for a range of operating conditions with varying levels of diluents (as much as 75% of fuel) in the fuel mixture and all the measurements are compared with numerical predictions based on leading kinetic models in order to verify their predictive capabilities. The results for CO_2 dilution are presented in the first section of this chapter followed by the results for N_2 dilution. Short conclusions are provided at the end of each sub section and highlighted by underlining the text.

5.1 Effects of CO_2 dilution

As discussed in Chapter 2, CO_2 can be more than not just a passive diluent; it can also influence flame propagation through its influence on flame chemistry and radiative heat transfer. For example, the presence of significant amounts of CO_2 in the reactant fuel mixtures permits it to absorb radiative energy from the hot product gases (e.g., CO_2 and H_2O), which would alter the flame propagation. Since the flame models considered here include diluent and chemical effects, but not radiation, comparisons between the

undiluted and CO_2 diluted cases are intended to examine the influence of radiation. Experiments were conducted for a range of syngas fuel mixtures at atmospheric and elevated pressure conditions as both chemical and radiation effects associated with CO_2 dilution are expected to have significant pressure dependence.

5.1.1 Atmospheric pressure results

The effects of CO_2 dilution at atmospheric pressure are examined for three H_2:CO compositions: 95:5, 50:50 and 5:95 (volume ratios). These compositions were chosen in order to cover a broad range of syngas mixture variations.

5.1.1.1 Medium H_2 content fuel mixtures

The equally weighted, 50:50 H_2:CO, fuel mixture was tested with 20% CO_2 dilution. The burner diameter used for these mixtures was 4.5 mm. For very lean fuel mixtures, the tip of the flame becomes less intense, and hence, the knife edge was used to make the tip more visible. Figure 5.1 shows the measured flame speeds for this fuel mixture, with horizontal error bars indicating the uncertainty in the measured equivalence ratios associated with the flow metering uncertainties. Also shown in Figure 5.1, is the result for the undiluted 50:50 H_2:CO fuel mixture in order to facilitate the comparison between the diluted and undiluted cases. The flame speed increases with equivalence ratio, and decreases with CO_2 dilution. This is not surprising, as dilution in general (with excess air or CO_2) decreases the flame temperature, which reduces the rate of CO and H_2 oxidation reactions and hence flame speed. Figure 5.1 also shows the flame speeds for these mixtures computed with the two reaction mechanisms.

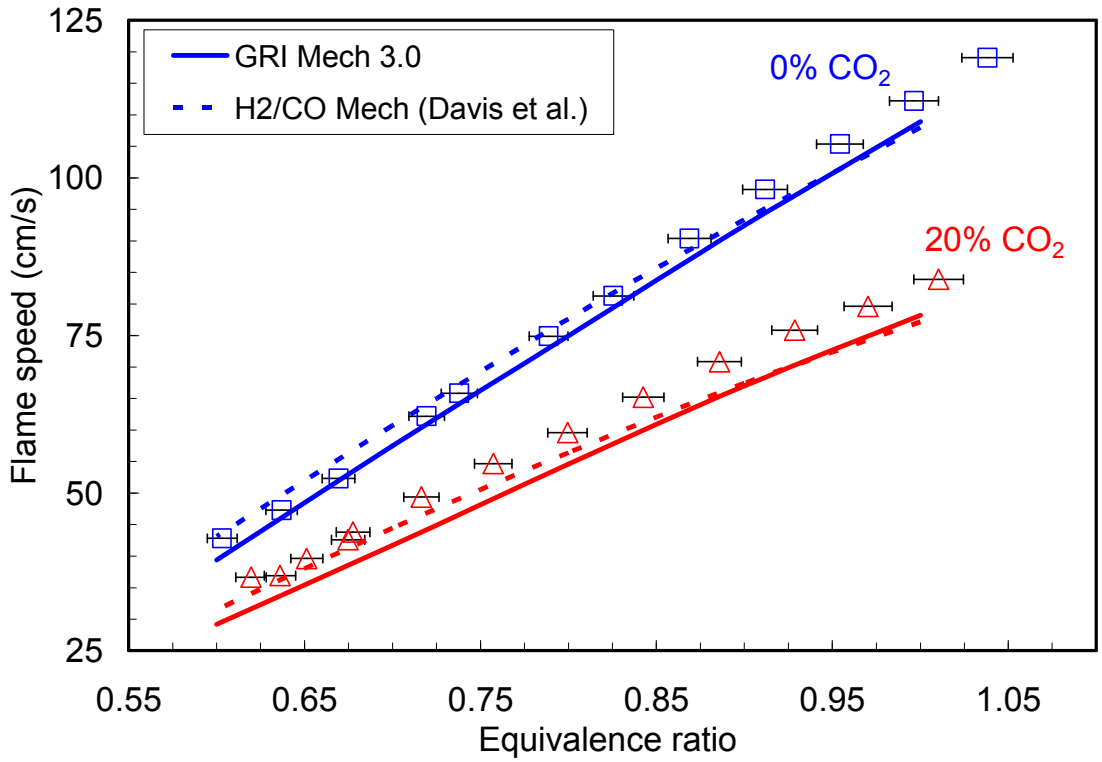

Figure 5.1. Laminar flame speeds for fuels with 50:50 H_2:CO composition, and 0 and 20% CO_2 dilution of the fuel at p=1atm and T_u≅300K; Bunsen flame measurements (symbols) and PREMIX predictions (lines).

Generally the GRI predictions are lower than the measurements for both diluted and undiluted mixtures. As noted earlier, the GRI predicted speeds are in good agreement (~5%) with the measured values over the whole equivalence ratio range tested for the undiluted fuel mixture. For 20% CO_2 dilution, however, the discrepancies between the measurements and the GRI results increase, especially for leaner equivalence ratios (0.6-0.8), where the model under predicts the measurements by 10%. On the other hand, the H_2/CO mechanism is able to more accurately predict the data, within ~5% for the undiluted and 20% CO_2 diluted mixture (see Figure 5.1). The Davis H_2/CO mechanism shows better agreement with the diluted data at lean conditions, compared to GRI, while it matches the GRI simulations closer to stoichiometric mixtures. Like the GRI results,

the Davis H_2/CO mechanism values consistently under predict the experimental data for 20% CO_2 dilution. At a minimum, the predicted flames speeds can be characterized as being in good agreement with the data for atmospheric pressure, ambient temperature conditions.

Strained flame speeds and strain sensitivities were also measured for this 20% CO_2 diluted, 50:50 H_2:CO fuel mixture in the stagnation flame configuration. The burner nozzle diameter *D* was 12.5 mm with *L*/*D*=1. The experimental data are shown in Figure 5.2, along with the predictions from two models, as a function of strain rate at two equivalence ratios ($\Phi \cong 0.59$ and 0.78.) The vertical bar on the measured flame speed indicates the rms fluctuation of the axial velocity at the minimum velocity location. As in the Bunsen flame results, the leanest mixtures still show the greatest fractional difference between experiments and predictions; however the models now tend to over predict the flame speeds (except at high Φ and low strain).

Both the measured and predicted flame speeds increase linearly with strain rate, and the expressions for the linear fits are also shown in Figure 5.2. The measured strain sensitivity, the slope of the linear fit, for the leanest mixture (Φ=0.59) is nearly twice as large as the measured strain sensitivity for the higher equivalence ratio (Φ=0.78). Similar to the experiments, the models also predict higher strain sensitivity for the leaner fuel mixtures. But there is a significant difference between the observed and predicted strain sensitivities. The strain sensitivity predicted by the two models is nearly the same, but roughly twice the measured strain sensitivity at Φ= 0.78 and 1.5 times the measured value for Φ=0.59.

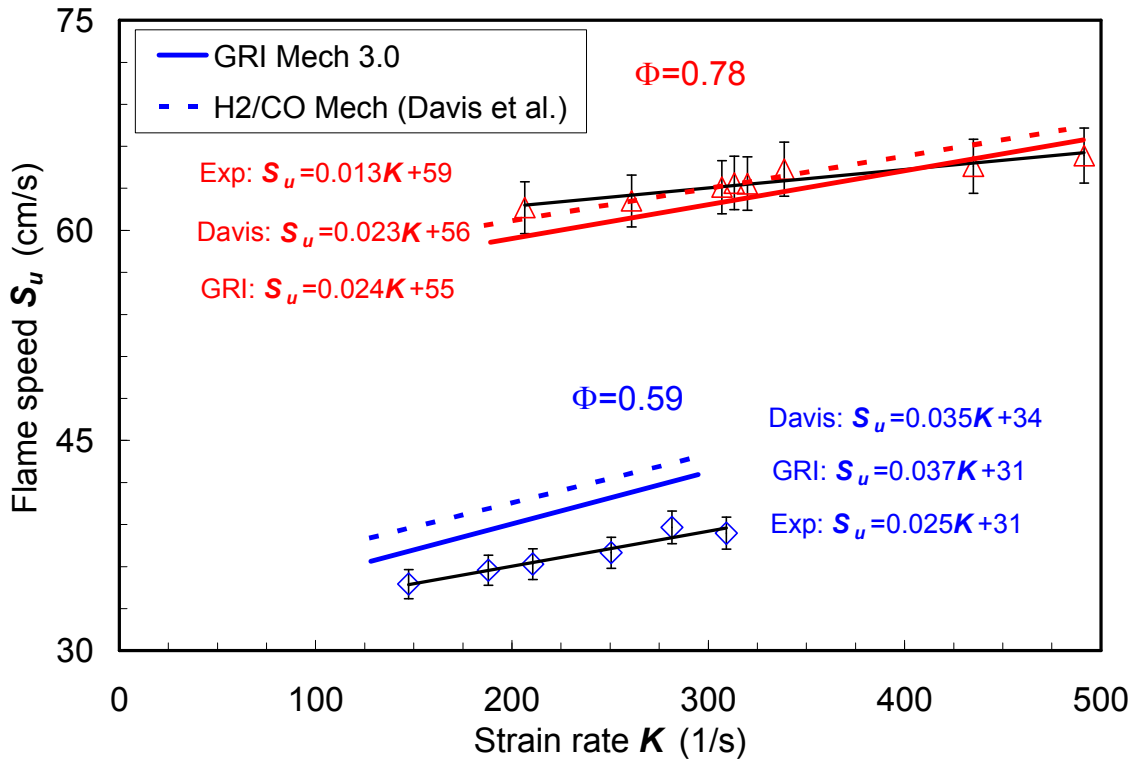

Figure 5.2. Strained flame speeds for lean mixtures with 50:50 H_2:CO fuel with 20% CO_2 dilution (i.e., 40:40:20 H_2:CO:CO_2) at p=1atm and T_u≅300K; Stagnation flame measurements (symbols and linear fit) and OPPDIF predictions (lines).

Unstrained flame speeds are determined from strained flame measurements by extrapolating the measured flame speeds to zero strain rate. Table 5.1 compares the Bunsen flame measurement and the linearly extrapolated strained flame speeds for this fuel composition at all three equivalence ratios. There is remarkably good agreement between the two distinct measurement approaches; for the experimental data, the difference is less than 4%. This further supports the accuracy of the conical Bunsen flame approach as developed in this thesis (i.e., using the reaction zone area). Recalling the discussion about the extrapolation uncertainty in the stagnation flame technique from Chapter 3, the unstrained flame speed calculated by linear extrapolation of strained flame speed always tends to over predict the true, unstrained flame speed.

Table 5.1. Measured and OPPDIFF predicted unstrained flame speed by linearly extrapolating to zero strain and their comparison with Bunsen flame measurements and PREMIX predictions for 40:40:20 H_2:CO:CO_2 mixture at three different equivalence ratios.

Φ	Experiment			GRIMech 3.0		
	Bunsen flame	Stagnation flame	%Δ	PREMIX	OPPDIFF	%Δ
0.78	57	59	4	52.5	54.4	4
0.68	44	45	2	39.7	42.0	6
0.59	32	31	-3	28.6	31.0	8

As shown in Table 5.1, the predicted unstrained flame speeds for the GRI mechanism by PREMIX and OPPDIFF differ as much as 8%, and the difference decreases with increasing equivalence ratio. Subtracting this linear extrapolation uncertainty from the stagnation flame measurements would indicate that the measured flame speed from the Bunsen flame technique slightly over predicts (~10%) the true, unstrained flame speed at the leanest condition (Φ=0.59). Since the observed discrepancies between the model prediction and measurement for the two dilution levels is within the uncertainty of the two measurement techniques, we conclude that the models ability to predict flame speed is good for this 50:50 H_2:CO fuel mixture with CO_2 dilution at atmospheric pressure and room temperature conditions. On the other hand, there is a significant difference between the measured and predicted strain sensitivities from both models.

In order to study the effect of CO_2 addition at elevated preheat temperature, experiments were conducted for the same 50:50 H_2:CO composition with 40% CO_2

dilution at lean equivalence ratios. Figure 5.3 shows the measured strained flame speeds for this composition at 700 K preheat temperature for Φ=0.6 and 0.8. The fuel composition and test conditions were selected such that the results can be directly compared with the undiluted case essentially for the same conditions, such as H_2 level, equivalence ratios, preheat temperature and pressure.(see Figure 4.6).

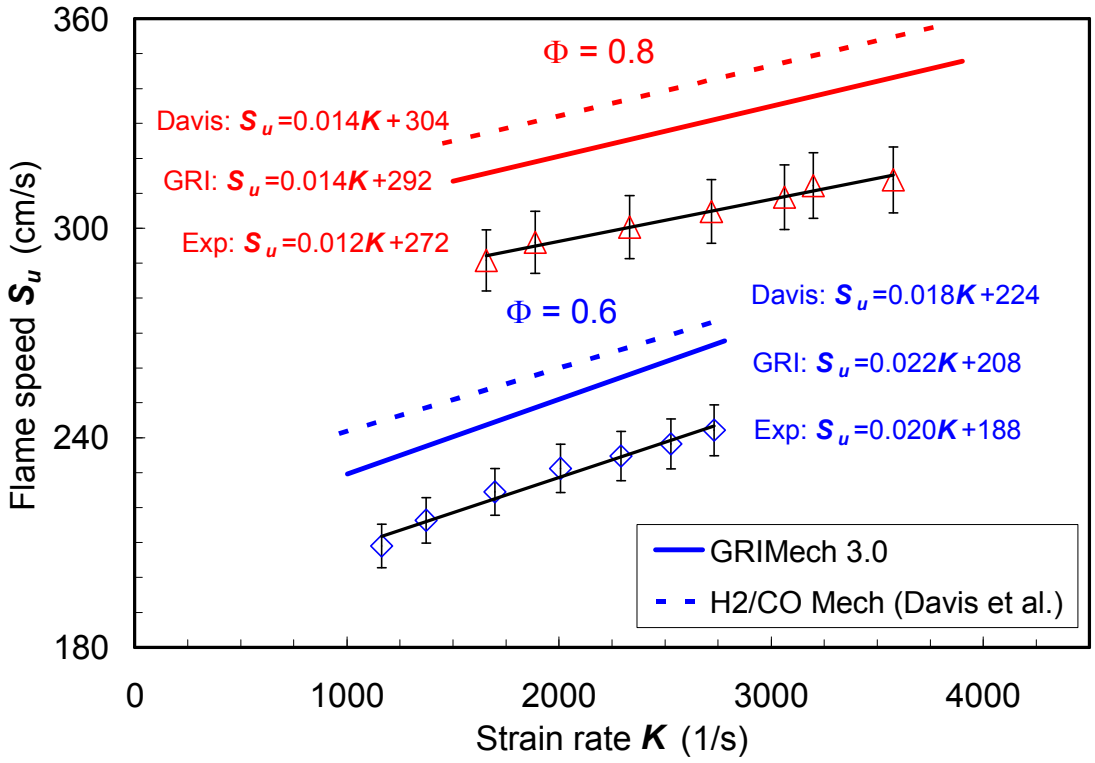

Figure 5.3. Strained laminar flame speeds for lean mixtures of fuel with 50:50 H_2:CO and 40% CO_2 dilution at p=1atm and T_u=700K; stagnation flame measurements (symbols and linear fits) and OPPDIF predictions (lines).

As expected, the flame speed decreases significantly for the diluted case due to the decreases in flame temperature and diffusivity of the reactants. The measured stained flame speed for Φ=0.6 decreases from ~350 cm/s for the undiluted case to ~230 cm/s for the diluted case. Consistent with both the room temperature and high preheat results for

the undiluted 50:50 H_2:CO mixture, the leaner mixture has a higher strain sensitivity than the Φ=0.8 mixture. Also for a given equivalence ratio, the diluted fuel mixture has higher strain sensitivity than the undiluted fuel mixture, especially for the leaner condition (Φ=0.6). Figure 5.3 also shows the predicted strained flame speeds for both equivalence ratios. The predictions with both mechanisms are consistently higher than the measurements, and the difference decreases with increasing Φ.

In fact, the deviations from the measurements are about the same levels seen in the undiluted, high preheat case; the GRI predictions are 10% (Φ=0.6) and 9% (Φ=0.8) above the measurements, while the H_2/CO mechanism results are 14% (Φ=0.6) and 12% (Φ=0.8) too high. This suggests that the radiation absorption/emission effect of CO_2 addition may not be important for this mixture even at these high preheat, lean conditions, at least at atmospheric pressure.

5.1.1.2 High H_2 content fuel mixture

Laminar flame speeds were measured with the Bunsen flame technique for high H_2 content fuel composition, 95:5 H_2:CO, with 20% CO_2 dilution. Due to the very high flame speeds of these mixtures, the burner diameter was reduced to 4.5 mm. For lean conditions with this high H_2 content fuel, the tip of the flame becomes less intense, and hence the knife edge was used to make the tip more visible for accurate flame area calculations. Figure 5.4 shows the measured and computed flame speeds for a range of lean equivalence ratios. Also shown in Figure 5.4 is the result for the undiluted, 95:5 H_2:CO fuel mixture in order to facilitate the comparison between the diluted and undiluted cases.

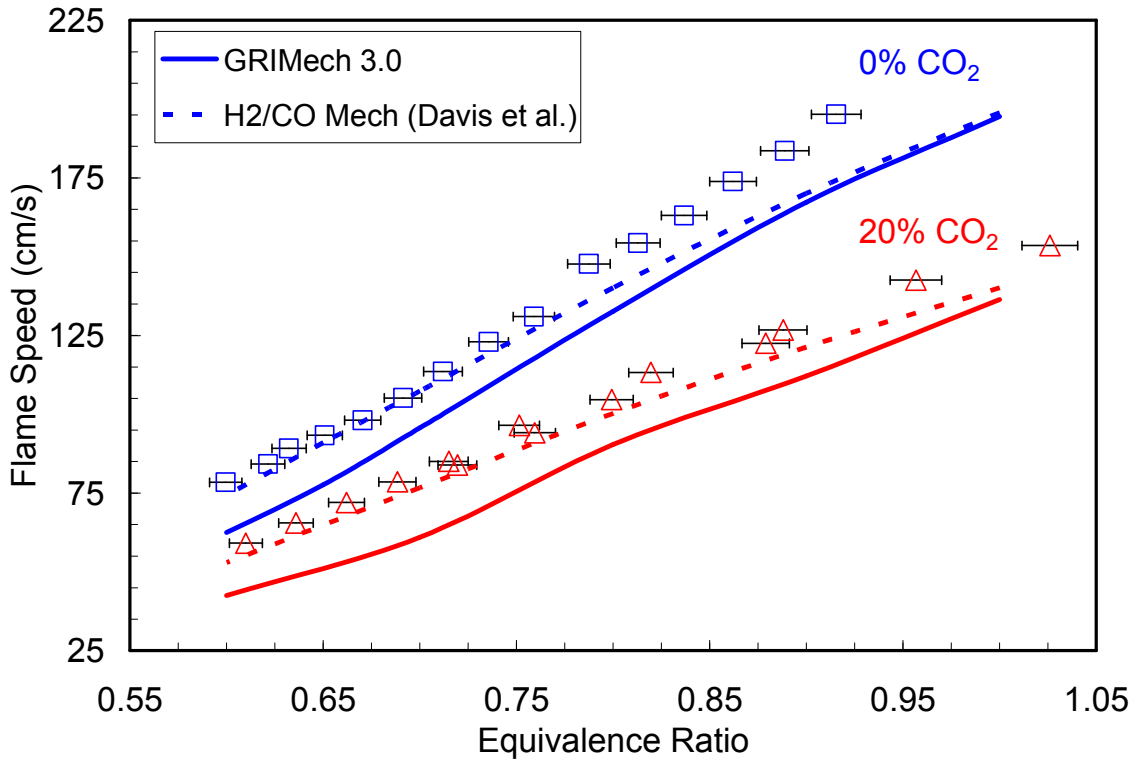

Figure 5.4. Laminar flame speed for fuels with 95:5 H_2:CO composition, and 0 and 20% CO_2 dilution at p=1atm and T_u≅300K; Bunsen flame measurements (symbols) and PREMIX predictions (lines).

The models predictions are consistently lower than the measured flame speeds for both undiluted and diluted fuel mixtures. As noted earlier for the undiluted mixture, the H_2/CO mechanism predictions are in better agreement with measurements especially at fuel lean conditions. The GRI mechanism under predicts the measurements by about 15% near stoichiometric conditions and as much as 20% at Φ=0.6. Though the H_2/CO mechanism predictions are similar to those from GRI at near stoichiometric conditions, the H_2/CO mechanism's deviations are within 3-4% at the leanest condition studied (Φ=0.6-0.75). Similar behavior is observed for the 20% CO_2 dilution case. However for the diluted case, the agreement between the GRI predictions and the measurement

improves near stoichiometric conditions, but worsens at lean conditions compared to undiluted case. For 20% CO_2 dilution, the GRI model under predicts the measurements by as much as 25-30% at very lean equivalence ratios. On the other hand, the H_2/CO mechanism predicts the measured flame speed within 5% at the very lean equivalence ratio for 20% dilution. Moreover, the H_2/CO mechanism predictions are much better for the diluted mixtures near stoichiometric conditions compared to that of the undiluted mixture.

Overall, the laminar flame speed predictions with the H_2/CO mechanism are considerably more accurate than with GRIMech 3.0 for this high H_2 content fuel mixture, especially at lean equivalence ratios. Since the H_2/CO mechanism shows good agreement with measurements for both diluted and undiluted cases, it can be concluded that CO_2 radiation does not play a significant role for this fuel mixture and the current test conditions.

5.1.1.3 Low H_2 content fuel mixture

The low H_2 content fuel mixture, 5:95 H_2:CO, was tested with 10% CO_2 dilution due to the difficulty in achieving a stable flame for 20% CO_2 dilution. The burner diameter used for these mixtures was 13.6 mm. Figure 5.5 shows the measured and predicted flame speeds for this mixture over a range of lean equivalence ratios. For comparison, the figure also includes the result for the undiluted 5:95 H_2:CO fuel. As was seen for the undiluted case, the models predictions are essentially the same for all the lean conditions, and they are in good agreement (within 5-7% over most of the range) with the measurements.

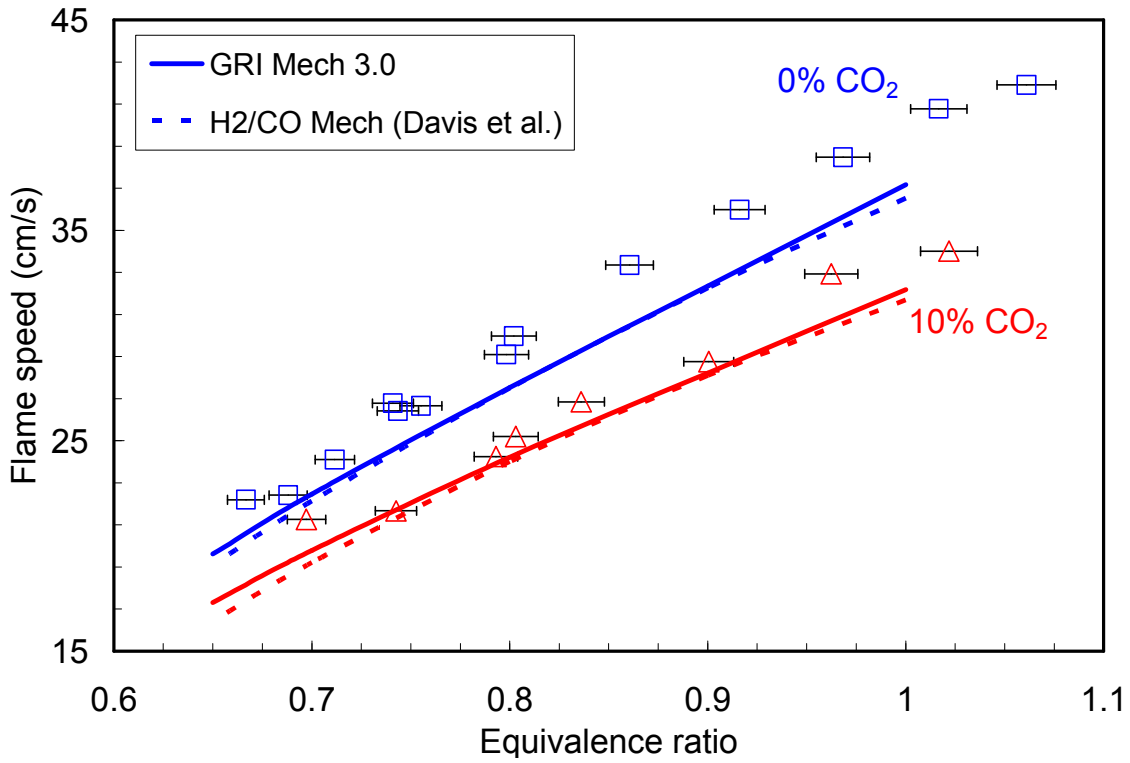

Figure 5.5. Laminar flame speed for fuels with 5:95 H_2:CO composition, and 0 and 10% CO_2 dilution at p=1atm and $T_u \cong 300K$; Bunsen flame measurements (symbols) and PREMIX predictions (lines).

Overall the atmospheric pressure results show that the predictive capability of the models does not change considerably with CO_2 dilution for a range of syngas fuel mixtures and reactant preheat temperatures. This indicates that the flame temperature and chemical effects, if any, associated with CO_2 dilution are modeled reasonably well. Also it can be concluded that other effects, such as the influence of radiation is small/negligible at these conditions (because the PREMIX code does not include such effects). This agrees with previous findings for other fuels [28] that found the radiation has little influence on flame speeds as long as the fuel mixture is not near the flammability limits or *at elevated pressure*. Pressure can influence the chemical effects associated with CO_2 dilution (through the pressure dependent reaction $CO+OH=CO_2+H$),

and radiation (through changes in the optical thickness). Therefore, the next section examines flame speeds at high pressure.

5.1.2 Elevated pressure results

Experiments were conducted for a range of H_2/CO ratios (50-90% H_2) with 40% CO_2 dilution (with respect to the amount of fuel) at 15 atm, 600 K preheat temperature and a fixed equivalence ratio of 0.75. This equivalence ratio was chosen to maintain nearly the same flame temperature as that of the undiluted case presented earlier (see Figure 4.13). This approach is helpful as it isolate the influence of CO_2 dilution while maintaining the pressure, preheat temperature and the flame temperature essentially the same between the diluted and the undiluted cases. The adiabatic flame temperature varies somewhat for the different diluted fuel compositions, from 1845 K at 20% H_2 to 1770 K at 90% H_2. Similar to the undiluted case, an O_2/He mixture with a 1:9 volumetric ratio was chosen to be the oxidizer in order to suppress the hydrodynamic instabilities at elevated pressure conditions. Since the GRI mechanism was not optimized for reactant mixtures containing He, the C_1 mechanism of Li *et al.* is considered together with H_2/CO mechanism of Davis *et al.* for elevated pressure conditions.

The measured and predicted flame speeds are presented in Figure 5.6, with results for the undiluted case included for comparison. In the figure, the indicated percentage of H_2 represents its volume fraction of the combustible (fuel) gases, i.e., H_2 and CO. Hence, though the flame temperature is maintained the same between the undiluted and diluted cases for a given fraction of H_2, the flame speeds for diluted mixtures are significantly lower than the undiluted fuel mixtures due to the decreased thermal and mass diffusivity of the reactant mixtures.

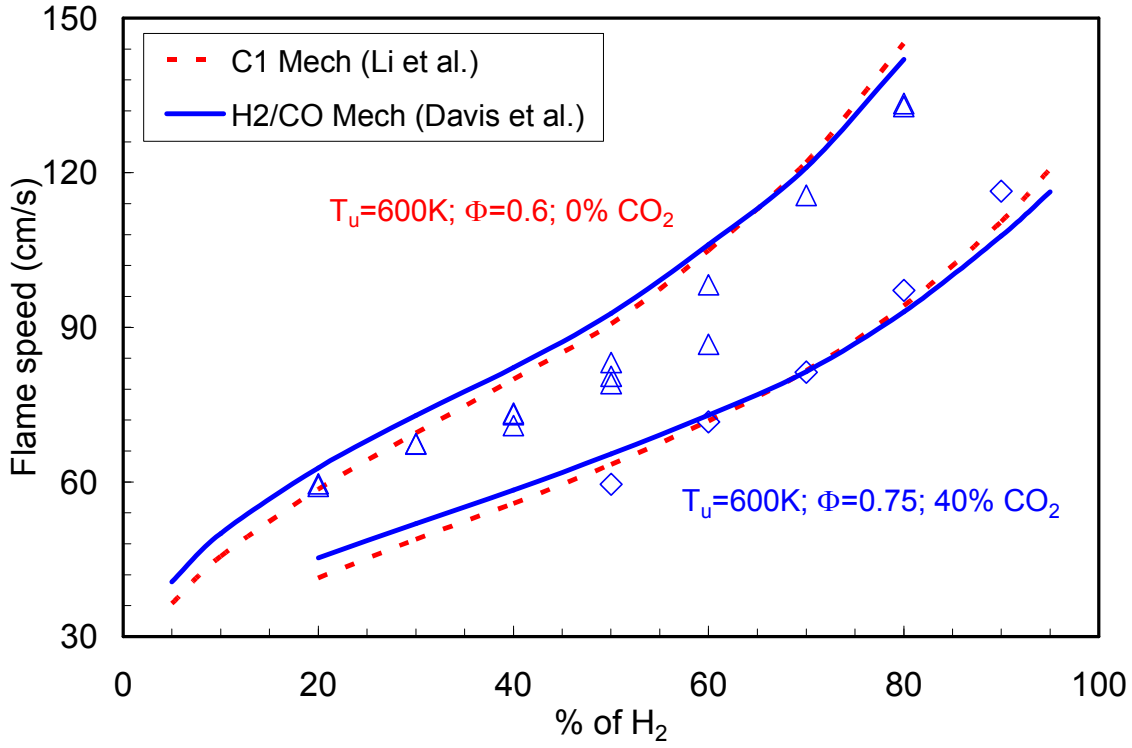

Figure 5.6. Laminar flame speeds for a range of H_2/CO fuel mixtures (O_2:He 1:9 oxidizer) with 0% and 40% CO_2 dilution at a fixed equivalence ratios, p=15 atm and T_u=600 K; Bunsen flame measurements (symbols) and PREMIX predictions (lines).

Similar to the undiluted results, the two models predict essentially the same flame speeds for medium and high H_2 fuel mixtures, though the H_2/CO mechanism predictions are slightly higher (up to 10%) as the amount of H_2 drops to 20%. Compared to the measurements, the C_1 mechanism predictions are in excellent agreement (within ~5%) for 50-90% H_2; it slightly over predicts for 50% H_2 and slightly under predicts for 90%. The H_2/CO mechanism predictions are similar, but with slightly higher discrepancy (up to ~10%) at both 50 and 90% H_2.

Comparing the diluted high H_2 mixtures with the undiluted results, we find that the models slightly under predict the measurements with dilution and slightly over predict the data without dilution. For medium H_2 content fuels, the amount of over prediction

decreases with CO_2 dilution. Thus in general, CO_2 dilution decreases the flame speed less than the amount predicted by the models. This suggests that radiative heat transfer (between products and reactants diluted with high amounts of CO_2) may slightly increase the flame speed for high pressure conditions (~5% in this 15 atm case). This effect would likely be more pronounced at higher pressures. It should be noted, however, that the amount of increase observed here is close to the uncertainty in the measurements; thus it is difficult to provide a quantitative value for the radiation effects.

To conclude, the flame temperature and chemical effects associated with CO_2 dilutions are well predicted by current models for a range of syngas fuel mixtures. The radiation absorption/emission characteristics of CO_2 dilution does not significantly affect the measured flame speed at least for fuel mixtures, dilution levels and test conditions (pressure and temperature) studied here.

5.2 Effects of N_2 dilution

Syngas mixtures often contain large amounts of N_2; hence it is important to understand its influences on the measured flame speeds and strain sensitivities. In particular, the goal here is to investigate the effects of N_2 dilution on the higher temperature dependence observed for the predicted flame speeds in medium and high H_2 content fuel mixtures (as revealed in Chapter 4). Since this effect was most prominent for high H_2 content fuel mixtures (see Figure 4.11), pure H_2 with highly N_2 diluted air (O_2:N_2 volume ratio of 1:9) is considered here at both room and elevated preheat temperatures. To elucidate the effect of N_2 dilution, the results are compared with undiluted results, i.e., pure H_2 and standard air. Also, the hydrogen mechanism of Li *et al*. [36] is included in the analysis.

5.2.1 Eleveated preheat temperature reactants

Laminar flame speeds and strain sensitivities were measured with the stagnation flame approach at elevated preheat temperature (700 K) for a range of fuel air ratios (Φ=0.8 to 1.6). The fuel air ratios were chosen to keep the adiabatic flame temperature similar to that for the undiluted cases. This approach isolates the influence of dilution while maintaining the preheat temperature and flame temperature between the two cases. The burner diameter used for this fuel mixture was 9 mm with an *L/D* of 0.66.

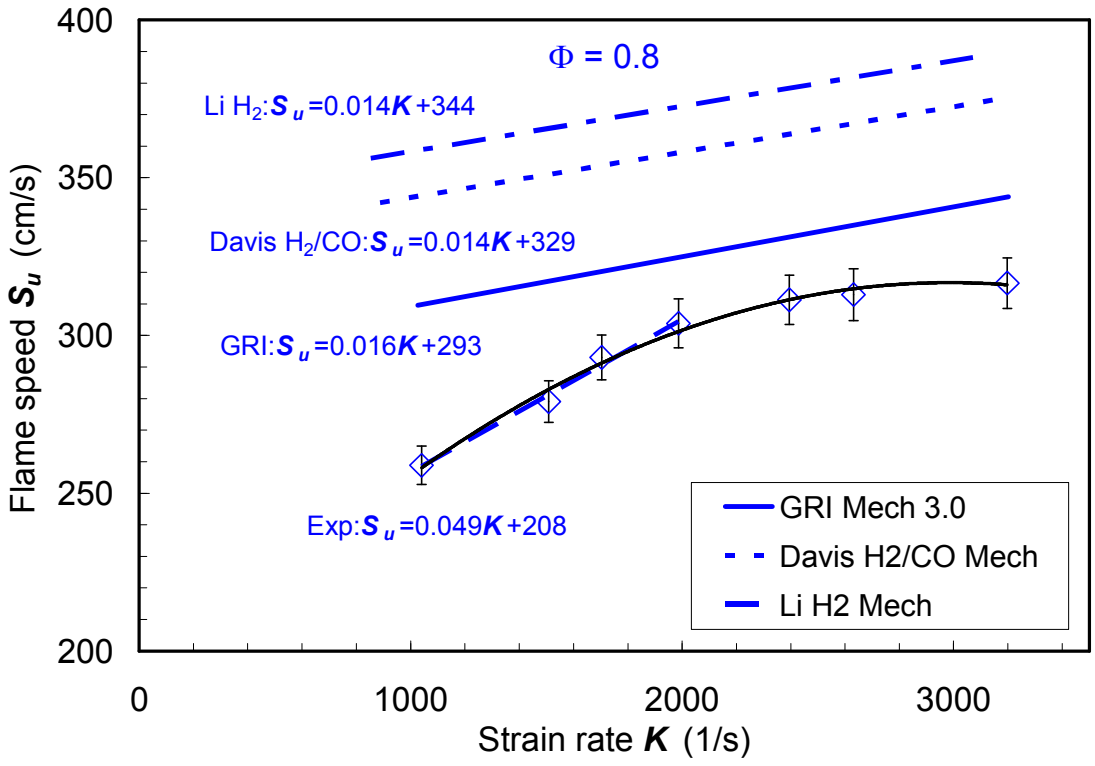

Figure 5.7. Strained laminar flame speeds for mixture of H_2 with N_2 diluted air (O_2:N_2 1:9) at Φ=0.8 and 700 K preheat temperature; stagnation flame measurements (symbols and fits) and OPPDIF predictions (lines).

Figure 5.7 shows the measured strained flame speeds at Φ=0.8 and 700 K preheat temperature for a range of strain rates. The measured flame speed increases nonlinearly

with the imposed strain rate, though the data appear closer to linear at low strain. Also shown in Figure 5.7 are the predicted strained flame speeds. Unlike the measurements, the predicted flame speeds increase linearly with strain rate. Also, all three models over predict the measured flame speed. As in the undiluted cases (see Figure 4.9 and Figure 4.10), the GRI mechanism results are closest to the measurements, while the H_2 mechanism produces the highest flame speeds. The GRI mechanism results are higher than the measurements by ~20% at lower strains, with the over prediction decreasing to 10% as strain increases. The H_2/CO and H_2 mechanism results are higher than the measurements by 30% and 35%, respectively, at low strain rates, with the discrepancy again decreasing at high strain.

Though the measured flame speed increases nonlinearly with strain, we can estimate the strain sensitivity by a linear fit to the experimental results in the low strain region (1000-2000 s^{-1}) where the data are close to linear (see Figure 5.7). The magnitudes of the strain sensitivities predicted by the models are again similar to one another (140 to 160 μm), but nearly three times lower than the measured sensitivity (490 μm). Thus if the results are extrapolated back to zero strain (to produce estimates of the unstrained flame speed), this leads to even larger discrepancies (~40 to 65%) between the extrapolated model values (293-344 cm/s) and the extrapolated measurements (208 cm/s).

It is interesting to recall that the models were in reasonable agreement for the undiluted case, i.e., pure H_2 with standard air (see Figure 4.9 and Figure 4.10), but now significantly over predict the measured flame speeds at very similar test conditions. Essentially, the difference between the two cases is that part of the excess O_2 in the lean mixture of pure H_2 and standard air is replaced with N_2 in the diluted case. Since the

adiabatic flame temperature is maintained roughly constant by varying the equivalence ratio, the initial H_2 concentration is the same for the two cases. Yet, the predicted flame speeds are slightly different. For example, the H_2 mechanism's predicted flame speed for H_2 with N_2 diluted air at Φ=0.8 (~331 cm/s) is lower than the predicted flame speed for H_2 with standard air at Φ=0.385 (~374 cm/s), even though the preheat temperature (700 K) and the flame temperature (1736 K) are the same for both cases. This is mainly because the reduced O_2 concentration in the reactants reduces the reaction rates of the key chain branching reaction $H+O_2 \leftrightarrow O+OH$ (R1), which in turn significantly reduces the heat release rates of $H_2+OH \leftrightarrow H_2O+H$ (R3), $H+O_2+M \leftrightarrow HO_2+M$ (R13) and $HO_2+H \leftrightarrow OH+OH$ (R15).

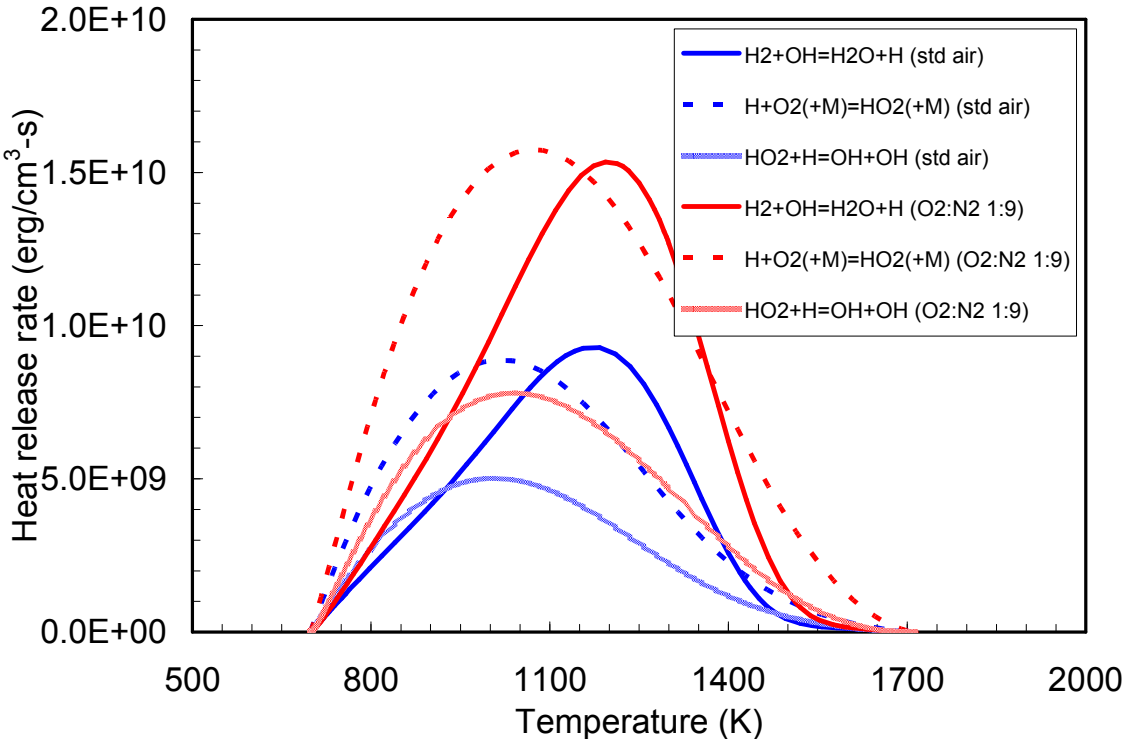

Figure 5.8. Variation of the heat release rates for R3, R13 and R15 reactions for pure H_2 with standard air and N_2 diluted air (O_2:N_2 1:9) at Φ=0.385 and Φ=0.8, respectively.

Figure 5.8 shows the variation of the heat release rates of these three reactions with local flame temperature for these two cases. It should be recalled that reaction R3 is one of the main heat release reaction in the H production zone (or main reaction zone). Consequently the important minor species (O, HO_2, OH, etc.) concentrations are also observed to be lower for the diluted case.

Similar to the undiluted case, the sensitivity analysis shows the flame speed is highly sensitive to the rate constants of reactions R1, R3, R13 and R15 for the diluted case. As discussed earlier, there is significant uncertainty associated with the rate coefficients of these key reactions, which could lead to significant uncertainty for the flame speed predictions. The estimated combined uncertainty on the predicted flame speed is about ±30% at these conditions, which is similar to the observed discrepancy between the measurements and models predictions. Again like the undiluted case, the major contribution (about 20%) to the combined uncertainty is due to reaction R15 ($HO_2+H \leftrightarrow OH+OH$).

Experiments were also conducted for stochiometric and rich (Φ=1.6) mixtures of H_2 and N_2 diluted air (Figure 5.9). Unlike the lean case, there is a fairly linear relationship between the measured flame speed and imposed strain rate. Similar to the lean case, all three models over predict the measurements. Now however, the model results are closer to one another than to the measurements. The GRI mechanism again has the smallest amount of over prediction (12% at Φ=1.0 and 10% at Φ=1.6), the H_2 mechanism produces the highest flame speeds (over prediction of 22% at Φ=1.0 and 15% at Φ=1.6), and the H_2/CO mechanism is in between (18% high at Φ=1 and 12% at Φ=1.6).

By comparing the results at Φ=0.8, 1.0, and 1.6 (Figure 5.7 and Figure 5.9), we find that the difference between the model predictions and the measurements increases for the N_2 diluted mixtures as the mixture becomes leaner. This trend is very similar to the results for the undiluted medium and high H_2 content fuel mixtures at elevated preheat temperatures presented in the previous chapter.

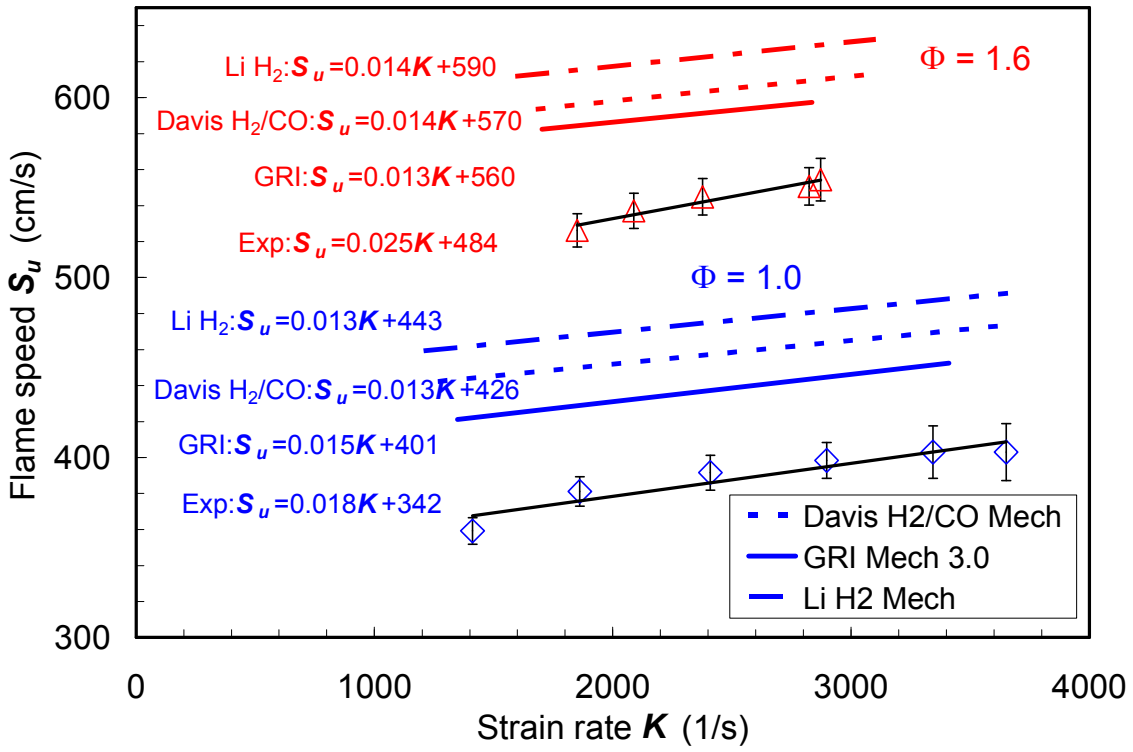

Figure 5.9. Strained laminar flame speeds for stoichiometric and rich mixtures of H_2 with N_2 diluted air (O_2:N_2 1:9) at 700 K preheat temperature; stagnation flame measurements (symbols and fits) and OPPDIF predictions (lines).

It is also interesting to consider the measured and predicted strain sensitivity variation with equivalence ratio as reported in Table 5.2. The magnitude of the measured strain sensitivity decreases from 490 μm at Φ=0.8 to 180 μm at Φ= 1.0, and then increases to 250 μm as the equivalence ratio increases further to 1.6. This nonomonotonic

behavior is expected and can be explained by the variation of the flame thickness and the concentration of the deficient species (H_2 or O_2 in the fuel lean or rich conditions, respectively) as the equivalence ratio varies. As we move away from stoichiometric on either side, the flame thickness increases and the deficient species concentration decrease. Both increase in flame thickness and decrease in deficient species concentration tend to increase strain sensitivity which is consistent with the measurements here. The model predicted strain sensitivities by all three models are very similar and they consistently under predict the measurements especially away from stoichiometric conditions. More importantly, in contrast to the measurements, the models predicted strain sensitivities change only slightly despite the significant variation in equivalence ratio. The more likely reason for this poor models prediction is the kinetics as the flame speeds were also poorly predicted at this condition, but the validity of the one dimensional assumption in the strained flame model should also be considered, due to the increased flame thickness (as it is the highest of all the other cases tested).

Table 5.2. Variation of the measured and models predicted unburned strain sensitivities for mixtures of H_2 with N_2 diluted air (O_2:N_2 1:9) at 700 K preheat temperature.

Φ	Unburned strain sensitivity (in μm)			
	Measurements	GRI	Davis H_2/CO	Li H_2
0.8	490	160	140	140
1.0	180	150	130	130
1.6	250	130	140	140

Overall the results at elevated reactants temperature for H_2 with N_2 diluted air (O_2:N_2 1:9) mixtures show that the models over predict the measured flame speeds and the amount of over prediction decreases with increase in equivalence ratio. The models consistently under predict the strain sensitivities especially away from stoichiometric conditions.

5.2.2 Room temperature reactants

To elucidate the effect of preheat temperature on the observed discrepancy between measurements and model predictions, it is important to consider the models' performance at low preheat. To this end, the predicted unstrained laminar flame speeds (from PREMIX) at room temperature are compared with measured, unstretched laminar flame speeds from Egolfopoulos *et al.* [40] for essentially the same fuel and oxidizer mixtures and equivalence ratios used in the high preheat results presented above. In their work, the unstretched laminar flame speed is calculated by linear extrapolation of the measured strained flame speeds determined in a counter flow flame.

The ratio of predicted and measured flame speeds for H_2 with N_2 diluted air are shown in Figure 5.10. As indicated previously, the models over predict the measurements for high preheat with the amount of over prediction decreasing as the equivalence ratio increases from 0.8 to 1.6. Like the undiluted results, all the mechanisms under predict the measurements for room temperature reactants. In addition, the amount of under prediction increases as the mixture moves away from near stoichiometric conditions. For lean mixtures, as opposed to the elevated preheat case, the H_2 mechanism is closest to the measurements (within 10% and 30% at Φ=1.0 and 0.8), and the GRI mechanism results are the farthest (15% and 50% at Φ=1.0 and 0.8). As the mixture becomes fuel rich, all

three mechanisms produce essentially the same flame speeds. Comparing the low and high temperature results, similar to the undiluted fuel mixture case, the models predict higher temperature dependence for the flame speed than is found from the measurements.

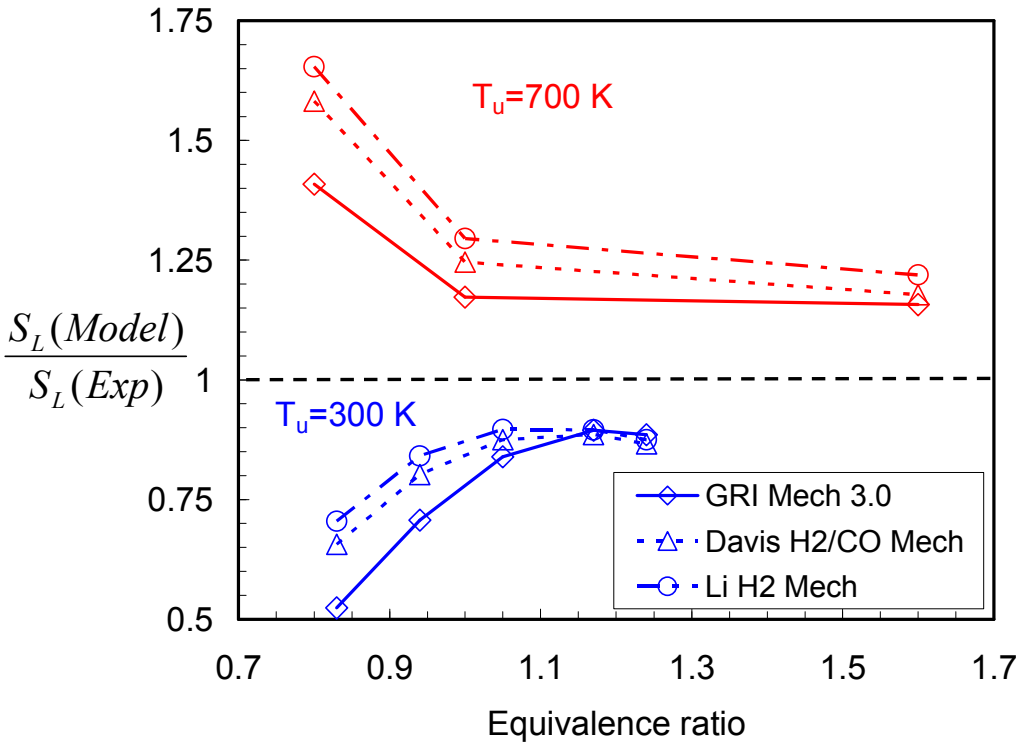

Figure 5.10. Ratios of the models predicted (PREMIX) and measured unstrained laminar flame speeds for lean mixtures of H_2 with N_2 diluted air (O_2:N_2 1:9) at 300 K and 700 K preheat temperatures.

To conclude, the predictive capability of the models for both flame speed and strain sensitivity does not change significantly with CO_2 dilution. Hence it is concluded that the flame temperature and chemical effects associated with CO_2 dilutions are well predicted by current models, and that the radiation absorption/emission issues associated with CO_2 dilution do not have significant impact on the flame speed under the current conditions. On the other hand, the predictive accuracy of the models deteriorates with N_2 dilution. At elevated temperature, the models significantly over predict the measured

strained flame speeds for N_2 diluted fuel mixtures, whereas the model predictions are in good agreement for undiluted fuel mixtures. Also, the models fail to predict the increased strain sensitivity for N_2 diluted mixtures especially away from stoichiometric conditions whereas the models predicted strain sensitivities are in good agreement for the undiluted and CO_2 diluted mixtures.

CHAPTER 6

CONCLUSIONS AND FURTHER RECOMMENDATIONS

6.1 Summary and conclusions

The objectives of this thesis were to measure laminar flame speeds and strain sensitivities of practical syngas fuel mixtures at realistic gas turbine conditions, and to identify potential avenues for improvement of the current chemical kinetic mechanisms used to predict syngas flame properties. To accomplish these goals, two flame speed measurement approaches were developed: a ***modified*** Bunsen flame approach based on reaction zone area imaging and a stagnation flame approach employing velocity measurements along the flame axis. Detailed numerical simulations of strained and unstrained laminar flames were performed with leading kinetic mechanisms and the model predicted flame speeds and strain sensitivities were compared with the measurements, leading to identification of conditions that result in low fidelity.

***Flame Speed Measurement Methods*:** In the modified Bunsen flame approach, the reaction zone area (measured from chemiluminescence images of the flame) is used for flame speed calculations in order to reduce the influence of curvature, which is the dominant source of stretch for a conical flame, on the measured flame speed. Flame speeds measured with this approach have shown to be in very good agreement (always less than 10% difference) with results obtained from stretch-corrected (extrapolated to zero stretch) data from expanding spherical flames and stagnation flames over a range of fuels (e.g. CH_4, and H_2/CO mixtures with 5% and

50% H_2 and 0 and 20% CO_2 dilution), pressures (up to 10 atm) and preheat temperatures (up to 700 K). Thus it is concluded that this modified Bunsen flame approach, based on reaction zone area, is reasonably accurate for a range of fuel mixtures and test conditions.

Strained flame speeds and strain sensitivities were measured using a wall stagnation flame, with the standard approach modified to use a rounded plug to improve flame stability at high flow rates. For highly preheated fast burning reactants, a burner stabilized stagnation flame is also found to be more stable. The uncertainty in the experimental boundary conditions, mainly the downstream heat loss from the products to the wall and the velocity boundary condition at the wall were shown to have a minor effect (less than 3%) on the measured unburned flame speeds and strain sensitivities.

***Flame Speed Data Condtions*:** Using these two measurement approaches, extensive flame speed and strain sensitivity information were obtained for various lean syngas mixtures at pressure and temperature conditions relevant to gas turbine engines. In particular, results were obtained for: 1) H_2/CO fuel mixture with 5 to 100% H_2, 2) preheat temperatures of 300- 700 K, 3) pressures of 1-15 atm, and 4) dilution with CO_2 or N_2 of the fuel up to 70%. These data, especially the high reactant temperature results, significantly extend the existing database for syngas mixtures.

Influence of preheat temperature: Comparison of predicted flame speeds with measurements from two very distinct experimental techniques show that the current mechanisms predicted flame speeds increase faster than measurements with preheat

temperature for the ***medium*** and ***high*** H_2 fuel mixtures, especially at fuel lean conditions.

For the medium H_2 syngas fuels, the models predictions are in good agreement with measurements up to 500 K. However, they significantly over predict (by as much as ~40%) the measurements as the preheat temperature increases to 700 K, especially for leaner mixtures. Results from strained flame measurement approach also confirm this trend that the models over predict increase in flame speed with preheat temperature.

Similarly for high H_2 content fuels, the Bunsen measurements of 95% H_2 syngas mixtures and strained flame speed measurement for pure H_2 fuel show the same trends. Unlike the medium H_2 content fuels, where all the models behave similarly, the model that is closest to the measurements at room temperature (the H_2/CO mechanism) tends to over predict the data at high temperature, while the model that under predicts at low reactant temperature (GRI Mech) fortuitously provides more accurate predictions at higher preheat temperature.

Experiments were also performed at elevate pressure conditions to find the influence of pressure on this exaggerated temperature dependence. The results generally agree with the findings at atmospheric pressure that the predicted flame speeds exhibit too high a temperature dependence, though the effect is not as pronounced as at atmospheric pressure.

Thus, we conclude that the current mechanisms predict higher preheat temperature dependence for flame speed than measurements for the medium and high H_2 fuel mixtures, especially at fuel lean conditions. The failure of the current models is

most likely caused by deficiencies in the rate parameters of one or more reactions in the chemical mechanisms.

The results from sensitivity analysis show that the normalized sensitivity of the flame speed to the rate constant (specifically the pre-exponential factor) of key reactions increases with preheat temperature for both medium and high H_2 content fuel mixtures. The identified key reactions, which also have significant uncertainty in the rate coefficients, are the HO_2 formation ($H+O_2+M \leftrightarrow HO_2+M$) and destruction ($HO_2+H \leftrightarrow OH+OH$) reactions, and the main heat release reaction in the H production zone ($H_2+OH \leftrightarrow H_2O+H$). Importantly, the first two reactions, which are responsible for heat release in the very early part of the flame (low temperature regime), are altered significantly with an increase in preheat temperature. By adjusting the rate coefficients of these three key reactions within the uncertainty limits provided in the literature, the model predictions can be made to better match the experiments. In particular, the HO_2 destruction reaction ($HO_2+H \leftrightarrow OH+OH$) is identified to have the largest contribution to the uncertainty in the predicted flame speed, and the temperature dependence of this reaction seems to be the possible error which need further investigation.

***Influence of CO_2 dilution*:** The chemical and radiative heat transfer influence of CO_2 dilution on the laminar flame speeds of syngas fuel mixtures was examined for a wide range of operating conditions that include elevated pressure and preheat temperature. Results at atmospheric pressure show that the predictive capability of the models does not change considerably with CO_2 dilution, i.e., if the models poorly predict the measured flame speed for undiluted mixtures then the same is

true for mixtures diluted with CO_2 up to 40%. Results at elevated pressure and preheat temperature suggest that radiative heat transfer may slightly increase the flame speed, but the increase in measured flame speeds is well within the uncertainty of the modeling results, and also close to the uncertainty in the measurements. Hence it is concluded that the flame temperature and chemical effects associated with CO_2 dilutions are well predicted by current models and the radiation absorption/emission characteristics of CO_2 dilution do not significantly affect the measured flame speed, at least for the dilution levels and test conditions (pressure, temperature and flame size) studied here.

Influence of N_2 dilution: The influence of N_2 dilution on models predictions of laminar flame speeds was examined for pure H_2 at room and elevated preheat temperature. Results show that, the models significantly over predict the measured flame speeds at elevated preheat temperature while they under predict the measurements at room temperature especially at fuel lean conditions. This is again in accordance with the earlier discussion that the models have higher preheat temperature dependence of the predicted flame speeds for syngas mixtures with significant amount of H_2.

Inferences on strain sensitivities: The models predicted strain sensitivities are in reasonably good agreement with the measurements for a range of undiluted syngas mixtures at both room and elevated preheat temperatures. Also the models are able to predict the variation in the measured strain sensitivity with equivalence ratio for the undiluted mixtures. For the diluted syngas mixtures, while the predictive capabilities are similar to undiluted mixtures for CO_2 dilution, they deteriorate for

heavy N_2 dilution. It is observed that the strain sensitivities predicted by all three models consistently under predict the measurements for pure H_2 with N_2 diluted air at elevated preheat temperatures and also they fail to predict the variation with equivalence ratio. The most likely reason for this deviation is again the chemical kinetics, as the flame speeds were poorly predicted at this condition. However, the validity of the one dimensional assumption in the strained flame model must also be a considered suspect, due to the increased flame thickness (as it is the highest of all the cases tested).

To conclude, leading models for syngas combustion predict the laminar flame speed and strain sensitivities reasonably well for majority of the conditions. One of the major drawbacks of the models is that the uncertainty involved with the predictions progressively increases with reactant preheat temperature for medium and high H_2 content fuel mixtures. This is particularly relevant to gas turbine combustors operating with syngas fuels and improving the accuracy of the models would enhance their use in detailed design. This failure of the current models is shown to be caused by uncertainties in rate coefficients of key reactions. A more detailed sensitivity analysis based on temperature dependent reaction rate parameters (e.g., activation energy) should be considered as the problem seems to be in the intermediate temperature range (~800-1200 K) for the key reactions.

6.2 Recommendations for further studies

It is important to develop an accurate flame speed measurement approach that can be used for measurements at elevated pressure and preheat temperature conditions. In this

regard, the Bunsen flame approach has significant potential. The use of reaction zone area to calculate the flame speed was justified by analytic results showing that the reaction zone area of a weakly stretched steady flame is insensitive to curvature. Though the analysis assumes weakly stretched flames, the flame speeds obtained with the modified Bunsen flame approach are close to results from stretch corrected methods even for "highly" stretched flames. For example, the flame speeds obtained with the modified Bunsen flame approach for a 4.5 mm diameter burner and 50:50 H_2/CO fuel mixtures at 700 K preheat temperature are in good agreement with the stagnation flame measurements (see discussion at the end of section 4.2.2). The flame thickness and flame speed at this condition are estimated to be 0.5 mm and 3 m/s. Since the radius of the burner itself is only few times the flame thickness and because the flame speed is high, the overall stretch imposed on this conical flame throughout the flame surface should be significant. Hence a more detailed numerical or experimental effort should be carried out to understand the limitations and applicability of this approach. Moreover this would help to estimate the *systematic uncertainty* (stemming from stretch and curvature effects) associated with this approach as well. Also the applicability of this approach to other fuels, especially the higher order hydrocarbons such as ethane, propane has to be tested.

To identify the relevant reactions responsible for the observed deviation in the dependence of flame speed on reactant temperature, a sensitivity analysis was performed in the current work. The main drawback of this analysis is that the perturbed rate parameter is the pre-exponential factor in the modified Arrhenius rate constant, rather than the temperature dependent parameters (e.g., activation energy). Increasing the pre-exponential factor increases the reaction rate at all temperatures as opposed to in a

particular temperature range. Hence it would be more appropriate to perform sensitivity analysis based on temperature dependent reaction rate parameters or by using "temperature window sensitivity" [42], i.e., perturbing the rate constants only in a narrow range of temperatures especially in the low temperature regime (~800-1200 K) for the key reactions identified.

CO_2 dilution does not seems to affect the predictive capability of the kinetic models, i.e., if the models poorly predict the measured flame speed for undiluted mixtures then the same is true for CO_2 diluted mixtures. As discussed earlier, the most likely reason is that the flame temperature and chemical effects associated with CO_2 dilutions are well predicted by current models and the radiation absorption/emission characteristics of CO_2 dilution do not significantly affect the measured flame speed. But, there is also a possibility that the chemical effect (which tends to reduce the flame speed) could offset the radiative heat transfer effect (which tends to enhance the flame propagation). Hence, it would be insightful to include the radiation models to the flame model and study the significance of radiation effects on flame propagation independently. Also, since heavy N_2 dilution is observed to change the predictive capability of the models, a more detailed analysis focusing the influence of third body efficiencies of these diluents on highly sensitive reactions need to be performed.

REFERENCES

1 Moliere, M., "Benefiting from the wide fuel capability of gas turbines: A review of application opportunities." *ASME Paper GT-2002-30017*, *Proceedings of the ASME/IGTI Turbo Expo 2002*, Amsterdam, Netherlands, 2002.

2 Klimstra, J., "Interchangeability of Gaseous Fuels – The Importance of the Wobbe Index," *SAE Paper 861578*, 1986.

3 Richards, G.A., McMillian, M.M., Gemmen, R.S., Rogers,W.A., and Cully,S.R., "Issues for Low-Emission, Fuel-Flexible Power System", *Prog. Energy Comb. Sci.,* vol. 27, pp. 141-169, 2001.

4 Lieuwen, T., McDonell, V., Petersen, E., and Santavicca, D., "Fuel Felxibility Influences on Premixed Combustor Blowout, Flashback, Autoignition, and Stability" *Journal of Engineering for Gas Turbines and Power*, vol. 130, pp. 2008.

5 Scholte, T. G., and Vaags, P. B., "Burning velocities of mixtures of hydrogen, carbon monoxide, and methane with air." *Combustion and Flame* vol. **3**, pp. 511-524, 1959.

6 Günther, R. and Janisch, G., "Messwerte der Flammegeschwindigkeit von gasen und gasmischen." *Chemie-Ing-Techn*. vol. 43, pp. 975-978, 1971.

7 Strauss, W. A. and Edse, R., "Burning velocity measurements by the constant-pressure bomb method." *Proceedings of the Combustion Institute,* vol. **7**, pp. 377-385, 1958.

8 Yumlu, V. S., "Prediction of burning velocities of carbon monoxide-hydrogen-air flames." *Combustion and Flame,* vol. 11, pp. 190-194, 1967.

9 Andrews, G. E., and Bradley, D., "Determination of burning velocities – Critical review." *Combustion and Flame,* vol. 18, pp. 133-153, 1972

10 Vagelopoulos, C. M. and Egolfopoulos, F. N., "Laminar flame speeds and extinction strain rates of mixtures of carbon monoxide with hydrogen, methane, and air." *Proceedings of the Combustion Institute,* vol. 25, pp. 1317-1323, 1994.

11 McLean, I. C., Smith, D. B. and Taylor, S. C., "The use of carbon monoxide/hydrogen burning velocities to examine the rate of the CO + OH reaction." *Proceedings of the Combustion Institute,* vol. 25, pp. 749-757, 1994.

12 Brown, M. J., McLean, I. C., Smith, D. B. and Taylor, S. C., "Markstein lengths of CO/H_2/air flames, using expanding spherical flames." *Proceedings of the Combustion Institute,* vol. 26, pp. 875-881, 1996.

13 Hassan, M. I., Aung, K. T. and Faeth, G. M., "Markstein numbers and unstretched laminar burning velocities of wet carbon monoxide flames." *AIAA 96-0912*, *34th Aerospace Sciences Meeting & Exhibit*, Reno, NV, 1996.

14 Hassan, M. I., Aung, K. T. and Faeth, G. M., "Properties of laminar premixed CO/H_2/air flames at various pressures." *Journal of Propulsion and Power,* vol. 13(2), pp. 239-245, 1997.

15 Sun, H. Y., Yang, S. I., Jomass, G. and Law, C. K., "High pressure laminar flame speeds and kinetic modeling of carbon monoxide/hydrogen combustion." *Proceedings of the Combustion Institute,* vol. 31, pp. 439-446, 2006.

16 Ruan, J., Kobayashi, H., Niioka, T., and Ju, Y., "Combined effects of nongray radiation and pressure on premixed $CH_4/O_2/CO_2$ flames" *Combustion and Flame,* vol. 124, pp. 225-230, 2001.

17 Chen, Z., Qin, X., Xu, B., Ju, Y., and Liu, F., "Studies of radiation absorption on flame speed and flammability limit of CO_2 diluted methane flames at elevated pressures." *Proceedings of the Combustion Institute,* vol. 31, pp. 2693-2700, 2006.

18 Qiao, L., Kim, C. H., and Faeth, G. M., "Suppression effects of diluents on laminar premixed hydrogen/oxygen/nitrogen flames" *Combustion and Flame,* vol. 143, pp. 79-96, 2005.

19 Davis, S. G., Joshi, A. V., Wang, H. and Egolfopoulos, F. N., "An optimized kinetic model of H_2/CO combustion" *Proceedings of the Combustion Institute,* vol**.** 30, pp. 1283-1292, 2004.

20 Li, J., Zhao, Z., Kazakov, A., Chaos, M., Dryer, F. L. and Scire Jr, J. J., "A Comprehensive kinetic mechanism for CO, CH_2O, and CH_3OH combustion." *Int. J. Chem. Kin.,* vol. 39 (3), pp. 109-136, 2007.

21 Smith, G. P., Golden, D. M., Frenklach, M., Moriarty, N. W., Eiteneer, B., Goldenberg, M., Bowman, C. T., Hanson, R. K., Song, S., Jr Gardiner, W. C., Lissianski, V. V. and Qin, Z. http://www.me.berkeley.edu/gri_mech/

22 Law, C. K., "Combustion Physics", Cambridge University press, 2006.

23 Turns, S. R., "An Introduction to Combustion: Concepts and Applications", McGraw-Hill International Edition, 2000.

24 Glassman, I., "Combustion", Academic Press, 3rd ed. 1996.

25 Egolfopoulos, F. N., and Law, C. K., "Chain mechanisms in the overall reaction order in laminar flame propagation." *Combust. Flame,* vol. 80, pp. 7-16, 1997.

26 Ren, J.-Y., Qin, W., Egolfopoulos, F. N., Mak, H., and Tsotsis, T. T., "Methane reforming and its potential effect on the efficiency and pollutant emissions of lean methane-air combustion." *Chemical Engineering Science* vol. 56, pp. 1541-1549, 2001

27 Zhu, D. L., Egolfopoulos, F. N., and Law, C. K., "Experimental and numerical determination of laminar flame speeds of methane/(Ar, N_2, CO_2) – air mixtures as function of stoichiometry, pressure, and flame temperature." *Proceedings of the Combustion Institute* vol. 22, pp. 1537-1545, 1988.

28 Ju, Y., Masuya, G., and Ronney, P. D., "Effects of radiative emission and absorption on the propagation and extinction of premixed gas flames." *Proceedings of the Combustion Institute* vol. 27, pp. 2619-2626, 1998.

29 Sun, C. J., Sung, C. J., He, L., and Law, C. K., "Dynamics of weakly stretched flames: quantitative description and extraction of global flame parameters." *Combust. Flame* vol. 118, pp. 108-128, 1999.

30 Choi, C. W., and Puri, I. K., "Contribution of curvature to flame-stretch effects on premixed flames." *Combust. Flame,* vol. 126, pp. 1640-1654, 2001.

31 Law, C. K., and Sung, C. J., "Structure, aerodynamics and geometry of premixed flamelets." *Prog. Energy Comb. Sci.,* vol. 26, pp. 459-505, 2000.

32 Sun, H. Y., Yang, S. I., Jomass, G., and Law, C. K., "High pressure laminar flame speeds and kinetic modeling of carbon monoxide/hydrogen combustion." Proceedings of the Combustion Institute. vol. 31, pp. 439-446, 2006.

33 Egolfopoulos, F. N., Zhang, H. and Zhang, Z., "Wall effects on the propagation and extinction of steady, strained, laminar premixed flames." *Combustion and Flame* vol. 109, pp. 237-252, 1997.

34 Andac, M. G., Egolfopoulos, F. N. and Campbell, C. S., "Premixed flame extinction by inert particles in normal and micro-gravity." *Combustion and Flame* vol. 129, pp. 179-191, 2002.

35 Wu, C. K. and Law, C. K., "On the determination of laminar flame speeds from stretched flames." *Proceedings of the Combustion Institute* vol. 20: pp. 1941-1949, 1984.

36 Li, J., Zhao, Z., Kazakov, A. and Dryer, F. L., "An updated comprehensive kinetic model of hydrogen combustion" *Int. J. Chem. Kin.* Vol. 36**,** pp. 566-575, 2004.

37 Davis, S. G., Quinard, J., and Searby, G., "Determination of markstein numbers in counterflow premixed flames," *Combustion and Flame* vol. 130, pp. 112-122, 2002.

38 Egolfopoulos, F. N., Cho, P., and Law, C. K., "Laminar flame speeds of methane-air mixtures under reduced and elevated pressures," *Combustion and Flame* vol. 76, pp. 375-391, 1989.

39 Vagelopoulos, C. M., Egolfopoulos, F. N., and Law, C. K., "Further considerations on the determination of laminar flame speeds with the counterflow twin-flame technique." *Proceedings of the Combustion Institute,* vol. 25, pp. 1341-1347, 1994.

40 Egolfopoulos, F. N. and Law, C. K., "An experimental and computational study of the burning rates of ultra-lean to moderately-rich $H_2/O_2/N_2$ laminar flames with pressure variation" *Proceedings of the Combustion Institute,* vol. 23, pp. 333-340, 1990.

41 Brown, M. J., Smith, D. B., and Taylor, S. C., "Influence of uncertainties in rate constants on computed burning velocities" *Combustion and Flame,* vol. 117, pp. 652-656, 1999.

42 Zhao, Z., Li, J., Kazakov, A., and Dryer, F. L., "Temperature-dependent feature sensitivity analysis for combustion modeling" *Int. J. Chem. Kin.,* vol. 37 (5), pp. 282-295, 2005.